NORTHWESTERN UNIVERSITY

Additional Functions of Mitochondria-Lysosome Contact Sites in Health and Neurological Disease

A DISSERTATION

SUBMITTED TO THE GRADUATE SCHOOL
IN PARTIAL FULFILLMENT OF THE REQUIREMENTS

for the degree

DOCTOR OF PHILOSOPHY

Field of Neuroscience

By
Wesley Peng

EVANSTON, ILLINOIS

September 2021

ABSTRACT

Inter-organelle contact sites have become increasingly appreciated as important regulators of cellular homeostasis, and disruption of inter-organelle contact site dynamics and function has been observed in various pathologies. Recently, inter-organelle contact sites between mitochondria and lysosomes were discovered, offering a new mechanism by which these two organelles may directly interact, and were subsequently found to regulate mitochondrial fission. However, whether mitochondria-lysosome contacts like other inter-organelle contacts may serve additional functions has not been elucidated. Moreover, while both mitochondrial and lysosomal dysfunction have been implicated in many neurological diseases, whether alterations in mitochondria-lysosome contact site dynamics and function may further contribute to disease pathogenesis has not been described.

Here, we report two novel functions of mitochondria-lysosome contact sites—the regulation of inter-mitochondrial contact site tethering and direct calcium transfer from lysosomes to mitochondria—and describe dysregulation of these contact-dependent functions in two models of neurological disease. First, using super-resolution imaging, we demonstrate that inter-mitochondrial contacts frequently form and play a fundamental role in mitochondrial networks by restricting mitochondrial motility. Inter-mitochondrial contact untethering events are marked and regulated by mitochondria-lysosome contacts and moreover, inter-mitochondrial contact formation and untethering are regulated by Mfn1/2 and Drp1 GTP hydrolysis, respectively. Importantly, we find that multiple Charcot-Marie-Tooth Type 2 disease-linked mutations in Mfn2 (CMT2A), RAB7 (CMT2B) and TRPV4 (CMT2C) converge on prolonged inter-mitochondrial contacts and defective mitochondrial motility.

Additionally, using high spatial and temporal resolution live-cell microscopy, we identify a role for mitochondria–lysosome contacts in regulating mitochondrial calcium dynamics through the lysosomal calcium efflux channel, transient receptor potential mucolipin 1 (TRPML1). Lysosomal calcium release by TRPML1 promotes calcium transfer to mitochondria, which is mediated by tethering of mitochondria–lysosome contact sites. Mitochondrial calcium uptake at mitochondria–lysosome contact sites is further modulated by the outer and inner mitochondrial membrane channels, voltage-dependent anion channel 1 and the mitochondrial calcium uniporter, respectively. Importantly, mucolipidosis type IV (MLIV) patient fibroblasts harboring loss-of-function mutations in TRPML1 show both altered mitochondria-lysosome contact site dynamics and defective contact-dependent mitochondrial calcium uptake.

Together, our findings highlight a role of mitochondria-lysosome contact sites in mitochondrial network regulation and interorganelle calcium dynamics and furthermore, demonstrate the potential contribution of mitochondria-lysosome contact site dysfunction to the pathophysiology of several neurological disorders.

ACKNOWLEDGEMENTS

The work presented in this thesis would not have been possible without the support of my mentor Dr. Dimitri Krainc. I thank him for taking me on as his first MD-PhD trainee and for providing me such a supportive environment for my thesis work. His mentorship has been instrumental to my growth as a researcher and clinician, and I am grateful to have found a role model and lifelong mentor on my path towards becoming a physician-scientist. I am also incredibly thankful for the mentorship provided by Dr. Yvette Wong including the many hours she has spent meeting with me to discuss experiment ideas and helping me with grant and paper writing. Her dedication to her mentees and ability to see the "big picture" are one-of-a-kind. I wish her all the best as she begins her own laboratory at Northwestern and am excited to see the contributions she will continue to make in the fields of cell biology and neuroscience. I would also like to thank Krainc lab members: Dr. Pingping Song, who patiently taught me about iPSC and dopaminergic neuronal cultures; Leonie Schröder, a fellow graduate student who has provided me so much support through the day-to-day challenges of this PhD journey; and Dr. Niccolò Mencacci, another physician-scientist role model and fellow board game enthusiast.

My thesis work would also not have been possible without the support of my committee members Drs. D. James Surmeier, Navdeep Chandel and Robert Kalb. Their scientific insights have challenged me to think critically about my work and I am grateful to have had the opportunity to work with these experts in organelle biology and neuroscience.

Finally, I would like to thank my friends and family who have supported me throughout my training: my medical school "Day Ones," Shivani Baisiwala and Eva Morgun, lifelong friends and future physician-scientist colleagues; my sister, Chelsea Peng, who continues to be one of my

biggest supporters through all of my endeavors and who has also put up with my many shenanigans throughout the years; and most importantly, my parents Ching-lin Peng and Tsui-Yi Tseng who have made many sacrifices to afford me the opportunities I have been so fortunate to have thus far in my life and who have always encouraged me to pursue my passions.

This work was supported by the following: NIH NINDS (National Institute of Neurological Disorders and Stroke) and NIA (National Institute of Aging) grants F30 AG066333 (to W.P.), K99 NS109252 (to Y.C.W.), and R01 NS076054 and R37NS096241 (to D.K.).

DEDICATION

To my parents,

Ching-Lin Peng and Tsui-Yi Tseng

TABLE OF CONTENTS

ABSTRACT…….3

ACKNOWLEDGEMENTS…….5

LIST OF ABBREVIATIONS……..7

ILLUSTRATIONS……..9

CHAPTERS

1. Chapter 1. Introduction……..11
2. Chapter 2. Lysosomal regulation of inter-mitochondrial contact fate and motility in Charcot-Marie Tooth Type 2…….22
    - Introduction
    - Methods
    - Results
    - Conclusions
3. Chapter 3. Mitochondria-lysosome contacts regulate mitochondrial calcium dynamics via lysosomal TRPML1……...56
    - Introduction
    - Methods
    - Results
    - Conclusions
4. Chapter 4. Discussion……...94

REFERENCES……109

ILLUSTRATIONS

Figure 1. Super-resolution imaging of inter-mitochondrial contacts as important contributors to mitochondrial networks……..35

Figure 2. Lysosomes regulate inter-mitochondrial contact untethering events…….41

Figure 3. Mfn1/2 GTP hydrolysis regulates inter-mitochondrial contact formation…….43

Figure 4. Drp1 GTP hydrolysis regulates inter-mitochondrial contact untethering……..44

Figure 5. Drp1 oligomers mark sites of multiple mitochondrial events and modulation of mitochondria by mitochondrial and cellular stress…….46

Figure 6. Inter-mitochondrial contacts functionally restrict mitochondrial motility and are modulated by mitochondrial respiration and nutrient availability…….49

Figure 7. Multiple Charcot-Marie-Tooth type 2 mutants converge on defective inter-mitochondrial contact dynamics and mitochondrial motility…….53

Figure 8. TRPML1-mediated lysosomal calcium efflux leads to mitochondrial calcium influx…67

Figure 9. Activation of lysosomal TRPML1 leads to mitochondrial calcium influx……68

Figure 10. TRPML1 activation preferentially increases mitochondrial calcium at mitochondria-lysosome contacts……...72

Figure 11. TRPML1 mediates mitochondrial calcium transfer at mitochondria-lysosome contacts in multiple cell types……...73

Figure 12. TRPML1-mediated lysosomal transfer of calcium to mitochondria does not depend on ER calcium release…….74

Figure 13. TRPML1-mediated lysosomal transfer of calcium to mitochondria is not altered by chelation of cytosolic calcium…….76

Figure 14. Wild-type and dominant-negative (D471K) TRPML1 preferentially localize to lysosomes/late endosomes……79

Figure 15. TRPML1 specifically modulates mitochondrial calcium and mitochondria-lysosome contact dynamics……80

Figure 16. TRPML1-mediated mitochondrial calcium influx does not trigger sustained mPTP opening or cytochrome C release……82

Figure 17. TRPML1, VDAC1 and MCU modulate mitochondrial calcium influx at mitochondria-lysosome contact sites……86

Figure 18. VDAC1 and the MCU modulate mitochondrial uptake of lysosomal calcium at mitochondria-lysosome contact sites……..88

Figure 19. Loss of TRPML1 function in MLIV patient fibroblasts disrupts mitochondria-lysosome contact and calcium dynamics……92

Figure 20. Mitochondria-lysosome contact sites as regulators of mitochondrial dynamics…..…96

Figure 21. Mitochondria-lysosome contact sites as regulators of mitochondrial calcium dynamics……..102

CHAPTER 1.

INTRODUCTION

Mitochondria and lysosomes as critical organelles in cellular homeostasis

Both mitochondria and lysosomes are critical for maintaining cellular homeostasis, which is further evinced by the fact that dysfunction of both organelles is functionally and genetically linked to multiple human diseases (Burte, Carelli, Chinnery, & Yu-Wai-Man, 2015; Hutagalung & Novick, 2011; Mc Donald & Krainc, 2017; Plotegher & Duchen, 2017b; Wong, Kim, Peng, & Krainc, 2019). Mitochondria are necessary for cellular respiration but also function as storage compartments for metabolites including calcium, iron, lipids, protons and ATP, and as gatekeepers for apoptosis and inflammatory pathways (Friedman & Nunnari, 2014; N. Sun, Youle, & Finkel, 2016). Consequently, proper regulation of mitochondrial transport and dynamics is key to maintaining a functional mitochondrial network throughout the cell (Mishra & Chan, 2016). Mitochondrial fission has multiple roles including mitochondrial biogenesis and mitochondrial DNA (mtDNA) synthesis (Lewis, Uchiyama, & Nunnari, 2016; Mishra & Chan, 2016) and is regulated by the GTPase dynamin-related protein (Drp1), endoplasmic reticulum (ER), dynamin-2 and actin (Friedman et al., 2011; Ji, Hatch, Merrill, Strack, & Higgs, 2015; Korobova, Ramabhadran, & Higgs, 2013; J. E. Lee, Westrate, Wu, Page, & Voeltz, 2016; Manor et al., 2015; Moore, Wong, Simpson, & Holzbaur, 2016; Smirnova, Griparic, Shurland, & van der Bliek, 2001). In contrast, mitochondrial membrane fusion allows for mixing of mitochondrial proteins, mtDNA and metabolites, and is mediated by the outer membrane GTPases Mitofusin1 (Mfn1) and Mitofusin2 (Mfn2) in consort with the inner membrane GTPase Opa1 (Mishra & Chan, 2016). Properly balanced mitochondrial fission and fusion is crucial as mutations in these proteins result

in various diseases (Alexander et al., 2000; Burte et al., 2015; Delettre et al., 2000; Zuchner et al., 2004).

Similarly, lysosomes are highly dynamic organelles and are responsible for the turnover of cellular contents including proteins and lipids via mature enzymes localized in the lysosomal lumen. Lysosomes can also act as calcium and iron stores, as well as mediate cell death pathways through the initiation of lysosomal membrane permeabilization (Aits & Jaattela, 2013), highlighting a critical role for lysosomes in the maintenance of cellular homeostasis. Lysosomes must undergo strict regulation of their maturation, positioning and network dynamics via the master regulator Rab7. Active, GTP-bound Rab7 is recruited to late endosomal/lysosomal membranes by guanine nucleotide exchange factors (GEFs) such as Mon1-Ccz1 but dissociates upon Rab GTP hydrolysis mediated by Rab GTPase-activating proteins (GAPs) resulting in an inactive, cytosolic GDP-bound form of Rab7 (Hutagalung & Novick, 2011; Zhen & Stenmark, 2015). Importantly, GTP-bound Rab7 promotes lysosomal tethering and fusion and can further bind Rab7 effectors to mediate lysosomal transport in the cell (Langemeyer, Frohlich, & Ungermann, 2018). Importantly, mutations in Rab7 lead to peripheral neuropathy (Houlden et al., 2004; Meggouh, Bienfait, Weterman, de Visser, & Baas, 2006; Verhoeven et al., 2003; X. Wang, Han, Liu, Wang, & Zhang, 2014), further emphasizing the importance of proper lysosomal dynamics in maintaining cell viability. However, the role and regulation of direct mitochondrial and lysosomal interactions at inter-organelle contact sites has only been recently studied.

Previous Crosstalk between Mitochondria and Lysosomes

Previous studies have demonstrated several pathways for indirect interactions between mitochondria and lysosomes. Mitochondrial function, including respiration has been shown to be

critical for regulating lysosomal function as deletion of mitochondrial proteins (AIF, Opa1 or PINK1), chemical inhibition of oxidative phosphorylation (Brahimi-Horn et al., 2015; Demers-Lamarche et al., 2016), or expression of transcription factor A, mitochondrial (TFAM) mutations impair lysosomal activity (Baixauli et al., 2015). In addition, lysosomal biogenesis increases dramatically in response to short-term inhibition of mitochondrial respiration but is disrupted by long-term inhibition via rotenone (Fernández-Mosquera et al., 2017). Moreover, increased mitochondrial oxidative stress in human dopaminergic neurons contributes to reduced activity of oxidized lysosomal enzymes such as glucocerebrosidase, which impairs lysosomal glycolipid metabolism (Burbulla et al., 2017).

Conversely, lysosomal function has been shown to be essential for maintaining mitochondrial homeostasis. In skeletal muscle, the lysosomal biogenesis regulator transcription factor EB (TFEB) acts as a central coordinator for mitochondrial function in a peroxisome proliferator-activated receptor gamma coactivator 1-alpha (PGC1α)-independent manner (Mansueto et al., 2017). In neurons, the autophagy inhibitor mammalian target of rapamycin complex 1 (mTORC1) promotes an integrated mitochondrial stress response (Khan et al., 2017) and also regulates mitochondrial activity (Norambuena et al., 2018). In addition, disrupting lysosomal acidification is sufficient to decrease mitochondrial respiration (Monteleon et al., 2018). Finally, endolysosomal Rabs, including Rab5, Rab7A, Rab5-GEP (RABGEF1) and Rab7-GEF (MON1-CCZ1), also regulate mitochondrial function and can be recruited to damaged mitochondria (Hsu et al., 2018; Yamano et al., 2018). Moreover, Rab7 knockdown inhibits the assembly of ATG9A vesicles during Parkin-dependent mitophagy (Yamano et al., 2018), while translocation of Rab5 to mitochondria decreases oxygen consumption of cytochrome C release during mitochondrial oxidative stress (Hsu et al., 2018).

In addition, mitochondria and lysosomes have also been shown to directly interact upon cellular stress (Hamacher-Brady, Choe, Krijnse-Locker, & Brady, 2014; Pickrell & Youle, 2015; Sugiura, McLelland, Fon, & McBride, 2014), with the majority of these studies predominantly focusing on lysosomal degradation of mitochondria either through mitophagy (Pickrell & Youle, 2015) or fusion of mitochondrial-derived vesicles (MDVs) with lysosomes (Sugiura et al., 2014). Whole mitochondria can be degraded by autophagy (mitophagy), which involves engulfment of damaged mitochondria by an autophagosome followed by fusion with lysosomes to form an autolysosome for degradation of its contents. Mitophagy can occur either nonselectively or selectively via mitophagy receptors such as optineurin and NDP52, which are recruited to ubiquitinated mitochondria in a PINK1/Parkin-dependent manner and subsequently recruit LC3 on the autophagosome via their LC3 interaction region (Lazarou et al., 2015; Wong & Holzbaur, 2014). In contrast, MDVs are small vesicles (~ 100 nm) (Sugiura et al., 2014), which bud off from mitochondria and contain different subsets of mitochondrial outer membrane and matrix proteins. MDVs targeted to lysosomes are generated through a PINK1/Parkin-dependent manner (McLelland, Soubannier, Chen, McBride, & Fon, 2014) and may represent a pathway to selectively degrade a subset of mitochondrial proteins rather than entire mitochondria. However, whether mitochondria and lysosomes directly interact with one another under normal conditions in healthy mammalian cells via nondegradative pathways has not been previously well-studied.

Identification of dynamic mitochondria-lysosome membrane contact sites

Inter-organelle membrane contact sites are defined as contacts forming between the membranes of two distinct organelles at close proximity allowing for their intracellular communication (Gatta & Levine, 2017). While the ER forms many contacts with other parts of the

cell including the plasma membrane, Golgi, mitochondria, peroxisomes, lipid droplets and endosomes (H. Wu, Carvalho, & Voeltz, 2018), the discovery of additional inter-organelle contacts not involving the ER such as those between lysosomes, lipid droplets and peroxisomes have further demonstrated that many organelles within the cell are well connected (Valm et al., 2017). In addition, contacts between mitochondria and lysosomal-related organelles including melanosomes, multi-vesicular bodies and yeast vacuoles have also been previously described (Daniele et al., 2014; Elbaz-Alon et al., 2014; Honscher et al., 2014; Sugiura et al., 2014). Importantly, while contacts are maintained by tethering proteins which allow for the dynamic formation and subsequent untethering of organelle membranes, additional proteins may also be present at contact sites which do not physically bridge membranes but help to regulate contact function such as by mediating metabolite transfer, or regulatory proteins which help coordinate contacts and their response to the cellular environment (Eisenberg-Bord, Shai, Schuldiner, & Bohnert, 2016). Functionally, previous contact sites have been found to be important for mediating multiple cellular functions including the transfer of lipids, calcium and iron, the regulation of organelle dynamics such as mitochondrial division (Friedman et al., 2011) and endosomal division (Rowland, Chitwood, Phillips, & Voeltz, 2014) which are marked by ER tubules, and additional processes which occur at contact sites (Simmen & Herrera-Cruz, 2018; H. Wu et al., 2018), demonstrating a critical role for inter-organelle contact sites in maintaining cellular homeostasis.

Recently, multiple studies using diverse imaging techniques have demonstrated that inter-organelle contact sites also form between mitochondria and lysosomes in multiple different cell types under healthy conditions (Aston et al., 2017; Q. Chen et al., 2018; Fermie et al., 2018; Han, Li, Qiu, Zhang, & Zhang, 2017; Itoh et al., 2019; Valm et al., 2017; Wong, Ysselstein, & Krainc, 2018). Mitochondria-lysosome contacts were observed using 2D and 3D electron microscopy

(Aston et al., 2017) as well as correlative light electron microscopy (CLEM) of LysoTracker-positive vesicles in contact with mitochondria (Wong et al., 2018) or CLEM combined with focused ion beam scanning electron microscopy (FIB-SEM) which showed Lamp1 and dextran positive vesicles stably contacting mitochondria (Fermie et al., 2018). Contacts between mitochondria and lysosomes were also observed by lattice light sheet spectral imaging (Valm et al., 2017), and were found to be less frequent than contacts involving the ER (Valm et al., 2017). In addition, mitochondria-lysosome contacts were observed by structured illumination microscopy (SIM) imaging of organelles labeled by mitochondrial (Q. Chen et al., 2018) or lysosomal (Han et al., 2017) dyes or fluorescently-labeled proteins which showed that mitochondria could first contact one lysosome and subsequently move on to contact another lysosome (Han et al., 2017). Moreover, contacts were also seen by immunofluorescent staining of endogenous mitochondrial (Tom20) and lysosomal (Lamp1) membrane proteins by confocal microscopy (Itoh et al., 2019) or 3D SIM imaging (Wong et al., 2018). Finally, mitochondria-lysosome contacts were also labeled by sensitized emission fluorescence resonance energy transfer (SE-FRET) between TOM20–Venus on the outer mitochondrial membrane and LAMP1–mTurquoise2 on the lysosomal membrane (Wong et al., 2018).

Mitochondria-lysosome contact sites had an average distance between mitochondrial and lysosomal membranes (Aston et al., 2017; Wong et al., 2018) consistent with previously observed membrane contact sites (10–30 nm) (Csordas et al., 2006; M. J. Phillips & Voeltz, 2016). Approximately 15% of lysosomes were in contact with mitochondria at any point in time with mitochondria-lysosome contact sites remaining stably tethered for an average of 60 sec (Wong et al., 2018) although contacts demonstrated a varying range of tethering durations, lasting as long as 13 minutes (Han et al., 2017). Bulk transfer of either lysosomal luminal contents or

mitochondrial matrix or inter-membrane space proteins across organelles was not observed at sites of contact (Wong et al., 2018), and contacts did not represent autophagosome biogenesis events or mitophagy as they were negative for multiple autophagosome markers including ULK1, Atg5, and LC3 (Wong et al., 2018). In addition, mitochondria that formed contacts were distinct from MDVs as they contained both outer mitochondrial membrane and matrix proteins (Wong et al., 2018) and were substantially larger than previously described MDVs (~100 nm (MDVs) versus ~500 nm (mitochondria)) (Sugiura et al., 2014), suggesting that mitochondria-lysosome contact sites do not represent sites of mitophagy or lysosomal engulfment of bulk mitochondria.

Regulation of mitochondria-lysosome contacts by Rab7 GTP hydrolysis

Mitochondria-lysosome contact site tethering is mechanistically regulated by multiple proteins on the mitochondrial and lysosomal membranes. The small GTPase Rab7 which is a master regulator of lysosomal dynamics modulates mitochondria-lysosome contact site tethering and untethering dynamics through its ability to alternate between an active, lysosomal-localized GTP-binding state and an inactive, cytosolic GDP-binding state. Contact tethering is promoted by lysosomal GTP-bound Rab7 and may be tethered to mitochondria via Rab7 effector proteins which bind GTP-bound Rab7 on the lysosome. Importantly, expression of RAB7 Q67L, a constitutively active GTP-bound form which is unable to undergo GTP hydrolysis, is sufficient to increase the number of lysosomes contacting mitochondria and results in prolonged contacts (Wong et al., 2018).

Subsequent mitochondria-lysosome contact untethering is mediated by Rab7 GTP hydrolysis which first involves the recruitment of cytosolic TBC1D15 (Rab7 GAP) to mitochondria via the outer mitochondrial membrane protein Fis1 (Onoue et al., 2013; Peralta,

Martin, & Edinger, 2010; X. M. Zhang, Walsh, Mitchell, & Rowe, 2005). Once recruited to mitochondria, TBC1D15 is able to interact with lysosomal GTP-bound Rab7 to drive its hydrolysis to a GDP-bound state. GDP-bound Rab7 can no longer bind Rab7 effectors and also loses its lysosomal membrane localization (Langemeyer et al., 2018), leading to mitochondria-lysosome contact untethering (Wong et al., 2018) potentially via the loss of Rab7 effector tethering. Importantly, inhibition of Rab7 GTP hydrolysis with either TBC1D15 (D397A or R400K) mutants, which lack GAP activity (Onoue et al., 2013), prevents efficient mitochondria-lysosome contact untethering, resulting in prolonged contacts (Wong et al., 2018). Interestingly, TBC1D15 mutants have no effect on contact formation, suggesting that TBC1D15-dependent Rab7 GTP hydrolysis is limited to regulating contact untethering but not the formation of contacts. In addition, mutant Fis1 (LA), which is unable to recruit TBC1D15 to mitochondria (Onoue et al., 2013), as well as complete knockout of either TBC1D15 or Fis1, prevents efficient mitochondria-lysosome contact untethering, leading to prolonged contacts (Wong et al., 2018). Thus, Rab7 GTP hydrolysis, which requires interaction of both lysosomal (Rab7) and mitochondrial-localized (TBC1D15, Fis1) proteins at contact sites, provides a mechanism for the regulation of mitochondria-lysosome untethering.

Known and potential functions of mitochondria-lysosome contact sites

Several functions of mitochondria-lysosome contact sites have been discovered including the regulation of lysosomal and mitochondrial dynamics. Lysosomal dynamics are acutely regulated by Rab7 effector proteins which preferentially bind GTP-bound Rab7 on the lysosomal membrane, such as RILP and FYCO which mediate lysosomal retrograde and anterograde microtubule transport respectively (Jordens et al., 2001; Pankiv et al., 2010), and the HOPS

complex which mediates lysosomal tethering and fusion (Balderhaar & Ungermann, 2013). Mitochondria-lysosome contact sites thus offer a platform for mitochondrial-localized proteins to regulate lysosomal dynamics via modulation of Rab7-GTP binding. As mitochondrial TBC1D15 promotes Rab7 GTP hydrolysis at contacts leading to the termination of GTP-bound Rab7 (Wong et al., 2018), this simultaneously results in both contact site untethering and the release of Rab7 effector proteins from GTP-bound Rab7 and the lysosomal membrane, thus regulating lysosomal dynamics. Indeed, expression of mitochondrial-localized mutant TBC1D15 (D397A or R400K) lacking GAP activity leads to enlarged lysosomes (Wong et al., 2018), consistent with the lysosomal morphology observed upon inhibition of RAB7 GTP hydrolysis. Thus, mitochondria-lysosome contact sites may help promote Rab7 GTP hydrolysis and regulate the dynamics of a subset of lysosomes within the cell which are in contact with mitochondria.

Mitochondria-lysosome contact sites are also able to regulate mitochondrial dynamics, as the majority of mitochondrial fission events (>80%) are marked by LAMP1-positive vesicles but not early endosomes or peroxisomes (Wong et al., 2018). Disrupting mitochondria-lysosome contact untethering dynamics by inhibiting Rab7 GTP hydrolysis with mutants GTP-bound Rab7 Q67L, TBC1D15 (D397A or R400K) or Fis1 (LA) decreases rates of mitochondrial fission and disrupts the mitochondrial network (Wong et al., 2018). All mitochondrial fission events marked by lysosomes were also positive for Drp1, a dynamin-related GTPase that facilitates the constriction of the outer mitochondrial membrane during mitochondrial fission (Friedman & Nunnari, 2014). Mitochondria-lysosome contact sites were also recently found to regulate the untethering of inter-mitochondrial contacts, homotypic contact sites involving two distinct mitochondria that do not undergo fusion and which are important for regulating mitochondrial motility (Wong, Peng, & Krainc, 2019). Specifically, LAMP1-positive vesicles were found to

preferentially mark sites of inter-mitochondrial contact untethering (> 90%) (Wong, Peng, et al., 2019). Thus, mitochondria-lysosome contact sites additionally act to regulate the mitochondrial network by marking sites of mitochondrial fission and inter-mitochondrial contact untethering.

Although the function of mitochondria-lysosome contacts has been explored largely with regard to the regulation of organelle dynamics, additional functions, such as the transfer of ions or metabolites, are also possible given the importance of both organelles to ion homeostasis and metabolism. One such candidate is calcium, which is a highly regulated ion that plays a crucial role in various cellular processes such as exocytosis, gene transcription and apoptosis (Raffaello, Mammucari, Gherardi, & Rizzuto, 2016). While the primary cellular store of calcium is located in the ER, both mitochondria and lysosomes have also been implicated as important players in calcium homeostasis. Calcium is transported into mitochondria through the voltage-dependent anion channel-1 (VDAC1) on the outer mitochondrial membrane and the mitochondrial calcium uniporter (MCU) on the inner mitochondrial membrane, and serves to remove cytosolic calcium and drive metabolic processes such as ATP production (Todkar, Ilamathi, & Germain, 2017). Mitochondria-ER contact sites known as MAMs (mitochondrial-associated membranes) have previously been identified as regulators of calcium transfer and dynamics in mitochondria in various cell types (Bononi et al., 2012) including mammalian neurons (Hirabayashi et al., 2017). However, as lysosomes also play emerging roles in calcium signaling and storage, mitochondria-lysosome contact sites may serve as similar platforms for calcium transfer. Indeed, TRPML1, a mucolipin channel on the lysosomal membrane that releases calcium, functions as a sensor of cellular reactive oxygen species (ROS), which are produced in large part by mitochondria (Sena & Chandel, 2012). In addition, the activity of TRPML1 increases with rising levels of ROS, and TRPML1 activation promotes autophagy (X. Zhang et al., 2016). While this suggests an indirect

modulation of mitochondrial function and activity by lysosomal calcium, mitochondria-lysosome contact sites may support more direct mechanisms for calcium transfer and signaling between these two organelles.

Conclusions

The recent identification of mitochondria-lysosome membrane contact sites in mammalian cells and their regulation of Rab7 GTP hydrolysis and mitochondrial dynamics highlight the intricate crosstalk between these two organelles. These contact sites offer important insight into their bidirectional relationship and may help to explain the converging dysfunction of both organelles in multiple diseases. As both mitochondria and lysosomes are crucial for proper metabolism and degradation, investigating their interplay will be key to elucidating their overlapping pathways in cellular homeostasis.

CHAPTER 2.

LYSOSOMAL REGULATION OF INTER-MITOCHONDRIAL CONTACT FATE AND MOTILITY IN CHARCOT-MARIE-TOOTH TYPE 2

Introduction

Mitochondrial networks are critical for functional cellular metabolism and must be properly regulated (Wai & Langer, 2016), as reflected by multiple human diseases linked to defective mitochondrial dynamics (Alexander et al., 2000; Burte et al., 2015; Delettre et al., 2000; Zuchner et al., 2004). Mitochondria undergo both fission and fusion events to regulate the mitochondrial network, but the dynamic role and regulation of a third event - the formation of inter-mitochondrial contact sites - in shaping mitochondrial network dynamics is still not well understood. Indeed, the majority of previous studies have viewed mitochondrial tethering between two mitochondria merely as a transition step occurring prior to membrane fusion for generating a single mitochondria (Mishra & Chan, 2016), rather than as a distinct event which can dynamically modulate the mitochondrial network.

Mitochondria can additionally interact with other organelles such as the endoplasmic reticulum (ER) or lysosomes/late endosomes at membrane contact sites to mediate multiple forms of inter-organelle communication and maintain cellular homeostasis (Eisenberg-Bord et al., 2016; Gottschling & Nyström, 2017; M. J. Phillips & Voeltz, 2016; Wong et al., 2018; Y. Wu et al., 2017). However, while mitochondria fission events are marked by ER tubules and lysosomes (Friedman et al., 2011; Wong et al., 2018), how inter-organelle contacts interact with and modulate inter-mitochondrial contact tethering dynamics is still not known.

In addition, whether dysfunctional inter-mitochondrial contact site dynamics might contribute to human disease pathogenesis is also unclear. Charcot-Marie-Tooth (CMT) disease is the most common hereditary peripheral neuropathy, with Type 2 forms representing autosomal dominant forms linked to axonal degeneration (Harel & Lupski, 2014). Mitofusin 2 (Mfn2) is an outer mitochondrial membrane protein which regulates mitochondrial fusion and has been implicated in additional mitochondrial functions including mitophagy, mitochondrial transport, ER-mitochondria contacts and mtDNA stability (H. Chen et al., 2010; Y. Chen & Dorn Ii, 2013; De Brito & Scorrano, 2008; A. Misko, Jiang, Wegorzewska, Milbrandt, & Baloh, 2010; Santel & Fuller, 2001; Schrepfer & Scorrano, 2016), with Mfn2 mutations leading to CMT Type 2A (Zuchner et al., 2004). In contrast, Rab7 is a lysosomal/late endosomal regulator (Hutagalung & Novick, 2011), with Rab7 mutations resulting in CMT Type 2B (Houlden et al., 2004; Manganelli et al., 2012; Meggouh et al., 2006; Verhoeven et al., 2003; X. Wang et al., 2014). However, whether and how CMT2A (Mfn2) and CMT2B (RAB7) disease-linked mutations converge in disease pathogenesis is unclear.

Previously, using super-resolution confocal imaging of mitochondrial membranes in living cells, we identified inter-mitochondrial contact tethering as fundamental events which modulate mitochondrial network dynamics. Inter-mitochondrial contacts form 10x more frequently than mitochondrial fission/fusion events and functionally help to restrict mitochondrial motility. Interestingly, late endosomes/lysosomes actively promote inter-mitochondrial contact untethering which are regulated by lysosomal RAB7 GTP hydrolysis at mitochondria-lysosome contact sites. Inter-mitochondrial contact formation and untethering dynamics are further mediated by Mfn1/2 GTP hydrolysis and Drp1 GTP hydrolysis respectively and are modulated by mitochondrial respiration and nutrient availability. Importantly, multiple Charcot-Marie-Tooth Type 2 disease-

linked mutants including Mfn2 (CMT2A), RAB7 (CMT2B) and TRPV4 (CMT2C) converge on defective inter-mitochondrial contact untethering and disrupted mitochondrial motility. Our study thus identifies a crucial role for inter-mitochondrial contacts in modulating mitochondrial homeostasis and demonstrate its dysfunction in the pathogenesis of multiple forms of CMT2.

Methods

Cell lines. HeLa cells (gift from Michael Schwake (ATCC)) and HEK293 cells (human embryonic kidney cell line 293FT (Life Technologies)) were cultured in DMEM (Gibco; 11995–065) supplemented with 10% (vol/vol) FBS, 100 units/mL penicillin, and 100 µg/mL streptomycin. H4 neuroglioma cells (Mazzulli et al., 2011) were cultured in Optimem + 5% FBS, 200ug/ml geneticin and hygromycin, 1% penicillin / streptomycin (Life Technologies) and treated with 1ug/ml doxycycline (Sigma) for 3 days. Cells were derived from female (HeLa, HEK293) or male (H4) subjects. All cells were maintained at 37 °C in a 5% CO2 incubator and previously verified by cytochrome c oxidase subunit I (COI) and short tandem repeat (STR) testing and tested for Mycoplasma contamination. Cells were transfected using Lipofectamine 2000 (Invitrogen). For live imaging, cells were grown on glass bottom culture dishes (MatTek; P35G-1.5-14-C).

Plasmids. The following plasmids were obtained from Addgene: LAMP1-mGFP was a gift from Esteban Dell'Angelica (Addgene #34831) (Falcon-Perez, Nazarian, Sabatti, & Dell'Angelica, 2005), mito-BFP and mCh-Drp1 were gifts from Gia Voeltz (Addgene #49151, #49152) (Friedman et al., 2011), Snap-Omp25 was a gift from David Sabatini (Addgene # 69599) (Katajisto et al., 2015), mito-PAGFP was a gift from Richard Youle (Addgene # 23348) (Karbowski et al., 2004), EGFP-RAB7A WT was a gift from Qing Zhong (Addgene #28047) (Q. Sun, Westphal,

Wong, Tan, & Zhong, 2010), mApple-TOMM20-N-10, mEmerald-TOMM20-C-10, DsRed2-Mito-7, and mCherry-ER-3 were gifts from Michael Davidson (Addgene #54955, #54281, #55838, #55041), and Mfn1-Myc, Mfn1(K88T)-10xmyc, Mfn2-myc and Mfn2 K109A-myc were gifts from David Chan (Addgene #23212, #26050, #23213, #26051) (Y. Chen & Dorn Ii, 2013). GFP-RAB7-Q67L was a gift from Aimee Edinger (Rosales, Peralta, Guenther, Wong, & Edinger, 2009). N-terminal HA-tagged TBC1D15 (wild-type and D397A mutant) and Flag-FIS1 (wild-type and LA mutant) were generous gifts from Naotada Ishihara (Jofuku, Ishihara, & Mihara, 2005; Onoue et al., 2013), mCherry-Mfn1 and mCherry-Mfn2 were generous gifts from Elena Kolobova (Mason, Goldenring, & Kolobova, 2014), and pIRES2-ZsGreen1- TRPV4 (WT) and pIRES2-ZsGreen1- TRPV4 (R269H) were generous gifts from Han-Xiang Deng (Deng et al., 2010). mCherry-Drp1(K38A), bicistronic Mfn2(WT)+mApple, bicistronic Mfn2(T105M)+mApple, mNeonGreen-RAB7(WT) and mNeonGreen-RAB7(V162M) were generated using VectorBuilder.

Cell treatment. To modulate mitochondrial and cellular homeostasis, HeLa cells were incubated with control DMSO (3h, Sigma), mitochondrial respiration Complex I inhibitor Rotenone (3h, 1μM, Sigma) or cultured in low nutrient media Hank's Balanced Salt Solutions (2h HBSS, Corning) prior to confocal live-cell imaging experiments.

Confocal microscopy. All confocal images were acquired on a Nikon A1R laser scanning confocal microscope with GaAsp detectors using a Plan Apo λ 100× 1.45 NA oil immersion objective (Nikon) using NIS-Elements 4.20 (Nikon). Live cells were imaged in a temperature-controlled chamber (37 °C) at 5% CO2 at 1 frame every 2–3 sec. Cells transfected with Snap-OMP25 were

visualized by incubation for 30 min with 0.6 μM SNAP-Cell® 647-SiR (New England Biolabs; S9102S) and subsequently washed 4x with warm media before imaging. The matrix of individual mitochondria were selectively labeled by localized photoactivation of cells transfected with photoactivatable mitochondrial matrix marker mito-PAGFP using a 405 nm laser (100% for 4 sec) and mitochondrial matrix transfer at fusion or transient fusion events was subsequently tracked.

Electron microscopy. For transmission electron microscopy (TEM), cells were grown on coverslips and fixed in a mixture of 2.5% glutaraldehyde and 2% paraformaldehyde in 0.1M cacodylate buffer for 2–24 h at 4 °C. After post-fixation in 1% osmium tetroxide and 3% uranyl acetate, cells were dehydrated in series of ethanol, embedded in Epon resin and polymerized for 48 h at 60 °C. Ultrathin sections were made using UCT ultramicrotome (Leica Microsystems) and contrasted with 4% uranyl acetate and Reynolds's lead citrate. Samples were imaged using a FEI Tecnai Spirit G2 transmission electron microscope (FEI Company, Hillsboro, OR) operated at 80 kV. Images were captured with an Eagle 4k HR 200kV CCD camera.

Structured illumination microscopy. Structured illumination microscopy (SIM) super-resolution images were taken on a Nikon N-SIM system with an oil immersion objective lens 100×, 1.49 NA, Nikon. Images were captured using NIS-Elements (Nikon) at 1 frame every 6 sec and reconstructed using slice reconstruction in NIS-Elements (Nikon). Images for live cell imaging (live N-SIM) were taken at a single z-plane. Cells used for live cell imaging were maintained in a temperature-controlled chamber (37 °C) at 5% CO2 in a TokaiHit stagetop incubator.

Image analysis (detailed). Inter-mitochondrial contacts were defined as those which clearly showed two distinct mitochondria which came together to form a tether and subsequently untethered, and remained as two distinct mitochondria throughout the process without fusion. Mitochondrial fusion events were defined as those which clearly began as two distinct mitochondria and subsequently tethered together prior to outer mitochondrial membrane fusion to form a single mitochondria. Mitochondrial fission events were defined as those which clearly showed division of a single mitochondria into two distinct daughter mitochondria which transiently tethered prior to subsequently separating from one another. The percentage of mitochondria in inter-mitochondrial contacts at a given point in time were defined as those which were tethered (<0.1 μm) to another mitochondria for >10s. The frequency of duration of inter-mitochondrial contact tethering was calculated from contacts which showed both clear formation of tether and subsequent untethering. Mitochondrial events were defined as tether (formation of inter-mitochondrial contacts not leading to fusion), untether (untethering of inter-mitochondrial contacts), fusion and fission as analyzed from confocal time-lapse of outer mitochondrial membrane markers. Mitochondrial transient fusion events were defined as events involving transfer of photoactivated mitochondrial matrix marker mito-PAGFP from individual mitochondria selectively labeled by localized photoactivation, without the obvious fusion of outer mitochondrial membrane marker (mApple-TOM20). Tethered mitochondrial partners were tracked over time (10s) for their inter-mitochondrial contact site using ImageJ 1.51j8 (NIH) from time-lapse confocal images of outer mitochondrial membrane marker (mApple-TOM20), with the starting location for all contact sites set to the center of the graph. For motility analysis, mitochondria which were tethered in an inter-mitochondrial contact (distance traveled over 30 sec

prior to untethering) were compared to free mitochondria (distance traveled over 30 sec after untethering from an inter-mitochondrial contact).

Mitochondrial untethering, fusion and fission events marked by Drp1 or ER were analyzed from confocal time-lapse images of outer mitochondrial membrane marker (TOM20-mEmerald), matrix marker (mito-BFP) and Drp1 marker (mCherry-Drp1) or ER marker (mCherry-ER). Mitochondrial untethering events and tethered mitochondria (the state of being tethered) were further analyzed for the presence of ER or Drp1 and confirmed to be distinct from fission/fusion/transient fusion events by confocal time-lapse images of individually labeled locally photoactivated mitochondria (mito-PAGFP) with outer mitochondrial membrane marker (Snap-OMP25). The expected probability that Drp1 oligomers would be at the site of a mitochondrial division event by random chance was calculated as the density of mCherry-Drp1 on the outer mitochondrial membrane (mApple-TOM20) from n = 19 living cells, using ImageJ 1.51j8 (NIH). The expected probability that ER would be at the site of a mitochondrial division event by random chance was calculated as the density of mCherry-ER in the cytosol from n = 11 living cells, using ImageJ 1.51j8 (NIH). Analysis for Drp1 conditions was conducted from confocal time-lapse images of outer mitochondrial membrane marker (mEmerald-TOM20), matrix marker (mito-BFP) and mCherry-Drp1 (WT or K38A) and subsequently normalized to Control. The duration for different mitochondrial events were defined for fusion (time from formation of mitochondrial tether to fusion into a single mitochondria), untether (time from formation of mitochondrial tether to untethering as two distinct mitochondria throughout the process), and fission (time from the formation of transient tethering of two daughter mitochondria to their separation). The minimum

time to untethering or transient fusion were quantified from mitochondrial tethers already formed at the beginning of the video.

Mitochondrial untethering, fusion and fission events and tethered state marked by lysosomes/late endosomes contacts (M-L) were analyzed from confocal time-lapse images of outer mitochondrial membrane marker (mApple-TOM20) and lysosome/late endosome marker (LAMP1-mGFP). The expected probability that a LAMP1 vesicle would be at the site of a mitochondrial division event by random chance was calculated as the density of LAMP1-mGFP vesicles in the cytosol from n = 16 living cells, using ImageJ 1.51j8 (NIH). The fate of inter-mitochondrial contacts (either remaining tethered or untethering in ≤10s) was analyzed for tethered mitochondria which did not simultaneously contact lysosomes compared to those that did. Inter-mitochondrial (M-M) contact and M-L contact formation were defined as the time when two distinct organelles clearly came together to form a tether, while M-M and M-L contact untethering were defined as the time when two distinct organelles clearly separated. M-L contacts were only analyzed for LAMP1-mGFP-positive vesicles which were clearly in contact (<0.1 μm) with a mitochondria that was simultaneously in a M-M contact. M-L contact formation was quantified for any events occurring either prior or subsequent to M-M formation but prior to M-M untethering. M-L contact untethering was quantified for any events occurring after M-M contact formation but either prior or subsequent to M-M untethering. The minimum time to M-M untether (duration of M-M contacts) was analyzed from mitochondria already tethered at the beginning of the video and was defined as the time prior to mitochondrial untethering over a 150s video. Any contacts which lasted throughout the entire 150s video and which were still in contact by the end of the video were categorized as 150s in bar graphs, and as > 120s in histograms.

Inter-mitochondrial contacts marked by mitofusins were analyzed from confocal time-lapse images of outer mitochondrial membrane marker (mEmerald-TOM20), matrix marker (mito-BFP) and mitofusin markers (mCherry-Mfn1, mCherry-Mfn2). The percentage of inter-mitochondrial (M-M) contacts was quantified as the percentage of mitochondria tethered to another mitochondria for >10s divided by the total number of mitochondria in the region of interest, and the minimum duration of M-M contacts was analyzed from mitochondria already tethered at the beginning of the video, and defined as the time prior to mitochondrial untethering over a 180s video, with any contacts which lasted throughout the entire 180s video and which were still in contact by the end of the video categorized as 180s and as > 120s in histograms. Analysis for Mitofusin conditions was conducted from confocal time-lapse images of outer mitochondrial membrane marker (TOM20-mApple) and matrix marker (mito-BFP) with or without myc-tagged mitofusins. All analysis was subsequently normalized to Control.

Analysis for CMT type 2A conditions was conducted from confocal time-lapse images of outer mitochondrial membrane marker (mEmerald-TOM20), matrix marker (mito-BFP) and bicistronic Mfn2 WT or T105M in cells simultaneously expressing mApple, and was subsequently normalized to Mfn2 (WT). For comparison of mNeonGreen-RAB7 WT with V162M using outer mitochondrial membrane marker (mApple-TOM20), the percentage of lysosomes in M-L contact was quantified as the percentage of RAB7 vesicles that formed contacts lasting >10s with mitochondria divided by the total number of RAB7 vesicles in the region of interest, the rate of mitochondrial fission was analyzed from videos >180s, and the minimum duration of both M-L and M-M contacts were analyzed from mitochondria already tethered at the beginning of the video, and defined as the time prior to mitochondrial untethering over a 180s video, with any contacts

which lasted throughout the entire 180s video and which were still in contact by the end of the video categorized as 180s and as > 120s in histograms, and all analysis was subsequently normalized to RAB7 WT. Analysis for CMT type 2C was conducted from confocal time-lapse images of outer mitochondrial membrane marker (mApple-TOM20) and the minimum duration of M-M contacts were analyzed from mitochondria already tethered at the beginning of the video, and defined as the time prior to mitochondrial untethering over a 180s video, with any contacts which lasted throughout the entire 180s video and which were still in contact by the end of the video categorized as 180s and as > 120s in histograms, and was subsequently normalized to TRPV4 (WT). For motility analysis, the motility of 5 randomly selected mitochondria per cell was tracked over 3 min (only for mitochondria which remained in the field of view for the entire 3 min) and normalized to WT/control/DMSO conditions.

Statistical analysis, graphing and figure assembly. Data were analyzed using unpaired two-tailed Student *t* test (for two datasets), Fisher's exact test or one-way ANOVA with Tukey's post hoc test (for multiple data sets) (see figure legends for details). Data presented are means ± SEM (except in histograms). Statistics and graphing were performed using Prism 7 (GraphPad) software. All experiments were analyzed from n ≥3 independent experiments (biological replicates) per condition. All line scans were generated using ImageJ 1.51j8 (NIH) and normalized per protein. Examples of transient fusion and M-L contacts are shown after linear rescaling in NIS-Elements 4.20 (Nikon) and all videos and images were assembled using ImageJ 1.51j8 (NIH). All final figures were assembled in Illustrator CC (Adobe).

Results

Super-resolution imaging of inter-mitochondrial contacts

To investigate the formation and dynamics of inter-mitochondrial contacts, we performed electron microscopy and super-resolution live cell imaging of mitochondria in human cells. Consistent with previous studies demonstrating mitochondria in close apposition spanning <20 nm between the outer mitochondrial membrane in fixed cells without membrane fusion (Pease, 1962; Picard et al., 2015; Vernay et al., 2017), we observed inter-mitochondrial contact sites using transmission electron microscopy (TEM) in healthy untreated HeLa cells (**Fig. 1A**). Next, we examined their dynamics using super-resolution imaging of the outer mitochondrial membrane (mApple-TOM20) by time-lapse structured illumination microscopy (SIM) in living cells. Inter-mitochondrial contacts were stably tethered together over time (**Fig. 1B-E**), with contacts forming between mitochondria of different lengths including tubular mitochondria as observed by TEM (Fig. 1A), super-resolution (Fig. 1B) and confocal imaging. Importantly, contacts were indeed the result of two distinct mitochondria and were positive for both outer mitochondrial membrane (TOM20) and matrix (mito-BFP; COX4) proteins (Fig. 1F). At any given time, ~30% of mitochondria were in stable inter-mitochondrial contacts for >10 sec (**Fig. 1G**) and remained tethered for 39.8 ± 2.6 sec (**Fig. 1H**).

Using super-resolution imaging of the outer mitochondrial membrane (mApple-TOM20), we further confirmed that inter-mitochondrial contacts were indeed distinct from previously described mitochondrial fusion or fission events. Mitochondrial fusion events involved two separate mitochondria that tethered together for >20s on average (white arrows) but subsequently fused to form a single mitochondria. Conversely, mitochondrial fission events involved a single mitochondria which divided into two transiently tethered distinct daughter mitochondria prior to

separating. In contrast, the formation and untethering of tethered mitochondria began and ended with two distinct mitochondria (**Fig. 1D-E**).

We further found that the majority of tethered mitochondria in the cell represented inter-mitochondrial contacts which subsequently untethered from each other (**Fig. 1C-E**), rather than mitochondrial fusion events (89.3% untether versus 10.7% fusion, $p<0.0001$, n = 195 events) (Fig. 1I) with their outcomes independent of tethering duration (**Fig. 1J**). Thus, inter-mitochondrial contacts represent a previously underappreciated dynamic event which frequently occurs and are distinct from mitochondrial fission or fusion events.

Inter-mitochondrial contacts form without matrix transfer and modulate the mitochondrial network

As mitochondrial kiss-and-run transient fusion events between two mitochondria have previously been observed without requiring complete fusion of the outer mitochondrial membrane (Huang et al., 2013; Liu, Weaver, Shirihai, & Hajnóczky, 2009), we examined whether tethered mitochondria represented sites of transient fusion by selectively locally photoactivating the matrix of individual mitochondria labeled with mito-PAGFP (photoactivatable GFP) and tracking their fate. We found that the majority of mitochondria tethered to another mitochondria (labeled for both outer mitochondrial membrane (SNAP-Omp25) and matrix proteins (Dsred2-mito)) without mito-PAGFP transfer (**Fig. 1K-L**). Moreover, mitochondria remained stably tethered in inter-mitochondrial contacts over time, and even untethered from one another without mito-PAGFP transfer (**Fig. 1K**). While we did observe several examples of transient fusion events leading to mito-PAGFP transfer without outer mitochondrial membrane fusion (mApple-TOM20), the majority of mitochondrial tethering events resulted in untethering without bulk matrix transfer

rather than in transient fusion, and was not dependent on the amount of time mitochondria were tethered.

To further differentiate between physical tethering and non-specific close apposition of mitochondrial membranes, we traced the movements of tethered inter-mitochondrial contact partners by tracking the point of inter-mitochondrial contact over time (10s) from time-lapse confocal live cell images. As expected, we found that tethered mitochondria could move together over time consistent with physical tethering between mitochondria, resulting in inter-mitochondrial contact sites which persisted but could move within the cell.

Next, we investigated the rate of different mitochondrial events to determine which occurred the most frequently in the cell. Surprisingly, while the rates of both mitochondrial fission and fusion were <2 events/min in live HeLa cells, inter-mitochondrial contact tethering and untethering events occurred ten times more frequently (23.1 ± 3.8 tethering events/min, 27.4 ± 4.7 untethering events/min) (**Fig. 1M**). We further confirmed that inter-mitochondrial contact tethering and untethering occurred significantly more frequently in other cell types including HEK293 and H4 neuroglioma cells. Taken together, these results demonstrate that dynamic inter-mitochondrial contacts occur frequently without matrix transfer and significantly more often than mitochondrial fission or fusion events, suggesting they play a critical role in modulating the mitochondrial network.

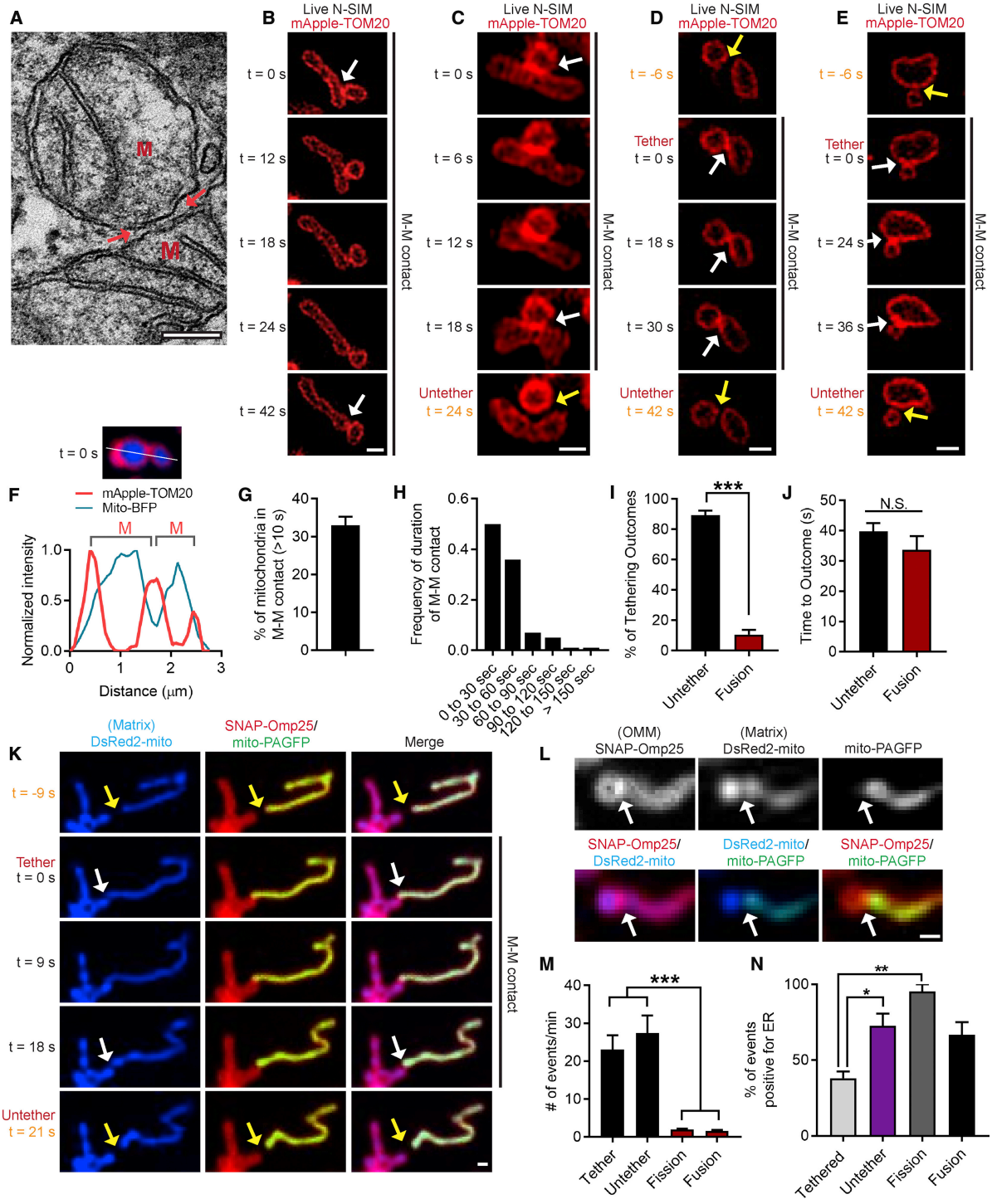
A
M
M
B
Live N-SIM
mApple-TOM20
t = 0 s
t = 12 s
t = 18 s
t = 24 s
t = 42 s
M-M contact
C
Live N-SIM
mApple-TOM20
t = 0 s
t = 6 s
t = 12 s
t = 18 s
Untether
t = 24 s
M-M contact
D
Live N-SIM
mApple-TOM20
t = -6 s
Tether
t = 0 s
t = 18 s
t = 30 s
Untether
t = 42 s
M-M contact
E
Live N-SIM
mApple-TOM20
t = -6 s
Tether
t = 0 s
t = 24 s
t = 36 s
Untether
t = 42 s
M-M contact
t = 0 s
F
mApple-TOM20
Mito-BFP
M
M
Normalized intensity
1.0
0.5
0.0
0
1
2
3
Distance (μm)
G
% of mitochondria in M-M contact (>10 s)
40
30
20
10
0
H
Frequency of duration of M-M contact
0.6
0.4
0.2
0.0
0 to 30 sec
30 to 60 sec
60 to 90 sec
90 to 120 sec
120 to 150 sec
> 150 sec
I
***
% of Tethering Outcomes
100
80
60
40
20
0
Untether
Fusion
J
N.S.
Time to Outcome (s)
50
40
30
20
10
0
Untether
Fusion
K
(Matrix)
DsRed2-mito
SNAP-Omp25/
mito-PAGFP
Merge
t = -9 s
Tether
t = 0 s
t = 9 s
t = 18 s
Untether
t = 21 s
M-M contact
L
(OMM)
SNAP-Omp25
(Matrix)
DsRed2-mito
mito-PAGFP
SNAP-Omp25/
DsRed2-mito
DsRed2-mito/
mito-PAGFP
SNAP-Omp25/
mito-PAGFP
M
***
# of events/min
40
30
20
10
0
Tether
Untether
Fission
Fusion
N
**
*
% of events positive for ER
100
50
0
Tethered
Untether
Fission
Fusion

Figure 1: Super-resolution imaging of inter-mitochondrial contacts as important contributors to mitochondrial networks. A, Transmission electron microscopy of inter-mitochondrial contacts (M, arrows) in untreated HeLa cells, corresponding to Figure S1B. Scale bar, 200 nm. **B,** Super-resolution time-lapse structured illumination microscopy (N-SIM) of inter-mitochondrial contact tethering (white arrows) in live HeLa cells (outer mitochondrial membrane (OMM) label mApple-TOM20). Scale bar, 0.5 μm. **C-E**, Super-resolution time-lapse structured illumination microscopy (N-SIM) of inter-mitochondrial contact tethering (white arrows) and subsequent untethering (yellow arrows) in live HeLa cells (outer mitochondrial membrane (OMM) label mApple-TOM20). Scale bars, 0.5 μm. **F,** Line scan of inter-mitochondrial contact positive for OMM label mApple-TOM20 and matrix label Mito-BFP (t = 0 s). **G, H,** Percentage of mitochondria forming inter-mitochondrial contacts (G) and frequency of contact duration (H) from confocal time-lapse images of live HeLa cells (OMM label mApple-TOM20 and matrix label Mito-BFP) (n = 176 events from 10 cells). **I, J,** Percentage of tethering outcomes (I) and time to outcome (J) for inter-mitochondrial contact untethering and mitochondrial fusion events from confocal time-lapse images of live HeLa cells (OMM label mApple-TOM20 and matrix label Mito-BFP) (n = 176 untethering and n = 19 fusion from 10 cells). **K,** Confocal time-lapse images of inter-mitochondrial contacts (white arrows), which do not undergo mitochondrial matrix mito-PAGFP transfer prior to untethering (yellow arrows) in live HeLa cells (OMM label SNAP-Omp25, matrix label DsRed2-mito, and individual mitochondrial matrix label mito-PAGFP). The matrix of individual mitochondria was selectively locally photoactivated and tracked over time. Scale bar, 0.5 μm. **L,** Confocal images of inter-mitochondrial contact (white arrows), which do not undergo mitochondrial matrix mito-PAGFP transfer in live HeLa cells (OMM label SNAP-Omp25, matrix label DsRed2-mito, and individual mitochondrial matrix label mito-PAGFP). The matrix of individual mitochondria was selectively locally photoactivated and tracked over time. Scale bar, 0.5 μm. **M,** Quantification of mitochondrial event rates from confocal time-lapse images of live HeLa cells (OMM label mApple-TOM20 and matrix label Mito-BFP) (n = 231 tether, n = 275 untether, n = 16 fusion, and n = 21 fission from 10 cells). **N,** Percentage of events marked by ER tubules for tethered mitochondria (confirmed as distinct mitochondria by selective local photoactivation of individual mitochondria by mito-PAGFP (OMM label SNAP-Omp25, individual mitochondrial matrix label mito-PAGFP, and ER label mCherry-ER) and mitochondrial untethering, fusion, and fission events (OMM label mEmerald-TOM20, matrix label Mito-BFP, and ER label mCherry-ER) in live HeLa cells (n = 88 tethered, n = 36 untether, n = 18 fusion, and n = 17 fission). Mean ± SEM; $^{*}p < 0.05$; $^{**}p < 0.01$; $^{***}p < 0.001$; NS, not significant; unpaired two-tailed t test for (I) and (J), ANOVA with Tukey's post hoc test for (M) and (N).

Lysosomes both mark and regulate inter-mitochondrial contact untethering events

As lysosomes/late endosomes could also simultaneously contact inter-mitochondrial contacts, we next examined whether the fate of inter-mitochondrial contact might be directly coupled to mitochondria-lysosome contacts. Surprisingly, using time-lapse confocal imaging of mitochondria (mApple-TOM20) and the lysosome/late endosome membrane marker LAMP1-mGFP, we found that the majority of inter-mitochondrial contact untethering events had at least one of the mitochondria simultaneously in contact with a LAMP1-positive vesicle within 10 s of untethering (94%, n = 50 events), which was significantly greater than expected by random chance (10.7%; ***$p < 0.001$, Fisher's exact test) (**Fig. 2A-B**). In contrast, very few tethered inter-mitochondrial contacts (Fig. 2C) or mitochondrial fusion events (**Fig. 2C**) were marked by lysosomes, suggesting that in contrast to ER tubules (**Fig. 1N**), mitochondria-lysosome contacts preferentially mark inter-mitochondrial contact untethering events over fusion events.

We further investigated the timing of inter-mitochondrial contact untethering and found that it was closely coupled to both mitochondria-lysosome (M-L) contact formation (**Fig. 2D**) and subsequent M-L contact untethering (**Fig. 2E**). In contrast, the formation of inter-mitochondrial contacts was not temporally coupled to either M-L contact formation (**Fig. 2F**) or M-L contact untethering (**Fig. 2G**). Indeed, M-L contacts which formed on a mitochondria that was in contact with another mitochondria resulted in rapid inter-mitochondrial contact untethering (≤10s) (**Fig. 2H-I**), as well as rapid subsequent M-L contact untethering (≤10s) (**Fig. 2J-K**). Moreover, we saw multiple examples of inter-mitochondrial contacts and M-L contacts which were tethered together (**Fig. 2A**), followed by simultaneous untethering of both contact sites (**Fig. 2A**).

Finally, to examine whether lysosomes directly promoted inter-mitochondrial contact untethering, we analyzed the fate of inter-mitochondrial contacts. In the absence of M-L contacts,

the majority of inter-mitochondrial contacts remained tethered (87.8%, n = 45 contacts from 21 cells) with very few subsequently untethering within 10s (12.2%, ***p<0.001) (**Fig. 2L**; left). In contrast, upon formation of M-L contacts, the majority of inter-mitochondrial contacts subsequently untethered within 10s (69.6%, n = 47 contacts from 21 cells) with few remaining tethered (30.3%,***p<0.001) (**Fig. 2L**; right), suggesting that mitochondria-lysosome contacts directly promote the untethering of inter-mitochondrial contacts.

Mfn1/2 and Drp1 GTP hydrolysis respectively regulate inter-mitochondrial contact formation and untethering

We next investigated whether GTPases such as mitochondrial Mfn1/2 and Drp1 might further regulate inter-mitochondrial contact dynamics. Both Mfn1 and Mfn2 localized to sites of inter-mitochondrial contact tethering (**Fig. 3A-B**) which were positive for both outer mitochondrial membrane (TOM20) and matrix (mito-BFP; COX4) proteins. Moreover, while the majority of tethered inter-mitochondrial contacts (>70%) were marked by Mfn1 (**Fig. 3C**) and Mfn2 (**Fig. 3D**), significantly fewer untethering events (<35%) were marked by Mfn1 or Mfn2 (**Fig. 3C-D**), suggesting that mitofusins might promote contact tethering rather than untethering events.

To directly examine the role of mitofusin GTP hydrolysis on inter-mitochondrial contact dynamics, we compared the effect of wild-type Mfn1 and Mfn2 and GTP hydrolysis deficient mutants on inter-mitochondrial contact tethering. Both wild-type Mfn1 and Mfn2 expression significantly increased the percentage of tethered inter-mitochondrial contacts by ~1.5 fold (**Fig. 3E, H**). In contrast, GTP hydrolysis deficient mutants Mfn1 (K88T) or Mfn2 (K109A) did not affect the percentage of tethered mitochondria (**Fig. 3E, H**), suggesting that inter-mitochondrial contact tethering is directly regulated by mitofusin GTP hydrolysis. Moreover, wild-type Mfn1 or

Mfn2 expression inhibited inter-mitochondrial contact untethering events resulting in significantly prolonged contact durations (**Fig. 3F-G**, I-J, ***p<0.001). In contrast, GTP hydrolysis deficient mutants Mfn1 (K88T) or Mfn2 (K109A) did not disrupt inter-mitochondrial contact untethering events, leading to decreased contact durations compared to wild-type Mfn1 and Mfn2 (**Fig. 3F-G**, I-J, ***p<0.001), suggesting that both Mfn1 and Mfn2 GTP hydrolysis promote inter-mitochondrial contact tethering.

We also found that Drp1 oligomers were gradually recruited to inter-mitochondrial contact sites and marked the majority of untethering events (>75%, n = 79), which was significantly greater than expected by random chance (18.7%; ***p<0.001, Fisher's exact test) (**Fig. 4A-B**, **Fig. 5A-C**). In addition, Drp1 oligomers preferentially marked inter-mitochondrial contact untethering events over stably tethered contacts (<40%; n = 94 tethered mitochondria from 19 cells) (**Fig. 4C**), suggesting that they might regulate inter-mitochondrial contact untethering dynamics.

Surprisingly, Drp1 oligomers were also recruited to the majority of both mitochondrial fission (**Fig. 5D**) and fusion events (**Fig. 4D, Fig. 5E**) as well as transient fusion events (**Fig. 5F-G**). While Drp1 oligomers were present for the majority of time during mitochondrial fission events, Drp1 oligomers were only present immediately prior to mitochondrial fusion or inter-mitochondrial contact untethering events (**Fig. 4E, Fig. 5H**). We further confirmed using selective local mito-PAGFP photoactivation of individual mitochondria that inter-mitochondrial contacts marked by Drp1 oligomers were indeed two distinct mitochondria lacking mito-PAGFP transfer, and thus not the result of fission or fusion events (**Fig. 4F**). Moreover, Drp1 oligomerization at mitochondrial untethering events occurred regardless of whether Drp1 oligomers were present during the initial tethering (**Fig. 4G**).

To directly examine the role of Drp1 in inter-mitochondrial contact dynamics, we compared the effect of wild-type Drp1 and its GTP hydrolysis deficient mutant on inter-mitochondrial contact tethering. Expression of the GTP hydrolysis mutant Drp1 (K38A) significantly increased the percentage of mitochondria forming inter-mitochondrial contacts (**Fig. 4H**, ***$p<0.001$), as compared to wild-type Drp1 or control conditions. Additionally, Drp1 (K38A) significantly prolonged the duration of inter-mitochondrial contacts by preventing efficient untethering (**Fig. 4I-J**, ***$p<0.001$), suggesting that Drp1 GTP hydrolysis regulates inter-mitochondrial contact site untethering.

Of note, two distinct tethered mitochondria at inter-mitochondrial contacts labeled by matrix markers (DsRed2-mito or mito-BFP) (**Fig. 1K-L**) appeared very similar to previously described mitochondrial constriction sites. Since inter-mitochondrial contact tethering occurred significantly more frequently than mitochondrial fission events (**Fig. 1M**), the majority of previously described mitochondrial constriction sites may have been tethering of two distinct mitochondria at inter-mitochondrial contact sites followed by untethering, rather than prolonged constriction of a single mitochondria followed by fission into two daughter mitochondria, which occurs much faster. Interestingly, we found that similar to what was previously proposed for mitochondrial constriction sites, Drp1 oligomers and ER tubules also both marked inter-mitochondrial contact untethering and mitochondrial fusion events (**Fig. 1N, Fig. 4D**).

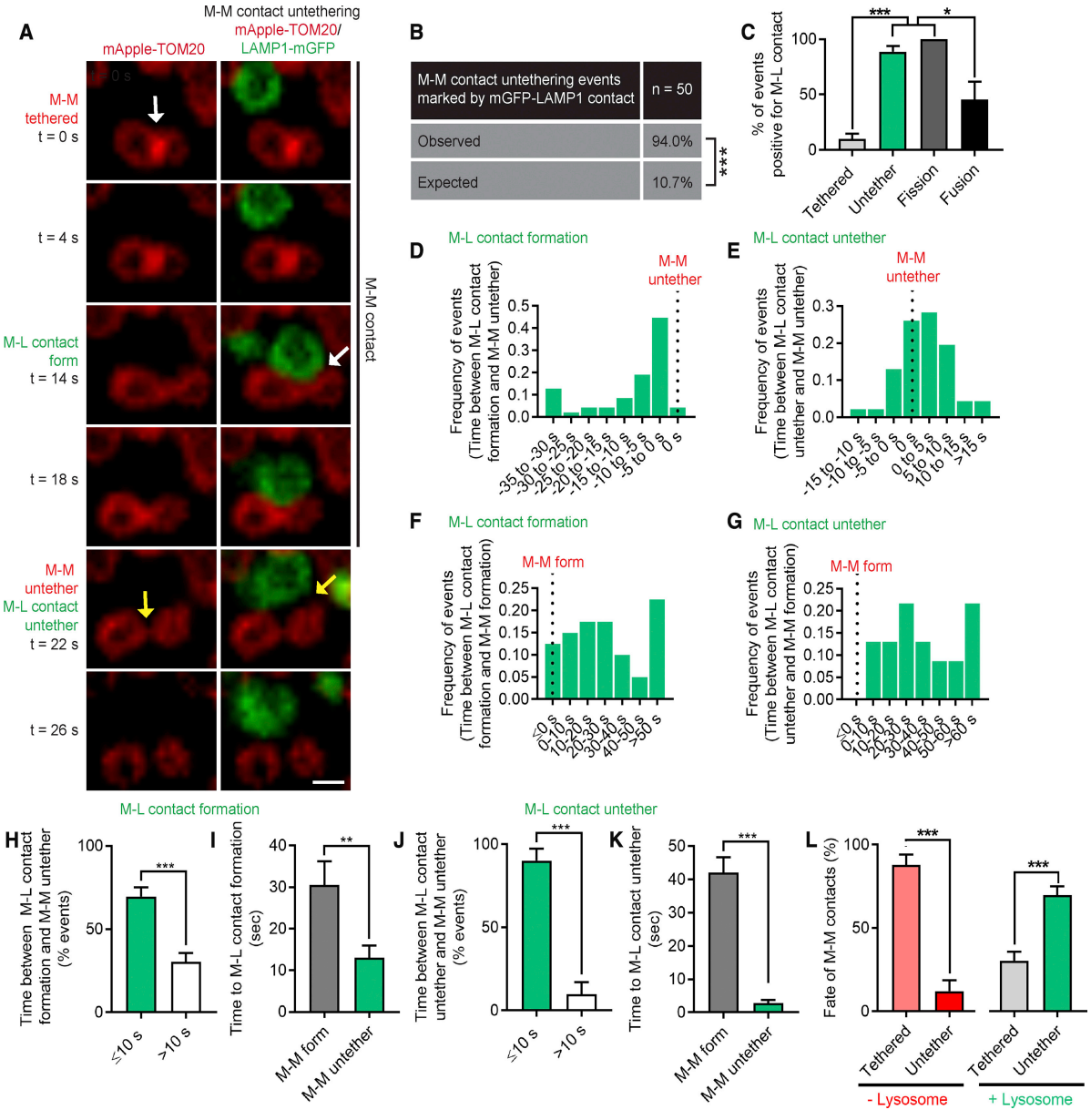
A
M-M contact untethering
mApple-TOM20/
LAMP1-mGFP
mApple-TOM20
M-M tethered t = 0 s
t = 4 s
M-L contact form t = 14 s
t = 18 s
M-M untether M-L contact untether t = 22 s
t = 26 s
M-M contact
B
M-M contact untethering events marked by mGFP-LAMP1 contact
n = 50
Observed
94.0%
Expected
10.7%
***
C
% of events positive for M-L contact
***
*
Tethered
Untether
Fission
Fusion
D
M-L contact formation
M-M untether
Frequency of events (Time between M-L contact formation and M-M untether)
E
M-L contact untether
M-M untether
Frequency of events (Time between M-L contact untether and M-M untether)
F
M-L contact formation
M-M form
Frequency of events (Time between M-L contact formation and M-M formation)
G
M-L contact untether
M-M form
Frequency of events (Time between M-L contact untether and M-M formation)
H
M-L contact formation
Time between M-L contact formation and M-M untether (% events)
≤10 s
>10 s
I
Time to M-L contact formation (sec)
M-M form
M-M untether
J
M-L contact untether
Time between M-L contact untether and M-M untether (% events)
K
Time to M-L contact untether (sec)
L
Fate of M-M contacts (%)
Tethered
Untether
- Lysosome
+ Lysosome

Figure 2: Lysosomes regulate inter-mitochondrial contact untethering events. A, Confocal time-lapse images of inter-mitochondrial contact (M-M) formation (white arrow) and subsequent untethering (yellow arrow) temporally coupled to mitochondria-lysosome (M-L) contact formation and untethering in live HeLa cells (OMM label mApple-TOM20 and lysosome/late endosome label LAMP1-mGFP). Scale bar, 0.5 μm. **B,** Observed localization of lysosomes marking inter-mitochondrial contact untethering events compared to lysosomal localization by random chance (expected) in live HeLa cells (OMM label mApple-TOM20 and lysosome/late endosome label LAMP1-mGFP) (n = 50 untethering events from 26 cells). **C,** Percentage of inter-mitochondrial contact untethering events and mitochondrial events (tethered state, untethering event, fission event, and fusion event) marked by LAMP1-mGFP vesicles in live HeLa cells (OMM label mApple-TOM20 and lysosome/late endosome label LAMP1-mGFP) (n = 25 tethered, n = 50 untether, n = 9 fission, and n = 17 fusion events from 26 cells). **D,** Histogram of time between mitochondria-lysosome (M-L) contact formation and inter-mitochondrial (M-M) contact untethering (n = 47 total events from 21 cells). **E,** Histogram of time between mitochondria-lysosome (M-L) contact untethering and inter-mitochondrial (M-M) contact untethering (n = 46 total events from 18 cells). **F,** Histogram of time between mitochondria-lysosome (M-L) contact formation and inter-mitochondrial (M-M) contact formation (n = 40 total events from 18 cells). **G,** Histogram of time between mitochondria-lysosome (M-L) contact untethering and inter-mitochondrial (M-M) contact formation (n = 46 total events from 18 cells). **H,** Graph of time between mitochondria-lysosome (M-L) contact formation and inter-mitochondrial (M-M) contact untethering (n = 47 total events from 21 cells). **I,** Graph of time between mitochondria-lysosome (M-L) contact formation and inter-mitochondrial (M-M) contact formation and untethering (n = 40 total M-M formation events from 18 cells and n = 47 total M-M untether events from 21 cells). **J,** Graph of time between mitochondria-lysosome contact untethering and inter-mitochondrial (M-M) contact untethering (n = 46 total events from 18 cells). **K,** Graph of time between mitochondria-lysosome (M-L) contact untethering and inter-mitochondrial (M-M) contact formation and untethering (n = 46 total M-M formation events from 18 cells and n = 46 total M-M untether events from 18 cells). **L,** Fate of inter-mitochondrial contacts either remaining tethered or untethering in ≤10 s depending on whether mitochondria simultaneously contact lysosomes (n = 45 events from 21 cells [no lysosomes] and n = 47 events from 21 cells [with lysosomes]). Mean ± SEM; $^{*}p < 0.05$; $^{**}p < 0.01$; $^{***}p < 0.001$; Fisher's exact test for (B), unpaired two-tailed t test for (H)–(L), and ANOVA with Tukey's post hoc test for (C).

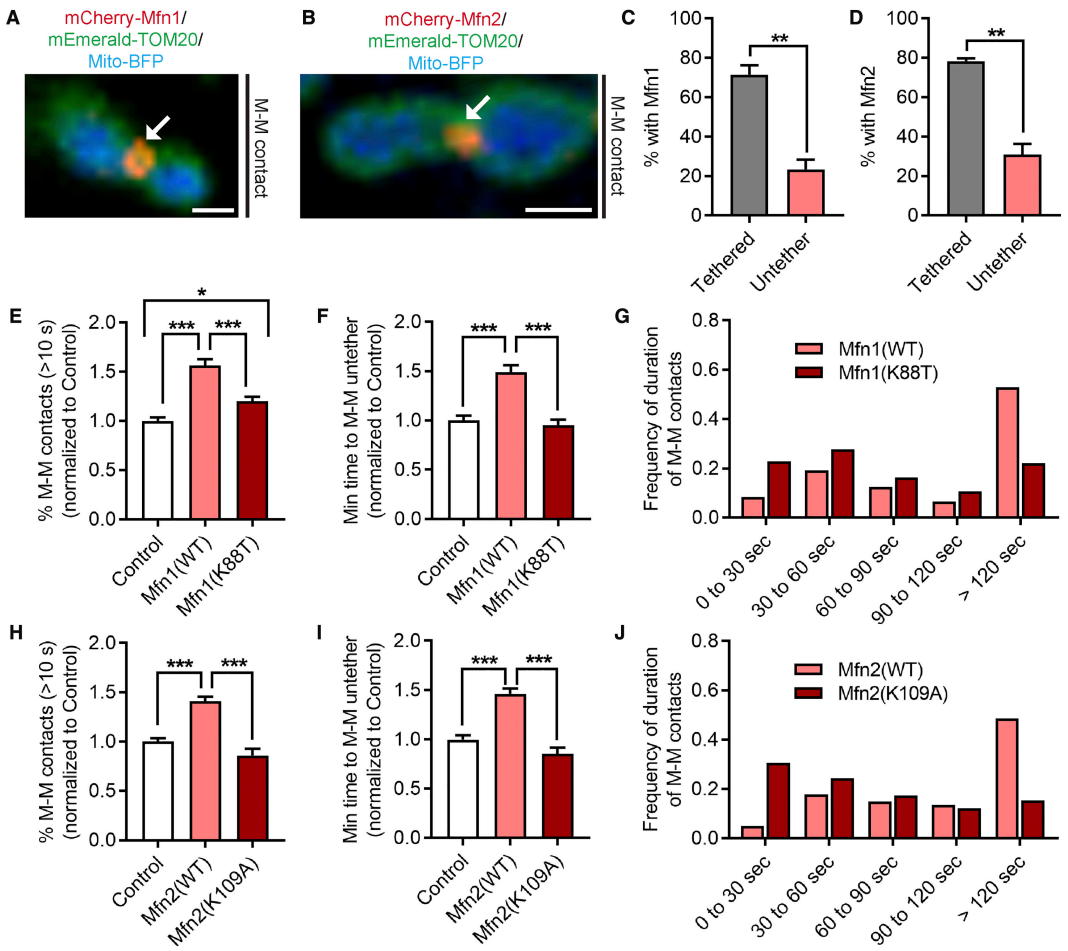

Figure 3: Mfn1/2 GTP hydrolysis regulates inter-mitochondrial contact formation. **A**, **B,** Confocal images of mCherry-Mfn1 (A) and mCherry-Mfn2 (B) localized to sites of inter-mitochondrial contact tethering (white arrows) in live HeLa cells (OMM label mEmerald-TOM20 and matrix label Mito-BFP). Scale bar, 0.5 µm. **C, D,** Percentage of inter-mitochondrial contact (in tethered state) and untethering events marked by mCherry-Mfn1 (C) and mCherry-Mfn2 (D) oligomers from confocal time-lapse images in live HeLa cells (OMM label mEmerald-TOM20 and matrix label Mito-BFP) (Mfn1, n = 105 events from 15 cells and Mfn2, n = 91 events from 13 cells). **E-G,** Percentage of mitochondria in inter-mitochondrial contact (E) and minimum time to untethering (F, histogram in G) in live HeLa cells expressing myc-tagged Mfn1 wild-type or GTP hydrolysis mutant K88T (n = 146 events from 21 cells (control), n = 119 events from 17 cells (Mfn1 [WT]) and n = 140 events from 20 cells (Mfn1 [K88T]). **H-J,** Percentage of mitochondria in inter-mitochondrial contact (H) and minimum time to untethering (I, histogram in J) in live HeLa cells expressing myc-tagged Mfn2 wild-type or GTP hydrolysis mutant K109A (n = 146 events from 21 cells (control), n = 140 events from 20 cells (Mfn2 [WT]), and n = 98 events from 14 cells (Mfn2 [K109A]). Mean ± SEM; $^{*}p < 0.05$; $^{**}p < 0.01$; $^{***}p < 0.001$; unpaired two-tailed t test for (C) and (D) and ANOVA with Tukey's post hoc test for (E), (F), (H), and (I).

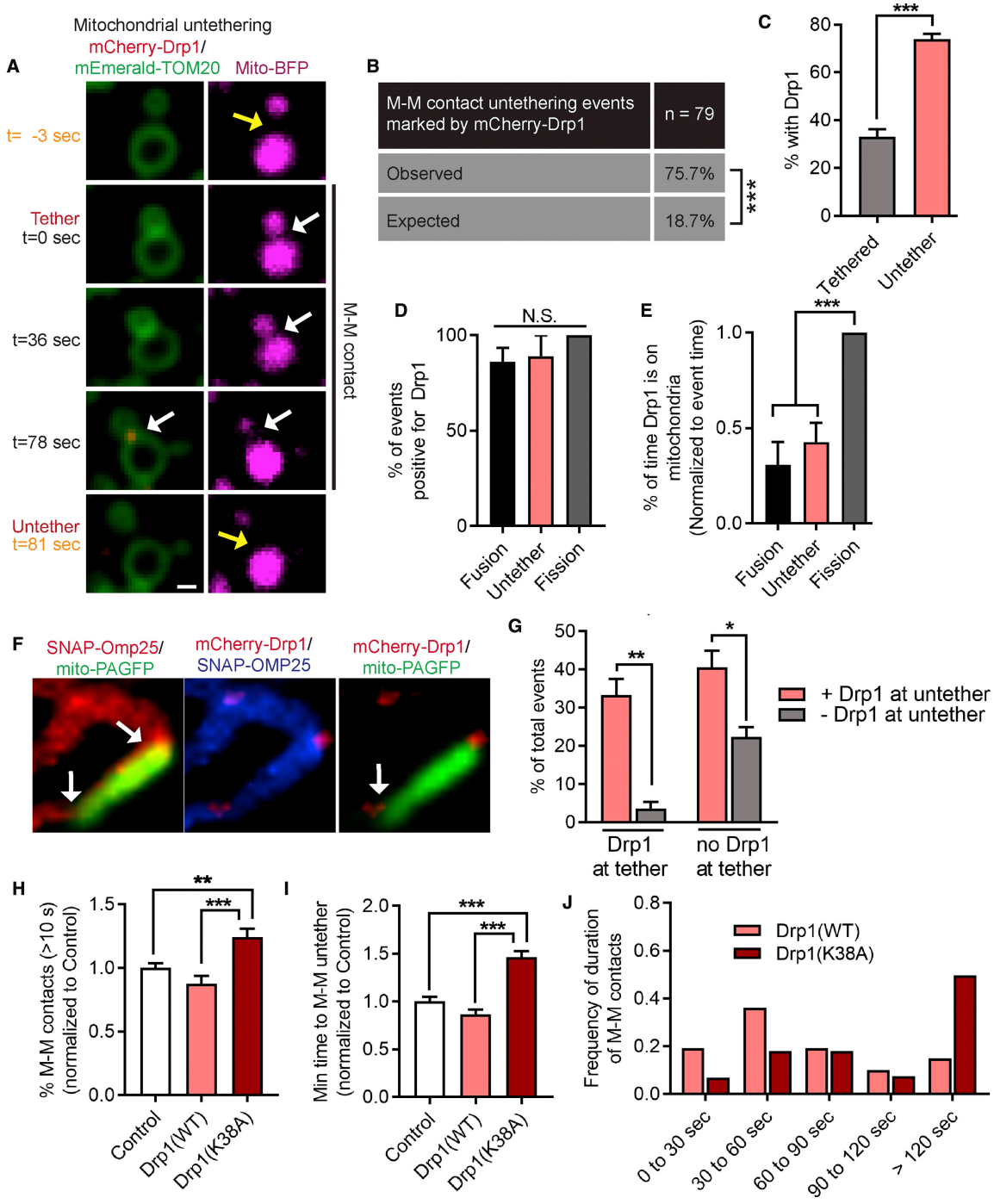
A
Mitochondrial untethering
mCherry-Drp1/
mEmerald-TOM20
Mito-BFP
t= -3 sec
Tether
t=0 sec
t=36 sec
t=78 sec
Untether
t=81 sec
M-M contact
B
M-M contact untethering events marked by mCherry-Drp1
n = 79
Observed
75.7%
Expected
18.7%
***
C
% with Drp1
***
Tethered
Untether
D
% of events positive for Drp1
N.S.
Fusion
Untether
Fission
E
% of time Drp1 is on mitochondria (Normalized to event time)
***
Fusion
Untether
Fission
F
SNAP-Omp25/
mito-PAGFP
mCherry-Drp1/
SNAP-OMP25
mCherry-Drp1/
mito-PAGFP
G
% of total events
**
*
+ Drp1 at untether
- Drp1 at untether
Drp1
at tether
no Drp1
at tether
H
% M-M contacts (>10 s)
(normalized to Control)
**
***
Control
Drp1(WT)
Drp1(K38A)
I
Min time to M-M untether
(normalized to Control)
***
***
Control
Drp1(WT)
Drp1(K38A)
J
Frequency of duration of M-M contacts
Drp1(WT)
Drp1(K38A)
0 to 30 sec
30 to 60 sec
60 to 90 sec
90 to 120 sec
> 120 sec

Figure 4: Drp1 GTP hydrolysis regulates inter-mitochondrial contact untethering. A, Confocal time-lapse images of inter-mitochondrial contact tethering (white arrows) and untethering (yellow arrows), showing Drp1 oligomerization in live HeLa cells (OMM label mEmerald-TOM20, matrix label Mito-BFP, and Drp1 label mCherry-Drp1). Scale bar, 0.5 μm. **B,** Observed localization of Drp1 oligomers marking inter-mitochondrial contact untethering events compared to Drp1 localization by random chance (Expected) from confocal time-lapse images in live HeLa cells, confirmed as distinct mitochondria by selective local photoactivation of individual mitochondria by mito-PAGFP (OMM label SNAP-Omp25, individual mitochondrial matrix label mito-PAGFP, and Drp1 label mCherry-Drp1). **C,** Localization of Drp1 oligomers marking inter-mitochondrial contact untethering events compared to tethered contacts from confocal time-lapse images in live HeLa cells, confirmed as distinct mitochondria by selective local photoactivation of individual mitochondria by mito-PAGFP (OMM label SNAP-Omp25, individual mitochondrial matrix label mito-PAGFP, and Drp1 label mCherry-Drp1) (n = 94 tethered mitochondria and n = 79 untethering events from 19 cells). **D, E,** Percentage of events marked by Drp1 oligomerization (D) and percentage of event time marked by Drp1 oligomers (E) for mitochondrial fusion, untethering, and fission events in live HeLa cells (OMM label mEmerald-TOM20, matrix label Mito-BFP, and Drp1 label mCherry-Drp1) ((D) n = 11 fusion, n = 24 untether, and n = 12 fission and (E) n = 7 fusion, n = 14 untether, and n = 12 fission from 6–9 cells). **F, G,** Confocal image of inter-mitochondrial contact marked by Drp1 oligomerization confirmed as distinct mitochondria by selective photoactivation of individual mitochondria by mito-PAGFP (F) and Drp1 oligomerization dynamics in live HeLa cells (G) (OMM label SNAP-Omp25, individual mitochondrial matrix label mito-PAGFP, and Drp1 label mCherry-Drp1). Scale bar, 0.5 μm. (G) n = total 79 events from 19 cells. **H-J,** Percentage of mitochondria forming inter-mitochondrial contacts (H) and minimum time to untethering (I, histogram in J) in live HeLa cells expressing mCherry-tagged Drp1 wild-type or GTP hydrolysis mutant K38A (n = 146 events from 21 cells (control), n = 119 events from 17 cells (Drp1 [WT]), and n = 133 events from 19 cells (Drp1 [K38A]). Mean ± SEM; $^{*}p < 0.05$; $^{**}p < 0.01$; $^{***}p < 0.001$; NS, not significant; Fisher's exact test for (B), unpaired two-tailed t test for (C) and (G), and ANOVA with Tukey's post hoc test for (D), (E), (H), and (I).

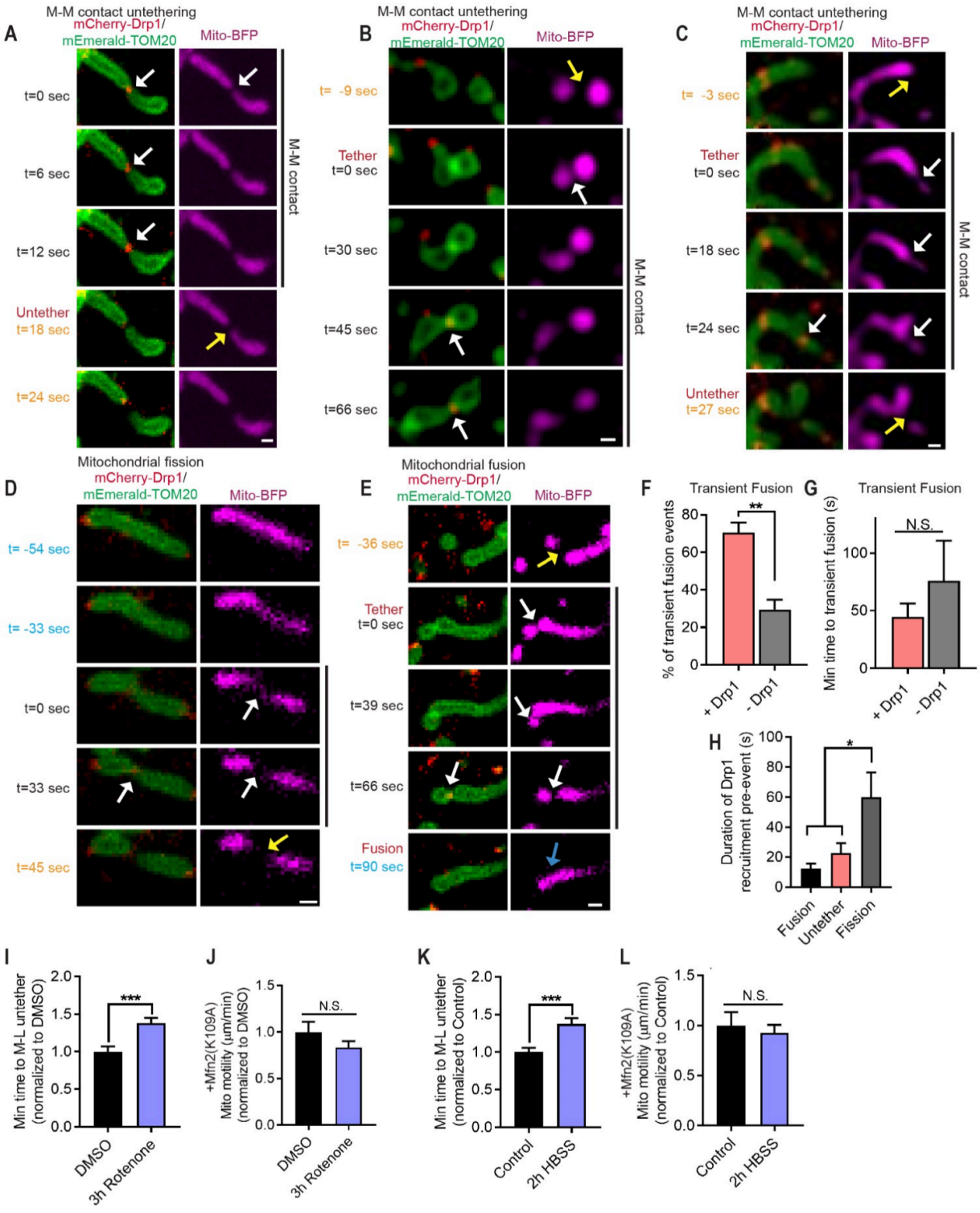
A
M-M contact untethering
mCherry-Drp1/
mEmerald-TOM20
Mito-BFP
t=0 sec
t=6 sec
t=12 sec
Untether
t=18 sec
t=24 sec
M-M contact
B
M-M contact untethering
mCherry-Drp1/
mEmerald-TOM20
Mito-BFP
t= -9 sec
Tether
t=0 sec
t=30 sec
t=45 sec
t=66 sec
M-M contact
C
M-M contact untethering
mCherry-Drp1/
mEmerald-TOM20
Mito-BFP
t= -3 sec
Tether
t=0 sec
t=18 sec
t=24 sec
Untether
t=27 sec
M-M contact
D
Mitochondrial fission
mCherry-Drp1/
mEmerald-TOM20
Mito-BFP
t= -54 sec
t= -33 sec
t=0 sec
t=33 sec
t=45 sec
E
Mitochondrial fusion
mCherry-Drp1/
mEmerald-TOM20
Mito-BFP
t= -36 sec
Tether
t=0 sec
t=39 sec
t=66 sec
Fusion
t=90 sec
F
Transient Fusion
% of transient fusion events
**
+ Drp1
- Drp1
G
Transient Fusion
Min time to transient fusion (s)
N.S.
+ Drp1
- Drp1
H
Duration of Drp1 recruitment pre-event (s)
*
Fusion
Untether
Fission
I
Min time to M-L untether (normalized to DMSO)
***
DMSO
3h Rotenone
J
+Mfn2(K109A) Mito motility (μm/min) (normalized to DMSO)
N.S.
DMSO
3h Rotenone
K
Min time to M-L untether (normalized to Control)
***
Control
2h HBSS
L
+Mfn2(K109A) Mito motility (μm/min) (normalized to Control)
N.S.
Control
2h HBSS

Figure 5: Drp1 oligomers mark sites of multiple mitochondrial events and modulation of mitochondria by mitochondrial and cellular stress. A-C, Confocal time-lapse images of two distinct mitochondria (yellow arrows) which form inter-mitochondrial contacts (white arrow) and subsequently untether (yellow arrow) marked by Drp1 oligomerization prior to separation (white arrows) in live HeLa cells (OMM label mEmerald-TOM20, matrix label Mito-BFP, Drp1 label mCherry-Drp1). Scale bars, 0.5 μm. **D,** Confocal time-lapse images of mitochondrial fission that are marked by Drp1 oligomerization (white arrows) in live HeLa cells (OMM label mEmerald-TOM20, matrix label Mito-BFP, Drp1 label mCherry-Drp1). Scale bar, 0.5 μm. **E,** Confocal time-lapse images of mitochondrial fusion prior to separation that are marked by Drp1 oligomerization (white arrows) in live HeLa cells (OMM label mEmerald-TOM20, matrix label Mito-BFP, Drp1 label mCherry-Drp1). Scale bar, 0.5 μm. **F, G,** Quantification of percentage of transient fusion events (observed as mito-PAGFP transfer without outer mitochondrial membrane fusion) marked by Drp1 oligomerization and time to transient fusion in live HeLa cells (OMM label SNAP-Omp25, individual mitochondrial matrix label mito-PAGFP, Drp1 label mCherry-Drp1) (F: n = 19 positive events for Drp1, n = 7 negative events for Drp1 from 9 cells; G: n = 30 positive events for Drp1, n = 14 negative events for Drp1 from 9 cells). **H,** Duration of Drp1 oligomerization pre-event for fusion, untethering and fission events in live HeLa cells (OMM label mEmerald-TOM20, matrix label Mito-BFP, Drp1 label mCherry-Drp1) (n = 7 fusion, n = 14 untether, n = 12 fission from 6-8 cells). **I,** Increased duration of mitochondria-lysosome contact sites in live HeLa cells treated with Rotenone (3h, 1 μM) compared to DMSO (3h) (n = 112 events from 15 cells per condition). **J,** Mitochondrial motility in live HeLa cells treated with Rotenone (3h, 1 μM) compared to DMSO (3h) expressing mutant Mfn2(K109A) (n = 90 mitochondrial from 18 cells per condition). **K,** Increased duration of mitochondria-lysosome contact sites in live HeLa cells cultured in low nutrient media (2h HBSS) compared to high nutrient media (Control) (n = 105 events from 15 cells per condition). Mean ± SEM; $^{*}p < 0.05$; $^{**}p < 0.01$; $^{***}p < 0.001$; NS, not significant (unpaired two-tailed t test for (F, G, I-L), ANOVA with Tukey's post hoc test for (H)).

Inter-mitochondrial contacts functionally restrict mitochondrial motility and are modulated by mitochondrial respiration and nutrient availability

We then analyzed how inter-mitochondrial contacts might functionally regulate the mitochondrial network, as they represented significant events occurring more frequently than fission or fusion (**Fig. 1M**). While mitochondria tethered in inter-mitochondrial contacts could move, their motility was significantly decreased compared to that of free mitochondria not in inter-mitochondrial contacts (**Fig. 6A-B**), suggesting that inter-mitochondrial contacts may functionally act to restrict individual mitochondrial motility. Indeed, disruption of inter-mitochondrial contact untethering by inhibiting RAB7 GTP hydrolysis via RAB7(Q67L), TBC1D15(D397A) or Fis1 (LA) mutants all resulted in significantly decreased mitochondrial motility (**Fig. 6C-E**).

We further examined whether inter-mitochondrial contact dynamics might respond to mitochondrial or cellular stress such as defective mitochondrial respiration or decreased nutrient availability as a way to modulate the mitochondrial network and its motility. Disruption of mitochondrial respiration with the mitochondrial respiratory chain complex I inhibitor Rotenone (1μM) or decreased nutrient availability (2h HBSS) resulted in inter-mitochondrial contact tethering/untethering rates which were still significantly higher than mitochondrial fusion/fission rates (**Fig. 6F, I**). This was consistent with our observations in control cells (Fig. 1M), suggesting that mitochondrial tethering is an important dynamic process that persists upon inhibition of mitochondrial respiration or decreased nutrient availability. Moreover, these conditions disrupted mitochondria-lysosome contact site dynamics (**Fig. 5I, K**), significantly increased the percentage of mitochondria forming inter-mitochondrial contacts (**Fig. 6G, J**), and led to a functional Mfn-dependent decrease in mitochondrial motility (**Fig. 5J, L**; **Fig. 6H, K**). Thus, upregulation of inter-

mitochondrial contacts in response to mitochondrial or cellular stress may contribute to restricted mitochondrial motility as a potential mechanism for preventing unnecessary energy expenditure.

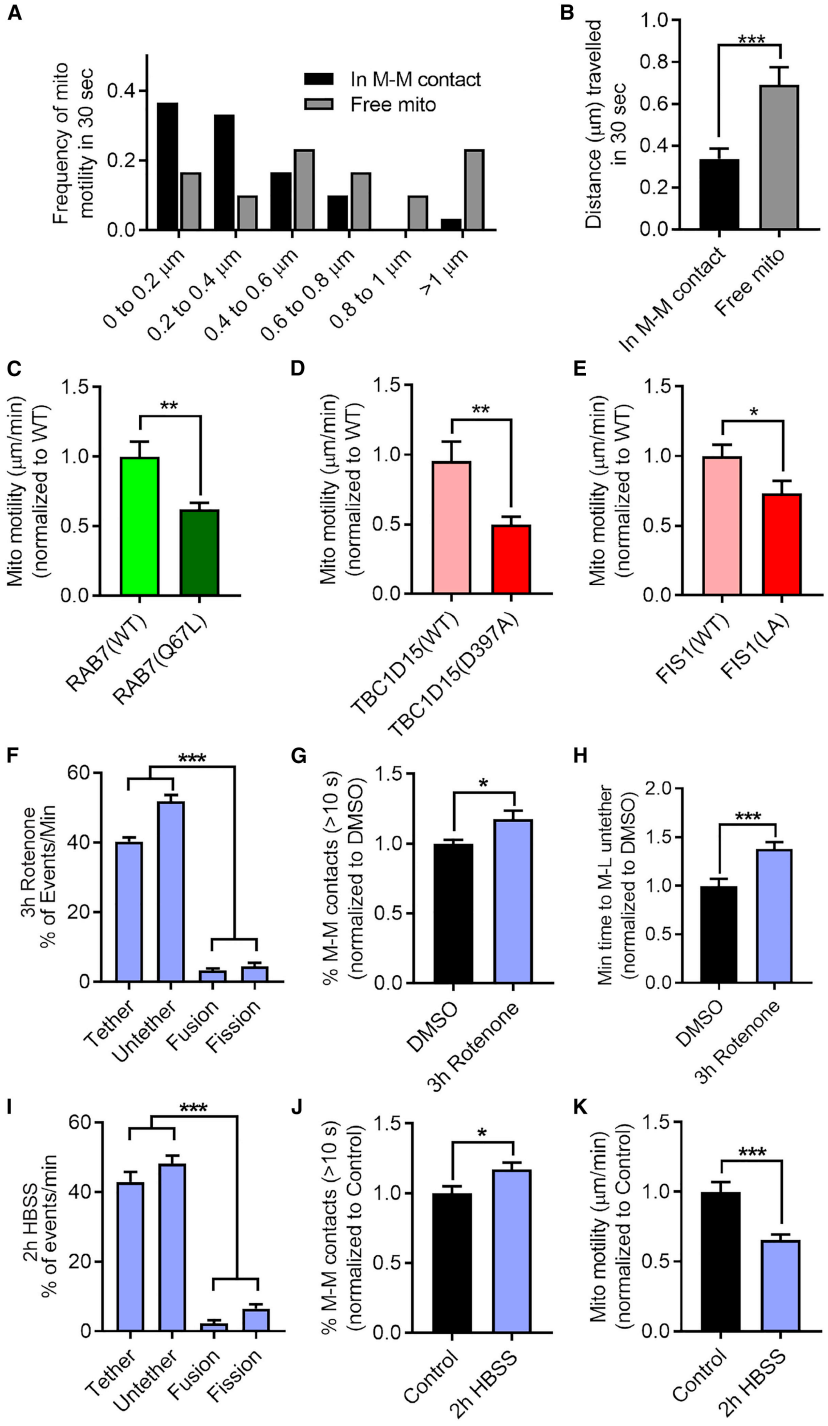

Figure 6: Inter-mitochondrial contacts functionally restrict mitochondrial motility and are modulated by mitochondrial respiration and nutrient availability. A, B, Decreased mitochondrial motility (B, histogram in A) in inter-mitochondrial contact (30 s before contact untethering) compared to free mitochondria (30 s after contact untethering) (n = 30 events per condition from 15 cells). **C-E,** Decreased mitochondrial motility upon inhibition of RAB7 GTP hydrolysis by mutant RAB7(Q67L) (C), TBC1D15 (D397A) (D), or FIS1(LA) (E) (OMM label mApple-TOM20 and matrix label Mito-BFP); n = 75 mitochondria from 15 cells (RAB7[WT], RAB7[Q67L], TBC1D15[D397A], and FIS1[WT]), n = 60 mitochondria from 12 cells (TBC1D15 [WT]), and n = 85 mitochondria from 17 cells (FIS1 [LA]). **F,** Quantification of distribution of mitochondrial events from confocal time-lapse images of live HeLa cells treated with mitochondrial respiration complex I inhibitor Rotenone (3 h, 1 μM) (OMM label mApple-TOM20 and matrix label Mito-BFP) (n = 493 events from 10 cells). **G,** Increased percentage of mitochondria forming inter-mitochondrial contacts in live HeLa cells treated with Rotenone (3 h, 1 μM) compared to DMSO (3 h) (n = 105 events from 15 cells (DMSO) and n = 105 events from 15 cells [Rotenone]). **H,** Decreased mitochondrial motility in live HeLa cells treated with Rotenone (3 h, 1 μM) compared to DMSO (3 h) (n = 90 mitochondria from 18 cells per condition). **I,** Quantification of distribution of mitochondrial events from confocal time-lapse images of live HeLa cells cultured in low-nutrient media (2 h HBSS) (OMM label mApple-TOM20 and matrix label Mito-BFP) (n = 297 events from 10 cells). **J,** Increased percentage of mitochondria forming inter-mitochondrial contacts in live HeLa cells cultured in low-nutrient media (2 h HBSS) compared to high-nutrient media (control) (n = 112 events from 16 cells (control) and n = 112 events from 16 cells [2 h HBSS]). **K,** Decreased mitochondrial motility in live HeLa cells cultured in low nutrient media (2 h HBSS) compared to high-nutrient media (control) (n = 90 mitochondria from 18 cells per condition). Mean ± SEM; $^{*}p < 0.05$; $^{**}p < 0.01$; $^{***}p < 0.001$; unpaired two-tailed t test for (B)–(E), (G), (H), (J), and (K) and ANOVA with Tukey's post hoc test for (F) and (I).

Multiple Charcot-Marie-Tooth Disease Type 2 mutants converge on defective inter-mitochondrial contact dynamics and mitochondrial motility

Mutations in the mitochondrial GTPase Mitofusin2 (Mfn2) result in Charcot-Marie-Tooth Disease Type 2A (Zuchner et al., 2004), while mutations in the GTPase RAB7 lead to Charcot-Marie-Tooth Disease Type 2B (Houlden et al., 2004). However, whether these different mutants functionally converge in CMT2 disease pathogenesis is not well understood. We first compared the effect of wild-type Mfn2 and the CMT2A disease-linked Mfn2 mutation (T105M) located in its GTPase domain (Chung et al., 2006; Lawson, Graham, & Flanigan, 2005) on inter-mitochondrial contact dynamics. Mutant Mfn2 (T105M) significantly prolonged the duration of inter-mitochondrial contacts leading to inefficient untethering compared to wild-type Mfn2 (**Fig. 7A, B**) and significantly decreased mitochondrial network motility (**Fig. 7C**), consistent with previous studies showing mitochondrial defects (Bannerman, Burns, Xu, Miers, & Pleasure, 2016; Detmer, Velde, Cleveland, & Chan, 2008; El Fissi et al., 2018; Franco et al., 2016; Rocha et al., 2018).

We next examined whether CMT2B mutations in RAB7 (**Fig. 7D**) which lead to defective GTP hydrolysis and increased GTP-binding (McCray, Skordalakes, & Taylor, 2010; Spinosa et al., 2008; K. Zhang et al., 2013) might similarly disrupt inter-mitochondrial contact dynamics. Using time-lapse confocal imaging, we investigated whether the most common CMT2B disease-linked RAB7 mutation (V162M) (Manganelli et al., 2012; Verhoeven et al., 2003) might disrupt mitochondria-lysosome contacts and further misregulate mitochondrial dynamics. Indeed, we found that similar to the RAB7 (Q67L) GTP hydrolysis mutant which locks RAB7 in a GTP-bound state, RAB7 (V162M) also significantly increased the formation of stable mitochondria-lysosome contacts (lasting >10s) (**Fig. 7E**) and increased the duration of mitochondria-lysosome contacts

resulting in inefficient untethering (**Fig. 7F, G**). Moreover, consistent with our data suggesting that mitochondria-lysosome contact dynamics regulate inter-mitochondrial contact untethering events, we found that RAB7 (V162M) led to prolonged inter-mitochondrial contacts unable to efficiently untether (**Fig. 7H, I**) and also decreased mitochondrial motility (**Fig. 7J**).

Finally, to test whether defective mitochondrial dynamics might be a common pathway across multiple forms of CMT2, we examined the CMT2C disease-linked TRPV4 mutation (R269H) (Auer-Grumbach et al., 2010; Deng et al., 2010; Landouré et al., 2010). Surprisingly, we found that mutant TRPV4 (R269H) also resulted in significantly prolonged inter-mitochondrial contacts which could not efficiently untether (**Fig. 7K, L**) and also decreased mitochondrial motility (**Fig. 7M**). Together, these results highlight a role for inter-mitochondrial contacts in regulating mitochondrial network motility and suggest that this pathway may be converging mechanism relevant to multiple forms of Charcot-Marie-Tooth Disease Type 2.

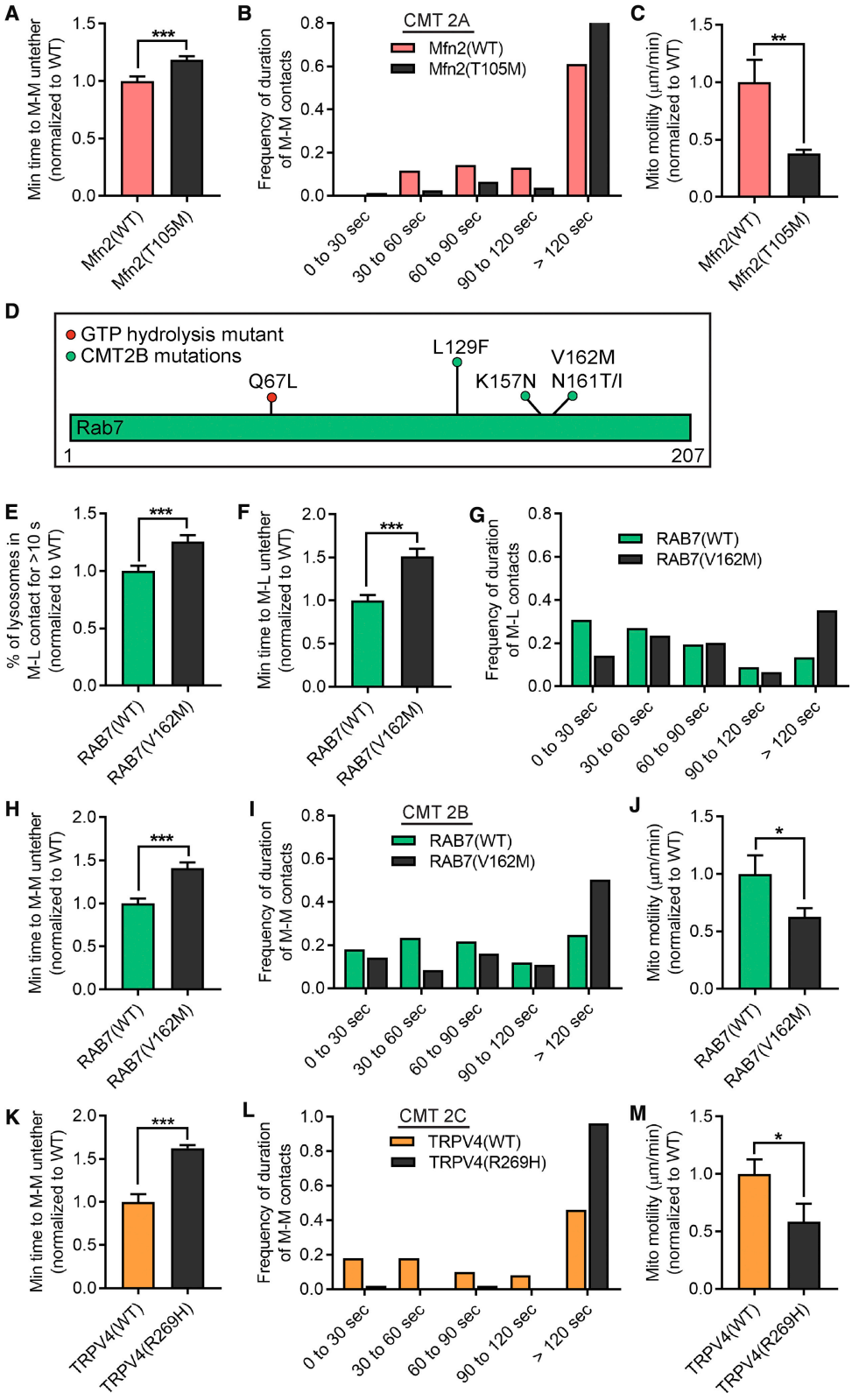
A
Min time to M-M untether (normalized to WT)
1.5
1.0
0.5
0.0
***
Mfn2(WT)
Mfn2(T105M)
B
Frequency of duration of M-M contacts
0.8
0.6
0.4
0.2
0.0
CMT 2A
Mfn2(WT)
Mfn2(T105M)
0 to 30 sec
30 to 60 sec
60 to 90 sec
90 to 120 sec
> 120 sec
C
Mito motility (µm/min) (normalized to WT)
1.5
1.0
0.5
0.0
**
Mfn2(WT)
Mfn2(T105M)
D
GTP hydrolysis mutant
CMT2B mutations
Q67L
L129F
K157N
V162M
N161T/I
Rab7
1
207
E
% of lysosomes in M-L contact for >10 s (normalized to WT)
1.5
1.0
0.5
0.0
***
RAB7(WT)
RAB7(V162M)
F
Min time to M-L untether (normalized to WT)
2.0
1.5
1.0
0.5
0.0
***
RAB7(WT)
RAB7(V162M)
G
Frequency of duration of M-L contacts
0.8
0.6
0.4
0.2
0.0
RAB7(WT)
RAB7(V162M)
0 to 30 sec
30 to 60 sec
60 to 90 sec
90 to 120 sec
> 120 sec
H
Min time to M-M untether (normalized to WT)
2.0
1.5
1.0
0.5
0.0
***
RAB7(WT)
RAB7(V162M)
I
Frequency of duration of M-M contacts
0.8
0.6
0.4
0.2
0.0
CMT 2B
RAB7(WT)
RAB7(V162M)
0 to 30 sec
30 to 60 sec
60 to 90 sec
90 to 120 sec
> 120 sec
J
Mito motility (µm/min) (normalized to WT)
1.5
1.0
0.5
0.0
*
RAB7(WT)
RAB7(V162M)
K
Min time to M-M untether (normalized to WT)
2.0
1.5
1.0
0.5
0.0
***
TRPV4(WT)
TRPV4(R269H)
L
Frequency of duration of M-M contacts
1.0
0.8
0.6
0.4
0.2
0.0
CMT 2C
TRPV4(WT)
TRPV4(R269H)
0 to 30 sec
30 to 60 sec
60 to 90 sec
90 to 120 sec
> 120 sec
M
Mito motility (µm/min) (normalized to WT)
1.5
1.0
0.5
0.0
*
TRPV4(WT)
TRPV4(R269H)

Figure 7: Multiple Charcot-Marie-Tooth type 2 mutants converge on defective inter-mitochondrial contact dynamics and mitochondrial motility. A, B, CMT2A disease-linked Mfn2 mutant (T105M) prevents efficient untethering of inter-mitochondrial contacts (A, histogram in B) (n = 77 events from 11 cells per condition). **C,** CMT2A disease-linked Mfn2 mutant (T105M) disrupts mitochondrial motility (n = 90 events from 18 cells per condition). **D,** Model of RAB7 showing GTP hydrolysis mutant (Q67L, red circle) and Charcot-Marie-Tooth type 2B (CMT2B) disease-linked mutations (green circles). **E-G,** RAB7 CMT2B disease-linked V162M mutation increases the percentage of lysosomes in mitochondria-lysosome (M-L) contacts (E) and the duration of M-L contacts (F, histogram in G). (n = 133 events from 19 cells (RAB7 [WT]) and n = 119 events from 17 cells (RAB7 [V162M]). **H, I,** RAB7 CMT2B disease-linked V162M mutation prevents efficient untethering of inter-mitochondrial contacts (H, histogram in I) (n = 133 events from 19 cells (RAB7 [WT]) and n = 119 events from 17 cells (RAB7 [V162M]). **J,** CMT2B disease-linked mutant RAB7 (V162M) disrupts mitochondrial motility (n = 90 events from 18 cells per condition). **K, L,** CMT2C disease-linked mutant TRPV4 (R269H) prevents efficient untethering of inter-mitochondrial contacts (K, histogram in L) (n = 50 events from 10 cells (TRPV4 [WT]) and n = 50 events from 10 cells (TRPV4 [R269H]). **M,** CMT2C disease-linked mutant TRPV4 (R269H) disrupts mitochondrial motility (n = 90 events from 18 cells per condition). Mean ± SEM; $^{*}p < 0.05$; $^{***}p < 0.001$; unpaired two-tailed t test for (A), (C), (E), (F), (H), (J), (K), and (M).

Conclusions

In summary, our study highlights an important role for inter-mitochondrial contact formation in regulating mitochondrial network dynamics. Inter-mitochondrial contacts did not result in fusion or bulk mitochondrial matrix exchange, but rather represented dynamic inter-mitochondrial contact site which formed under normal conditions in multiple cell types and whose dynamics were acutely regulated by multiple GTPases. Inter-mitochondrial contacts were further found to be modulated by mitochondrial respiratory activity and nutrient availability, suggesting that contact dynamics may be regulated to counter mitochondrial and cellular dyshomeostasis (Ichas, Jouaville, & Mazat, 1997; Picard et al., 2015; Rambold, Kostelecky, Elia, & Lippincott-Schwartz, 2011; Santo-Domingo, Giacomello, Poburko, Scorrano, & Demaurex, 2013; Vernay et al., 2017). Moreover, mitochondria in inter-mitochondrial contacts had significantly restricted motility, potentially allowing for contact formation to further modulate the dynamics of the global mitochondrial network. Importantly, we observed dysregulation of mitochondrial tethering and motility in various forms of CMT type 2, suggesting a potential contribution of inter-mitochondrial contacts to diseases pathogenesis.

CHAPTER 3.

MITOCHONDRIA-LYSOSOME CONTACTS REGULATE MITOCHONDRIAL CALCIUM DYNAMICS VIA LYSOSOMAL TRPML1

Introduction

Inter-organelle contact sites have become increasingly appreciated as essential regulators of cellular homeostasis. Contact sites, which form dynamically between two distinct organelles in close proximity, have been shown to have a variety of functions including the ability to act as platforms for the direct transfer of ions such as calcium (Bartok et al., 2019; Hayashi & Su, 2007; Hirabayashi et al., 2017; Lim et al., 2019; Rizzuto et al., 1998; Szabadkai et al., 2006). Recently, inter-organelle contact sites between mitochondria and lysosomes were characterized, revealing a novel mechanism of crosstalk between the two organelles (Han et al., 2017; Hoglinger et al., 2019; Wong, Kim, et al., 2019; Wong et al., 2018). Interestingly, both mitochondria and lysosomes are also important players in cellular homeostasis including intracellular calcium dynamics (Lawrence & Zoncu, 2019; J. H. Lee et al., 2015; Lie & Nixon, 2019; Misgeld & Schwarz, 2017), and a number of diseases presenting with mitochondrial and/or lysosomal dysfunction also exhibit dysregulation of cellular calcium (Abeliovich & Gitler, 2016; Burbulla et al., 2017; Burte et al., 2015; Mc Donald & Krainc, 2017; Pchitskaya, Popugaeva, & Bezprozvanny, 2018; Peng, Minakaki, Nguyen, & Krainc, 2019; Plotegher & Duchen, 2017b; Wong, Peng, et al., 2019). Although the calcium dynamics of mitochondria and lysosomes have previously been studied individually or in relation to other organelles (Bartok et al., 2019; Garrity et al., 2016; Hayashi & Su, 2007; Hirabayashi et al., 2017; Kilpatrick, Yates, Grimm, Schapira, & Patel, 2016; Rizzuto et al., 1998; Szabadkai et al., 2006), whether mitochondria and lysosomes can interact directly to

modulate their calcium states has not been elucidated. Mitochondria-lysosome contacts may thus enable the direct transfer of calcium between lysosomes and mitochondria and function as an additional pathway in regulating intracellular calcium homeostasis.

TRPML1 is a lysosomal/late endosomal cation channel that mediates lysosomal calcium efflux (Q. Chen et al., 2017; Dong et al., 2008; Fine, Schmiege, & Li, 2018; Hirschi et al., 2017; M. Li et al., 2017; Schmiege, Fine, Blobel, & Li, 2017) and function (Dayam, Saric, Shilliday, & Botelho, 2015; X. Li et al., 2016; Minckley et al., 2019; Samie et al., 2013; Scotto Rosato et al., 2019; W. Wang et al., 2015), and dysfunction in TRPML1 has been associated with several mitochondrial defects (Eichelsdoerfer, Evans, Slaugenhaupt, & Cuajungco, 2010; Jennings et al., 2006). In addition, loss of function mutations in TRPML1 cause Mucolipidosis type IV (MLIV), an autosomal recessive lysosomal storage disorder characterized by psychomotor retardation, retinal degeneration and developmental delay (Bassi et al., 2000; Dong et al., 2008; Marques & Saftig, 2019; M. Sun et al., 2000) and which has been associated with various lysosomal and mitochondrial aberrations (Eichelsdoerfer et al., 2010; Jennings et al., 2006; LaPlante et al., 2006; S. Park et al., 2016; Shen et al., 2012; Soyombo et al., 2006; Vergarajauregui, Connelly, Daniels, & Puertollano, 2008). However, whether TRPML1-mediated lysosomal calcium release modulates mitochondrial calcium dynamics via mitochondria-lysosome contact sites, and the role of mitochondria-lysosome contact site dysfunction in the pathophysiology of lysosomal storage disorders such as MLIV has not previously been studied.

Using live-cell high spatial and temporal resolution microscopy, we show that TRPML1 lysosomal calcium release mediates the direct transfer of calcium into mitochondria. Calcium transfer from lysosomes to mitochondria is modulated by mitochondria-lysosome contact site tethering and is modulated by the outer and inner mitochondrial membrane proteins, VDAC1 and

MCU, respectively. Importantly, MLIV patient fibroblasts with loss of TRPML1 function exhibit disrupted mitochondria-lysosome contact site dynamics and contact-dependent calcium transfer, suggesting a potential contribution of dysregulated mitochondria-lysosome contact site dynamics in lysosomal storage disorders. Our results thus elucidate a novel mechanism for regulating intracellular calcium dynamics via mitochondria-lysosome contact sites, which are further implicated in disease pathophysiology.

Methods

Reagents. The following plasmids were obtained from Addgene: CMV-mito-R-GECO1 was a gift from Robert Campbell (Addgene #46021), LAMP1-mGFP was a gift from Esteban Dell-Angelica (Addgene #34831) (Falcon-Perez et al., 2005), mito-BFP was a gift from Gia Voeltz (Addgene #49151) (Friedman et al., 2011), mTagBFP-Lysosomes-20, mApple-TOMM20-N-10 and mEmerald-TOMM20-N-10 were gifts from Michael Davidson (Addgene #55263, #54955, #54282) (Rizzo, Davidson, & Piston, 2009), pCMV-2E2-HA-mCh was a gift from Tim Stasevich (Addgene #129596) (Zhao et al., 2019), TRPML1-HA was a gift from Craig Montell (Addgene #18825) (Venkatachalam, Hofmann, & Montell, 2006), Mucolipin1 pHcRed C1, Mucolipin1 D471-472K-pHcRed C1 and Mucolipin-pEGFP C3 were gifts from Paul Luzio (Addgene #62959, #62961, #62960) (Pryor, Reimann, Gribble, & Luzio, 2006), pEGFP-N1-FLAG was a gift from Patrick Calsou (Addgene #60360) (Britton et al., 2014), and pDONR223-MCU and pDONR223-MCU-E264A were gifts from Vamsi Mootha (Addgene #31726, #31730) (Baughman et al., 2011). TRPML1 WT-Halo, TRPML1 D471K-Halo, VDAC1 WT-SNAP, VDAC1 E73Q-SNAP, bicistronic VDAC1 WT-IRES-BFP, bicistronic VDAC1 E73Q-IRES-BFP, MCU WT-SNAP and MCU E264A-SNAP were generated using VectorBuilder. The following reagents were also used:

ML-SA1 (Sigma; SML0627) (Shen et al., 2012), MK6-83 (Cayman Chemicals; 21944) (C. C. Chen et al., 2014), PI(3,5)P_2 diC8 (Echelon Biosciences; P-3508), Unlabeled Shuttle PIP Carrier 2 (Echelon Biosciences; P-9C2), BAPTA-AM (Cayman Chemicals; 15551), Xestospongin-C (Cayman Chemicals; 64950) (Gafni et al., 1997), DHBP dibromide (Tocris; 0839), SKF-96365 hydrochloride (Tocris; 1147), thapsigargin (abcam; ab120286), ionomycin (Cayman Chemicals; 10004974), staurosporine (abcam; ab120056), MitoTracker Red CMXRos (Invitrogen; M7512), calcein-AM (Invitrogen; 65-0853-78) and cobalt (II) chloride (Sigma; 232696).

Cell culture and transfection (detailed). HeLa cells (gift from Michael Schwake (ATCC)) and HEK293 cells were cultured in DMEM (Gibco; 11995-065) supplemented with 10% (vol/vol) heat inactivated FBS, 100 units/mL penicillin and 100 µg/mL streptomycin. Wild-type and *TBC1D15*$^{-/-}$ HCT116 cells were gifts from Richard Youle (Yamano, Fogel, Wang, van der Bliek, & Youle, 2014) and cultured in McCoy's 5A with L-glutamine (ATCC; 30-2007) supplemented with 10% (vol/vol) heat inactivated FBS, 100 units/mL penicillin and 100 µg/mL streptomycin. MLIV patient fibroblasts (GM02048 (MLIV #1), GM02527 (MLIV #2), GM02629 (MLIV #3)) and age-matched control fibroblasts (GM00498 (Con #1), GM00969 (Con #2), GM05658 (Con #3)) were obtained from the NIGMS Human Genetic Cell Repository at the Coriell Institute for Medical Research and cultured in DMEM (Gibco; 11995-065) supplemented with 15% (vol/vol) heat inactivated FBS, 100 units/mL penicillin and 100 µg/mL streptomycin. All MLIV patient fibroblast lines contain recessive mutations as described by the NIGMS Human Genetic Cell Repository at the Coriell Institute for Medical Research [GM02048 (MLIV #1; from same patient as GM02533a) is heterozygous for 1) a splice site mutation (IVS3AS-2A>G) leading to frameshift and premature termination resulting in a severely truncated protein containing only the first 21

amino acids of wild-type TRPML1 and 2) a deletion removing 6432 base pairs spanning from 938 base pairs upstream of the 5' end of the gene, including transcriptional regulatory elements, to exon 6 (Bassi et al., 2000). GM02527 (MLIV #2) is homozygous for the aforementioned splice site mutation (IVS3AS-2A>G) (Bassi et al., 2000)]. All cells were maintained at 37 ºC in a 5% CO_2 incubator and previously verified by cytochrome c oxidase subunit I (COI) and short tandem repeat (STR) testing and tested for Mycoplasma contamination. HeLa, HEK293 and HCT116 cells were transfected using X-tremeGENE HP DNA transfection reagent (Roche; XTGHP-RO), and fibroblasts were transfected using Lipofectamine LTX with PLUS reagent (Invitrogen; 15338100). For live imaging, cells were grown on glass bottom culture dishes (MatTek; P35G-1.5-14-C).

Immunofluorescence staining. All confocal images were acquired on a Nikon A1R laser scanning confocal microscopy with GaAsp detectors using a Plan Apo λ 100x 1.45 NA oil immersion objective (Nikon) using NIS-Elements (Nikon). Live HeLa cells on coverslips were treated with ML-SA1 (31.25 μM), staurosporine (1 μM, positive control) or vehicle control (DMSO) for 2 h or 4 h and in the last 15 minutes of drug treatment, cells were incubated with MitoTracker Red (200 nM). Following drug treatment, cells were washed three times in PBS then immediately fixed in 4% paraformaldehyde in PBS for 15 minutes. Cells were then blocked and permeabilized in 2% BSA/0.1% saponin in PBS for 30 minutes at room temperature then incubated with cytochrome C antibody (mouse; 1:200) (abcam; ab13575) overnight at 4 ºC. The following day, cells were washed three times in blocking solution then incubated with secondary antibody (Goat anti-mouse Alexa Fluor 488; 1:300) (Invitrogen; A28175) for 1 h at room temperature. Cells were washed three times in blocking solution then mounted (Vector Laboratories; H-1500-10). Mounted coverslips were allowed to dry for at least 1 h at 4 ºC prior to imaging.

Co-immunoprecipitation. HEK293 cells plated on 15 cm dishes were transfected with Mucolipin1-pEGFP C3 (5 µg) or pEGFP-N1-FLAG (5 µg, negative control). After 22-24 hours, cells were washed three times in PBS then scraped in ice-cold lysis buffer (10 mM Tris pH 7.5, 150 mM NaCl, 0.5 mM EDTA, 1% Triton X-100, 10% glycerol) with protease inhibitors (Roche; 11873580001). Cell suspensions were incubated on ice for 30 minutes with vigorous pipetting every 5 minutes followed by centrifugation at 14,000 rpm for 10 minutes at 4 ºC. Each supernatant was then applied to 50 µL pre-blocked GFP-Trap Magnetic Agarose beads (Chromotek; gtma) and incubated on a 4 ºC rotator for 1 hour. Beads were washed three times for 10 minutes with ice-cold lysis buffer on a 4 ºC rotator and then eluted by heating in 100 µL 2x Laemmli sample buffer (Bio-Rad; 1610737) at 95 ºC for 5 minutes. Samples were loaded onto a 4-20% Tris-Glycine gel (Invitrogen; XP04205BOX) and were subsequently analyzed by SDS-PAGE and Western blot for immunoprecipitation and co-immunoprecipitation. For co-immunoprecipitation blots, varying exposure times were used to image input (30-60 seconds) and IP (300 seconds) lanes. Antibodies used included anti-GFP (mouse; 1:1000) (Santa Cruz; SC-9996), anti-VDAC1 (mouse; 1:500) (abcam; ab14734), anti-VDAC2 (rabbit; 1:500) (Proteintech; 11663-1-AP), anti-VDAC3 (rabbit; 1:500) (Proteintech; 14451-1-AP).

Live-cell confocal microscopy (detailed). Baseline calcium fluorescence was acquired over the course of 60 seconds followed by the addition of the following drug treatments in 100 µL Krebs-Ringer solution (without calcium): TRPML1 agonists, ML-SA1 (31.25 µM, within the range used in previous studies) (Garrity et al., 2016; Kilpatrick et al., 2016; Minckley et al., 2019; Scotto Rosato et al., 2019; Shen et al., 2012) or MK6-83 (10 µM); or DMSO control. For calcium imaging with endogenous TRPML1 activator, $PI(3,5)P_2$ diC8 (1 mM in Ultrapure H_2O) was incubated with

Unlabeled Shuttle PIP Carrier 2 (1 mM in Ultrapure H_2O) for 10 min.; the lipid-histone complex or histone alone (control) was then diluted in 100 uL Krebs-Ringer solution (without calcium), delivered to cells as previously described (Ozaki, DeWald, Shope, Chen, & Prestwich, 2000) and imaged as described above. For calcium imaging with drug pre-treatment, cells were incubated with the following in Krebs-Ringer solution (without calcium) then imaged as described above: Xestospongin-C (10 μM in DMSO) for 20 min., BAPTA-AM (5 μM in DMSO) for 20 min., DHBP (50 μM in Ultrapure H_2O) for 10 min., SKF-96365 (20 μM in Ultrapure H_2O) for 10 min., thapsigargin (1 μM in DMSO) for 10 min. or vehicle control (DMSO or Ultrapure H_2O). For imaging experiments with Halo or SNAP-tagged proteins, cells were incubated with 30 nM PA Janelia Fluor 646 (a gift from Luke Lavis) or 100 nM SNAP-Cell 647 SiR (New England Biolabs; S9102S) for 30 min. then washed three times with fresh media prior to imaging.

For measurement of mPTP opening with the calcein-AM/cobalt assay, live HeLa cells were incubated with calcein-AM (1 μM), $CoCl_2$ (8 mM) and MitoTracker Red (200 nM) for 15 minutes in modified Krebs-Ringer solution as previously described (Bonora et al., 2016). Cells were then washed three times with modified Krebs-Ringer solution. Following verification of calcein-AM loading into mitochondria via colocalization with MitoTracker Red, cells were immediately imaged at 1 frame every 4 sec for 5 minutes. Baseline calcein fluorescence was acquired over the course of 60 seconds followed by addition of the following drug treatments in 100 μL modified Krebs-Ringer solution: TRPML1 agonist ML-SA1 (31.25 μM), ionomycin (2 μM, positive control) or DMSO control.

Image analysis (detailed). Calcium responses for total mitochondria were assessed using $\Delta F/F_0$ analysis defined as the difference in fluorescence at time *t* minus the initial fluorescence (F_0), all divided by the initial fluorescence (F_0). F_0 was defined as the mean fluorescence intensity from *t* = -5 s to *t* = 0 s, the time when drug was added, for thresholded mitochondria in a given cell drawn as a region of interest (ROI). Calcium fluorescence parameters were defined as follows: maximum calcium fluorescence as the maximum $\Delta F/F_0$ following addition of drug at *t* = 0 s; mean calcium fluorescence as the average $\Delta F/F_0$ across all time points following addition of drug at *t* = 0 s; and calcium fluorescence at 30 s, 60 s, 90 s and 120 s as the $\Delta F/F_0$ at the respective time points following addition of drug at *t* = 0 s. Expression levels of Halo and SNAP-tagged proteins in the cells analyzed for calcium responses were assessed by drawing ROIs around each cell and measuring the mean fluorescence intensities in the channel corresponding to the excitation of the Halo/SNAP ligands (far-red).

Contact-dependent mitochondrial calcium responses were assessed by comparing mean fluorescence intensity values for mitochondria in stable contact with lysosomes versus mitochondria not in contact with lysosomes following addition of TRPML1 agonist. Stable mitochondria-lysosome contacts imaged in living cells were categorized as those that showed mitochondria and lysosomes in close proximity (< 0.1 μm) for > 10 s in time-lapse images. ROIs were drawn for mitochondria in contact and not in contact with lysosomes at *t* = 0 s and were re-drawn for the same mitochondria at *t* = 30 s. Mean fluorescence intensity values at both time points were obtained using the ROI Statistics feature in NIS-Elements (Nikon).

For the analysis of mitochondria-lysosome contact dynamics, mitochondria-lysosome contacts were defined as has been previously described (Wong et al., 2018). In short, the percentage of lysosomes in contact was quantified as the percentage of lamp1-mGFP or mTagBFP-Lysosomes-20-positive vesicles that formed contacts with mApple-TOMM20-N-10 or mEmerald-TOMM20-N-10-labeled mitochondria (> 10 s) divided by the total number of vesicles in the ROI. The minimum duration of contacts was quantified as the time before contact untethering (mitochondria and lysosomes detaching from one another) over a 3-minute (180 s) video. All contacts analyzed for the minimum duration of contacts were those that had already formed at the beginning of the video and any contacts that lasted throughout the entirety of the video were categorized as 180 s in the analysis. Prior to analysis of contacts, videos were processed using the Denoise AI and equalize intensity over time feature in NIS-Elements (Nikon). Mitochondria-lysosome contact sites marked by TRPML1 were analyzed from confocal time-lapse images of outer mitochondrial membrane marker (mEmerald-TOMM20-N-10), lysosomal marker (mTagBFP-Lysosomes-20), TRPML1-HA and HA-mCherry nanobody (pCMV-2E2-HA-mCh). The expected probability that TRPML1-HA/HA-mCherry would be at the site of a mitochondria-lysosome contact site by random chance was calculated as the total density of TRPML1-HA/HA-mCherry vesicles in a given cell using NIS-Elements (Nikon).

Calcein fluorescence responses in mitochondria were assessed by analysis of fluorescence at time *t* as a % of initial fluorescence, defined as the average calcein fluorescence over the 60 second baseline acquisition period. Prior to analysis of calcein fluorescence, images were processed by background subtraction. Overall calcein fluorescence was defined as the average calcein

fluorescence as a % of initial fluorescence across all time points following addition of drug at t = 0 s.

Colocalization analysis of endogenous cytochrome C and MitoTracker Red in immunofluorescence staining was performed using ImageJ. Prior to colocalization analysis, images were processed by background subtraction and median filtering. Processed images were then analyzed using the Colocalization Threshold feature (ImageJ) and Pearson's correlation coefficients between endogenous cytochrome C and MitoTracker Red were calculated.

Statistical analysis, graphing and figure assembly. Data were analyzed using unpaired two-tailed Student *t*-test (for two datasets) or one-way ANOVA with Tukey's post hoc test (for multiple datasets). Data presented are means ± s.e.m. All statistical tests were justified as appropriate and were analyzed from $n \geq 10$ cells (see text and figure legends for details) from $n \geq 3$ independent experiments (biological replicates) per condition. Statistics and graphing were performed using MatLab and Prism 8 (GraphPad) software. All videos and images were analyzed and assembled using NIS-Elements (Nikon) and ImageJ. All final figures were assembled in Adobe Photoshop and Microsoft PowerPoint.

Results

TRPML1-mediated lysosomal calcium efflux leads to mitochondrial calcium influx

To evaluate whether lysosomal TRPML1 calcium efflux modulated mitochondrial calcium (**Fig. 8A**), we used live-cell confocal microscopy at high spatial and temporal resolution to image mitochondrial calcium dynamics using the mitochondria-targeted genetically encoded calcium sensor Mito-R-GECO1 (J. Wu et al., 2013) (**Fig. 8B**). We first verified correct localization of Mito-R-GECO1, which was found to localize to the mitochondrial matrix as demonstrated by colocalization with the mitochondria matrix-targeted BFP-mito (**Fig. 9A**). Next, mitochondrial calcium responses were measured in wild-type HeLa cells upon activation of TRPML1 lysosomal calcium release with the TRPML1 agonist ML-SA1 (Shen et al., 2012). Following treatment with ML-SA1, total mitochondrial calcium was significantly increased (**Fig. 8C-D**). Compared to control cells, cells treated with ML-SA1 showed a sustained elevation in mitochondrial calcium (**Fig. 8D**) and a significant increase in maximum mitochondrial calcium, mean mitochondrial calcium and mitochondrial calcium at multiple time points (**Fig. 8E-G**). These results were further validated by activation of TRPML1 with an additional small molecule agonist, MK6-83 (C. C. Chen et al., 2014) (**Fig. 9B-F**) as well as with its physiological activator, $PI(3,5)P_2$ (Dong et al., 2010) (**Fig. 9G-J**), both of which resulted in a sustained increase in mitochondrial calcium. Thus, lysosomal TRPML1 calcium efflux robustly modulates mitochondrial calcium dynamics by increasing calcium influx into the mitochondrial matrix.

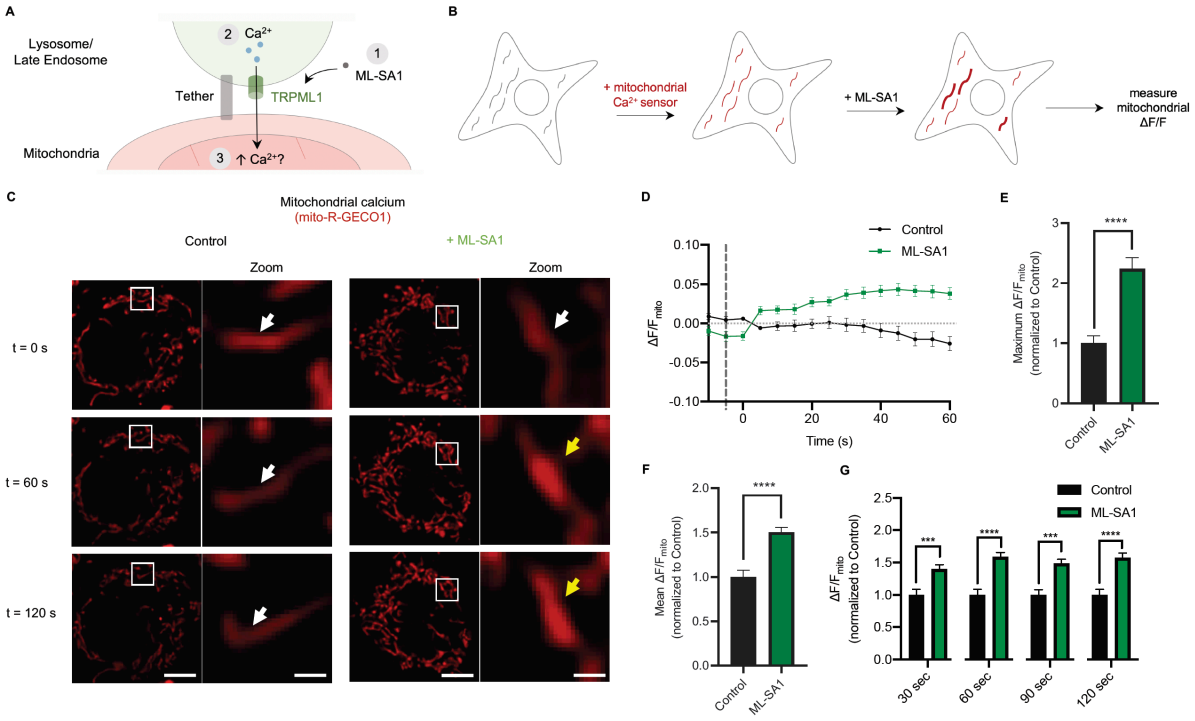

Figure 8: TRPML1-mediated lysosomal calcium efflux leads to mitochondrial calcium influx. A, Model of activation of lysosomal calcium release by TRPML1 agonist, ML-SA1, resulting in mitochondrial calcium influx at mitochondria-lysosome contacts. **B**, Experimental design for the assessment of mitochondrial calcium responses (ΔF/F) to TRPML1 activation in live cells. **C**, **D**, Mitochondrial calcium response in live HeLa cells expressing mitochondrial-matrix targeted calcium sensor, Mito-R-GECO1, in response to TRPML1 activation with ML-SA1 (31.25 µM) or control treatment at t = 0 s with representative time-lapse confocal images (**C**, n = 23 cells for ML-SA1, n =20 cells for control) and mitochondrial calcium traces (ΔF/F) (**D**, n = 23 cells for ML-SA1, n =20 cells for control). **E-G**, Quantification of maximum mitochondrial calcium response (**E**), mean mitochondrial calcium response (**F**) and mitochondrial calcium response at 30, 60, 90 and 120 seconds (**G**) after TRPML1 activation with ML-SA1 (31.25 µM) or control treatment from confocal time-lapse images (from **C**) (n = 23 cells for ML-SA1, n =20 cells for control). Data are means ± s.e.m. (***P<0.001, ****P<0.0001, unpaired two-tailed t-test). Scale bars, 10 µm (**C**); 1 µm (**C**, zoom).

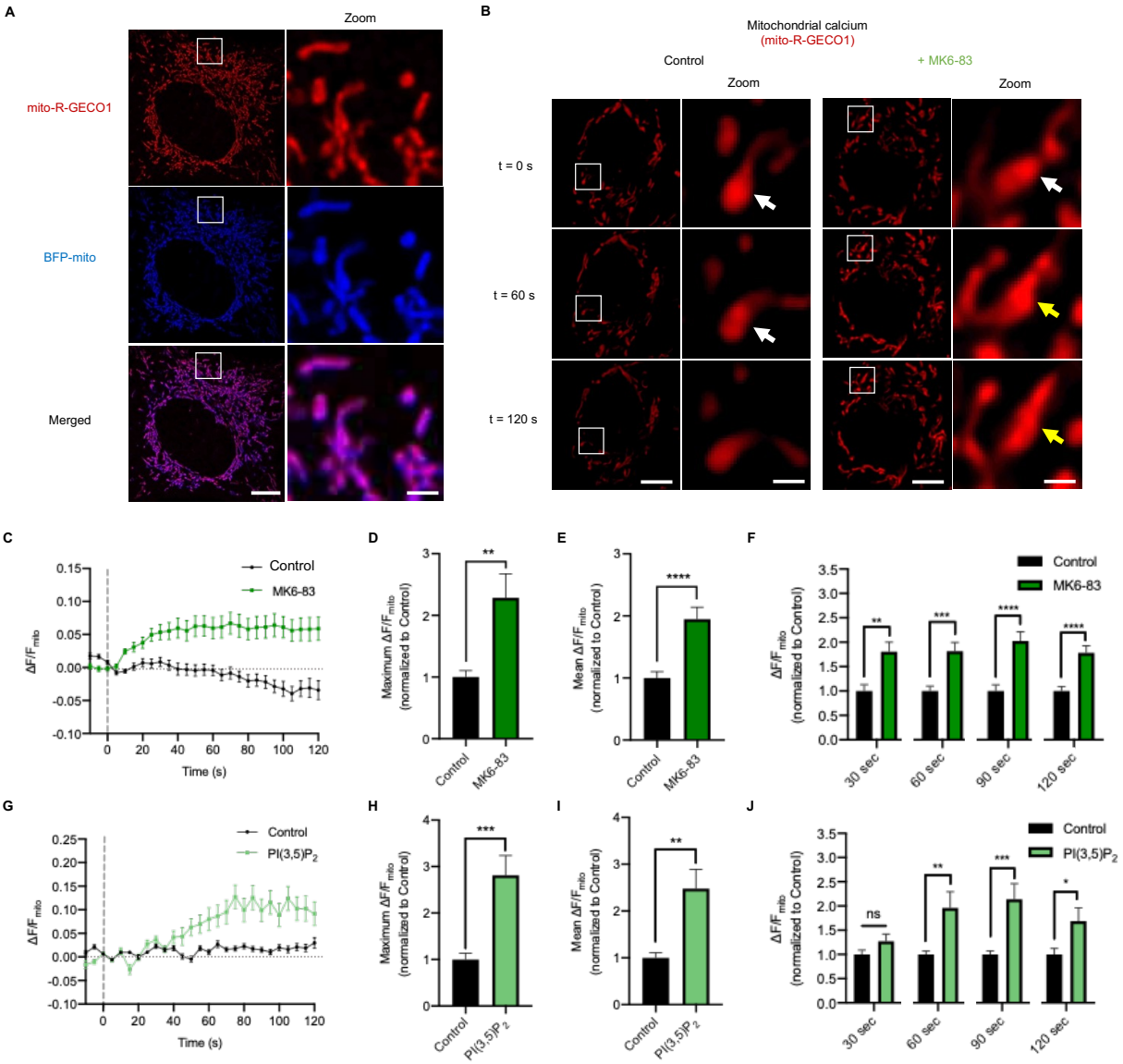
A
Zoom
mito-R-GECO1
BFP-mito
Merged
B
Mitochondrial calcium
(mito-R-GECO1)
Control
+ MK6-83
Zoom
Zoom
t = 0 s
t = 60 s
t = 120 s
C
Control
MK6-83
ΔF/F mito
Time (s)
D
Maximum ΔF/F mito (normalized to Control)
Control
MK6-83
E
Mean ΔF/F mito (normalized to Control)
Control
MK6-83
F
Control
MK6-83
ΔF/F mito (normalized to Control)
30 sec
60 sec
90 sec
120 sec
G
Control
PI(3,5)P2
ΔF/F mito
Time (s)
H
Maximum ΔF/F mito (normalized to Control)
Control
PI(3,5)P2
I
Mean ΔF/F mito (normalized to Control)
Control
PI(3,5)P2
J
Control
PI(3,5)P2
ΔF/F mito (normalized to Control)
ns
30 sec
60 sec
90 sec
120 sec

Figure 9: Activation of lysosomal TRPML1 leads to mitochondrial calcium influx. A, Colocalization of mitochondrial calcium sensor, Mito-R-GECO1, with mitochondrial matrix marker, BFP-mito, in live HeLa cells. **B**, **C**, Mitochondrial calcium response in live HeLa cells expressing Mito-R-GECO1, in response to TRPML1 activation with MK6-83 (10 μM) (yellow arrow) or control treatment (white arrow) at t = 0 s with representative time-lapse confocal images (**B**, n = 20 cells for each condition) and mitochondrial calcium traces (ΔF/F) (**C**, n = 20 cells for each condition). **D-F**, Quantification of maximum mitochondrial calcium response (**D**), mean mitochondrial calcium response (**E**) and mitochondrial calcium response at 30, 60, 90 and 120 seconds (**F**) after TRPML1 activation with MK6-83 (10 μM) or control treatment (from **B**) (n = 20 cells for each condition). **G**, Mitochondrial calcium response (ΔF/F) in live HeLa cells expressing Mito-R-GECO1 in response to TRPML1 activation with $PI(3,5)P_2$ (1 μM) or control treatment at t = 0 s (**G**, n = 24 cells for each condition). **H-J**, Quantification of maximum mitochondrial calcium response (**H**), mean mitochondrial calcium response (**I**) and mitochondrial calcium response at 30, 60, 90 and 120 seconds (**J**) after TRPML1 activation with $PI(3,5)P_2$ (1 μM) or control treatment (n = 24 cells for each condition). Data are means ± s.e.m. (*P<0.05, **P<0.01, ***P<0.001, ****P<0.0001, ns, not significant, unpaired two-tailed t-test). Scale bars, 10 μm (**A, B**); 1 μm (**A, B**, zoom).

TRPML1 activation preferentially increases mitochondrial calcium at mitochondria-lysosome contacts

Because activation of lysosomal calcium release via TRPML1 led to increased mitochondrial calcium, we next evaluated whether this increase in mitochondrial calcium preferentially occurred at mitochondria-lysosome contact sites. We found that stable mitochondria-lysosome contacts dynamically formed in wild-type HeLa cells, defined as lysosomes remaining tethered to mitochondria for over 10 seconds (**Fig. 10A**), as recently described (Wong, Kim, et al., 2019; Wong et al., 2018). To assess whether TRPML1 mediated the direct transfer of calcium at mitochondria-lysosome contacts, we analyzed the calcium dynamics of mitochondria that were either in contact or not in contact with lysosomes upon TRPML1 activation (**Fig. 10B**). Mitochondria stably in contact with lysosomes (> 10 seconds) had a significantly higher increase in calcium after TRPML1 activation, compared to mitochondria not in contact with lysosomes (**Fig. 10B-C**). This preferential increase in mitochondrial calcium at mitochondria-lysosome contacts was observed in multiple cell types including fibroblasts and HCT116 cells, which similarly showed a mitochondria-lysosome contact-dependent increase in mitochondrial calcium upon activation of TRPML1 lysosomal calcium release (**Fig. 11B-D**).

We then investigated whether directly modulating mitochondria-lysosome contact sites could increase the transfer of lysosomal calcium into mitochondria. We previously showed that mitochondria-lysosome contact site untethering is directly modulated by the activity of the mitochondrial-localized Rab7 GTPase-activating protein (TBC1D15) driving Rab7 GTP hydrolysis on lysosomes/late endosomes, and consequently, that TBC1D15 knockout significantly prolonged mitochondria-lysosome contact site tethering (Wong et al., 2018). To further investigate whether mitochondrial calcium dynamics could be regulated at mitochondria-lysosome contacts,

we compared HCT116 wild-type with TALEN-generated HCT116 TBC1D15 knockout cells (Yamano et al., 2014), as TBC1D15 knockout cells have significantly increased mitochondria-lysosome contact tethering duration (Wong et al., 2018). Upon TRPML1 activation with ML-SA1, TBC1D15 knockout cells showed a significantly greater increase in total mitochondrial calcium compared to wild-type cells (**Fig. 10D-E**) as well as significantly increased maximum mitochondrial calcium, mean mitochondrial calcium and mitochondrial calcium at multiple time points (**Fig. 10F-H**). Thus, directly modulating mitochondria-lysosome contact site tethering is sufficient to increase lysosomal calcium transfer into mitochondria.

We further confirmed that mitochondrial uptake of lysosomal calcium was not dependent on the endoplasmic reticulum (ER) (Garrity et al., 2016; Kilpatrick et al., 2016), as blocking ER calcium release using an inositol 1,4,5-triphosphate receptor (IP3R) antagonist (Xestospongin-C, pre-treatment for 20 minutes) (**Fig. 12A-D**) or ryanodine receptor (RyR) antagonist (DHBP, pre-treatment for 10 minutes) (**Fig. 12E-G**) did not prevent an increase in mitochondrial calcium (Mito-R-GECO1) upon TRPML1 activation. Similarly, neither blocking store-operated calcium entry (SOCE) with a Stim1 inhibitor (SKF-96365, pre-treatment for 10 minutes) (**Fig. 12H-J**) nor depleting ER calcium using a SERCA pump inhibitor (thapsigargin, pre-treatment for 10 minutes) (**Fig. 12K-M**) altered mitochondrial calcium increase (Mito-R-GECO1) upon TRPML1 activation. TRPML1-mediated mitochondrial calcium influx was also unaltered upon chelation of cytosolic calcium (BAPTA-AM, pre-treatment for 20 minutes), further suggesting that calcium transfer primarily occurs at mitochondria-lysosome contacts (**Fig. 13A-D**). Altogether, these findings indicate that TRPML1-mediated calcium influx into mitochondria occurs preferentially at mitochondria-lysosome contacts and furthermore, can be directly regulated by modulating mitochondria-lysosome contact tethering machinery.

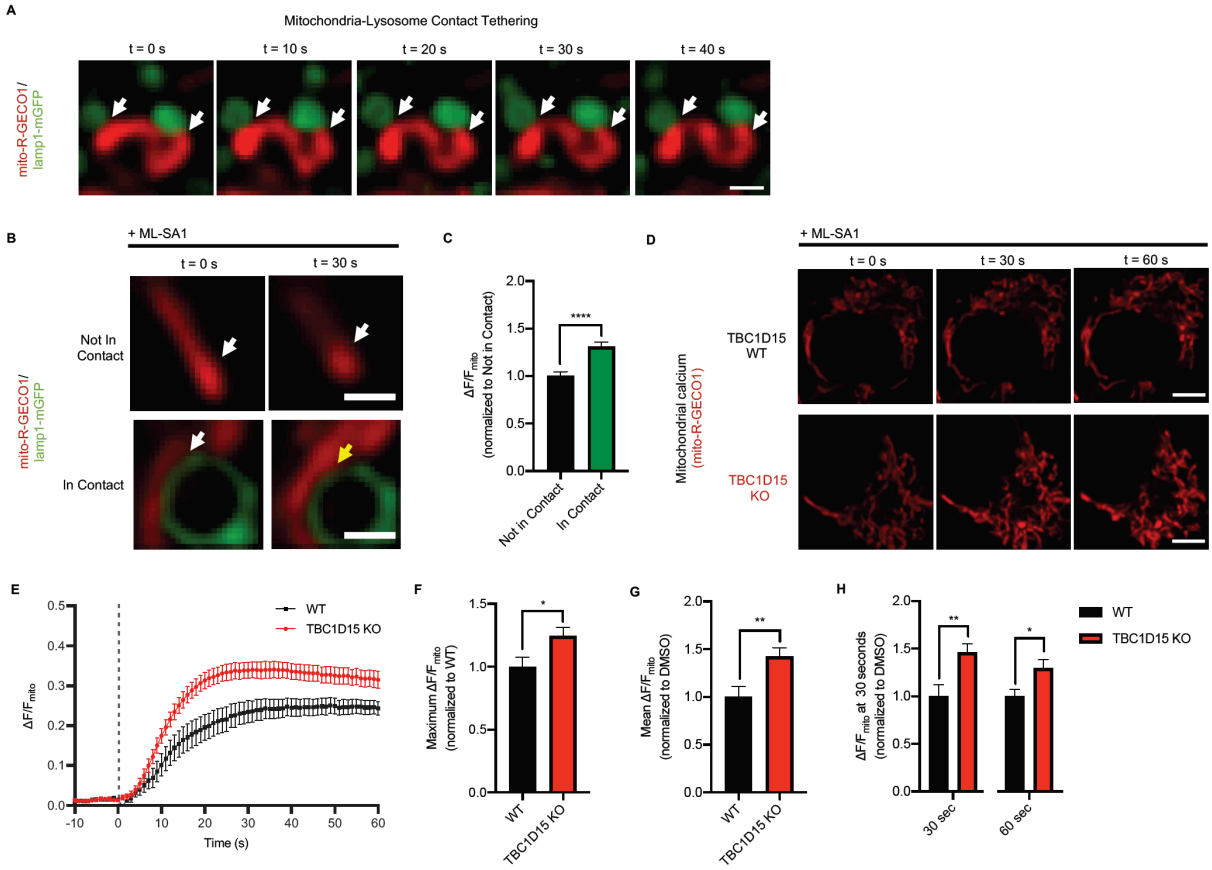

Figure 10: TRPML1 activation preferentially increases mitochondrial calcium at mitochondria-lysosome contacts. A, Representative time-lapse confocal images showing stable mitochondria-lysosome contact site tethering (white arrows) in live HeLa cells expressing lysosomal marker, lamp1-mGFP, and Mito-R-GECO1. **B**, Representative time-lapse confocal images of mitochondrial calcium at t = 30 s following TRPML1 activation with ML-SA1 (31.25 μM) in mitochondria in contact with lysosomes (bottom, yellow arrow) versus those not in contact with lysosomes (top, white arrow) in live HeLa cells expressing Mito-R-GECO1 and lamp1-mGFP (n = 100 events from 20 cells for each condition). **C**, Quantification of mitochondrial calcium responses from mitochondria in contact and not in contact with lysosomes following TRPML1 activation with ML-SA1 (31.25 μM) from **B** (n = 100 events from 20 cells for each condition). **D**, **E**, Mitochondrial calcium response (ΔF/F) in live wild-type (WT) or TBC1D15 knockout (KO) HCT116 cells expressing Mito-R-GECO1 following TRPML1 activation with ML-SA1 (31.25 μM) at t = 0 s with representative time-lapse confocal images (**D**, n = 18 cells for each condition) and mitochondrial calcium traces (ΔF/F) (**E**, n = 18 cells for each condition). **F-H**, Quantification of maximum mitochondrial calcium response (**F**), mean mitochondrial calcium response (**G**) and mitochondrial calcium response at 30 and 60 seconds (**H**) after treatment with ML-SA1 (31.25 μM) in live WT or TBC1D15 KO HCT116 cells from confocal time-lapse images (from **D**) (n = 18 cells for each condition). Data are means ± s.e.m. (*P<0.05, **P<0.01, ****P<0.0001, unpaired two-tailed t-test). Scale bars, 1 μm (**A**, **B**); 5 μm (**D**)

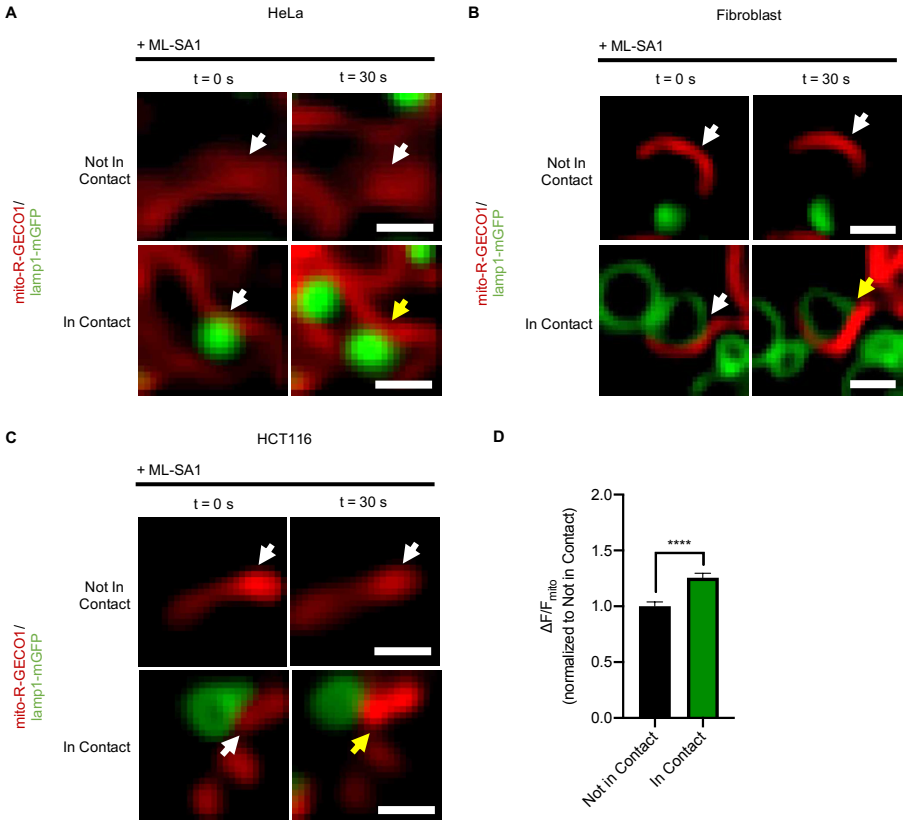

Figure 11: TRPML1 mediates mitochondrial calcium transfer at mitochondria-lysosome contacts in multiple cell types. A-C, Representative time-lapse confocal images of increase in mitochondrial calcium at t = 30 sec following TRPML1 activation with ML-SA1 (31.25 μM) in mitochondria in contact with lysosomes (bottom, yellow arrows) versus those not in contact with lysosomes (top, white arrows) in live HeLa cells (**A**), fibroblasts (**B**) and HCT116 cells (**C**) expressing mitochondrial matrix calcium sensor, Mito-R-GECO1, and lysosomal marker, lamp1-mGFP (n = 100 events from 20 cells for **A**, **B**; 90 events from 18 cells for **C**). **D**, Quantification of mitochondrial calcium responses from mitochondria in contact and not in contact with lysosomes following TRPML1 activation with ML-SA1 (31.25 μM) in HCT116 cells from confocal time-lapse images (from **C**) (n = 90 events from 18 cells for each condition). Data are means ± s.e.m. (****P<0.0001, unpaired two-tailed t-test). Scale bars, 1 μm (**A-C**).

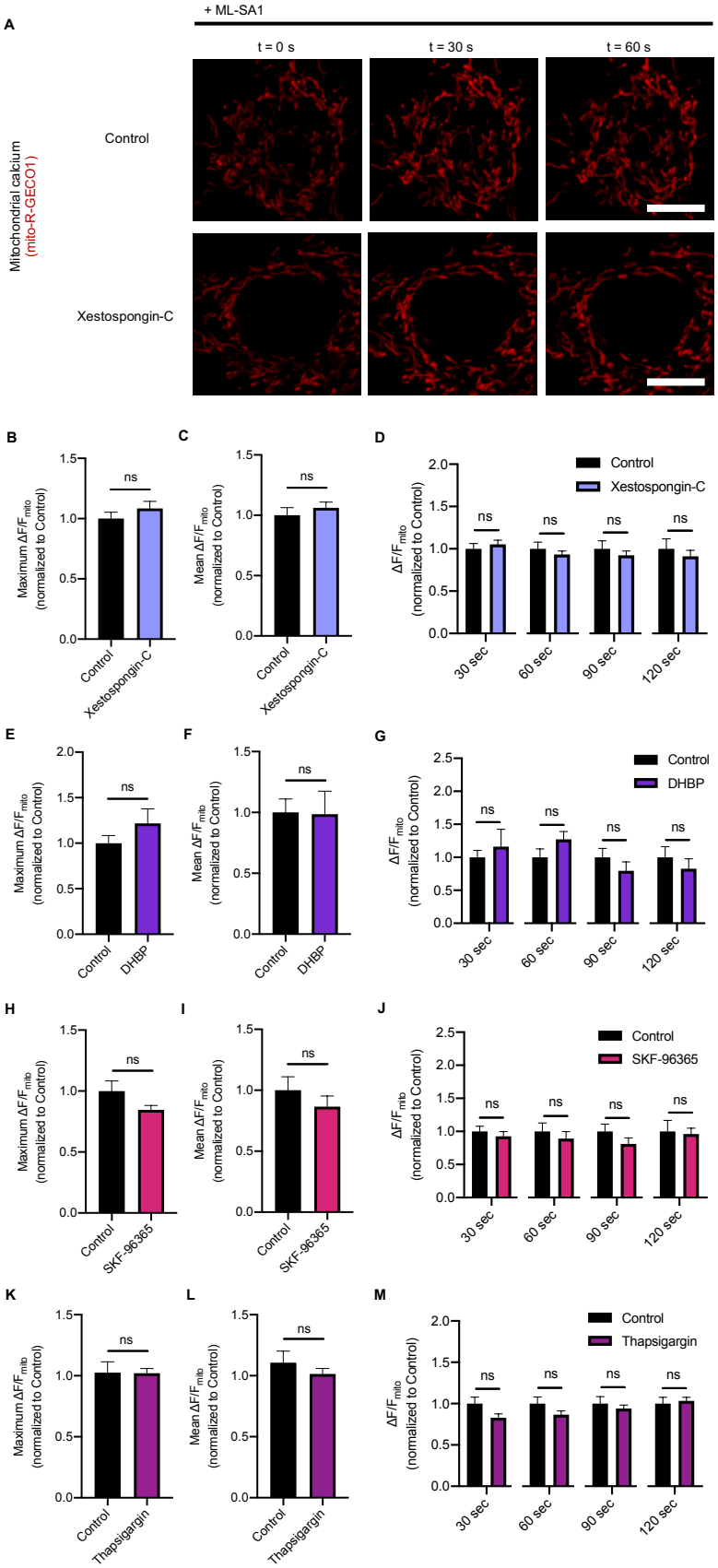
A
+ ML-SA1
t = 0 s
t = 30 s
t = 60 s
Control
Xestospongin-C
Mitochondrial calcium
(mito-R-GECO1)
B
Maximum ΔF/F mito (normalized to Control)
ns
Control
Xestospongin-C
C
Mean ΔF/F mito (normalized to Control)
D
ΔF/F mito (normalized to Control)
Control
Xestospongin-C
30 sec
60 sec
90 sec
120 sec
E
DHBP
F
G
H
SKF-96365
I
J
K
Thapsigargin
L
M

Figure 12: TRPML1-mediated lysosomal transfer of calcium to mitochondria does not depend on ER calcium release. A, Representative time-lapse confocal images of live HeLa cells expressing mitochondrial-matrix targeted calcium sensor, Mito-R-GECO1, in response to TRPML1 activation with ML-SA1 (31.25 μM) at t = 0 sec following 20-minute pre-treatment with either vehicle control or ER calcium release blocker (IP3R antagonist), Xestospongin-C (10 μM) (n = 15 cells for each condition). **B-D**, Quantification of maximum mitochondrial calcium response (**B**), mean mitochondrial calcium response (**C**) and mitochondrial calcium response at 30, 60, 90 and 120 seconds (**D**) after TRPML1 activation with ML-SA1 (31.25 μM) in live HeLa cells pre-treated with vehicle control or Xestospongin-C from confocal time-lapse images (from **A**) (n = 15 cells for each condition). **E-G**, Quantification of maximum mitochondrial calcium response (**E**), mean mitochondrial calcium response (**F**) and mitochondrial calcium response at 30, 60, 90 and 120 seconds (**G**) after TRPML1 activation with ML-SA1 (31.25 μM) in live HeLa cells pre-treated for 10 minutes with vehicle control or ER calcium release blocker (RyR antagonist), DHBP (50 μM) (n = 18 cells for each condition). **H-J**, Quantification of maximum mitochondrial calcium response (**H**), mean mitochondrial calcium response (**I**) and mitochondrial calcium response at 30, 60, 90 and 120 seconds (**J**) after TRPML1 activation with ML-SA1 (31.25 μM) in live HeLa cells pre-treated for 10 minutes with vehicle control or SOCE blocker (STIM1 inhibitor), SKF-96365 (20 μM) (n = 18 cells for each condition). **K-M**, Quantification of maximum mitochondrial calcium response (**K**), mean mitochondrial calcium response (**L**) and mitochondrial calcium response at 30, 60, 90 and 120 seconds (**M**) after TRPML1 activation with ML-SA1 (31.25 μM) in live HeLa cells pre-treated for 10 minutes with vehicle control or SERCA pump inhibitor, thapsigargin (1 μM) (n = 19 cells for each condition). Data are means ± s.e.m. (ns, not significant, unpaired two-tailed t-test). Scale bars, 10 μm (**A**).

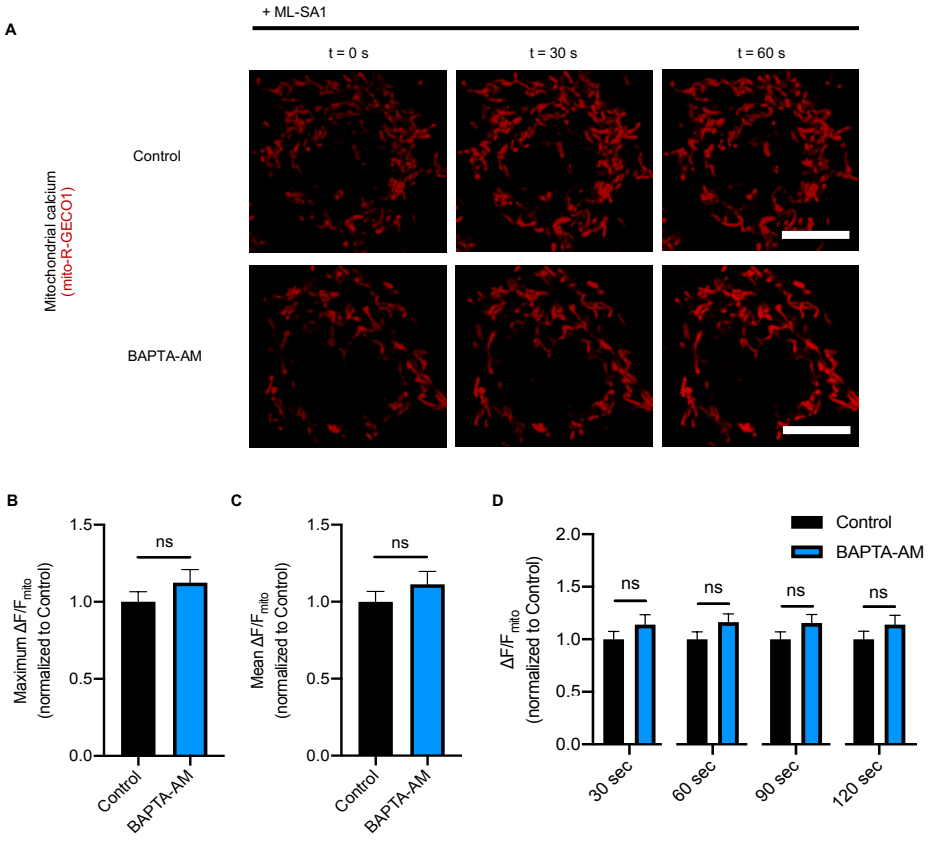

Figure 13: TRPML1-mediated lysosomal transfer of calcium to mitochondria is not altered by chelation of cytosolic calcium. A, Representative time-lapse confocal images of live HeLa cells expressing mitochondrial-matrix targeted calcium sensor, Mito-R-GECO1, in response to TRPML1 activation with ML-SA1 (31.25 μM) at t = 0 sec following 20 minute pre-treatment with either vehicle control or cytosolic calcium chelator, BAPTA-AM (5 μM) (n = 15 cells for each condition). **B-D**, Quantification of maximum mitochondrial calcium response (**B**), mean mitochondrial calcium response (**C**) and mitochondrial calcium response at 30, 60, 90 and 120 seconds (**D**) after TRPML1 activation with ML-SA1 (31.25 μM) in live HeLa cells pre-treated with vehicle control or BAPTA-AM from confocal time-lapse images (from **A**) (n = 15 cells for each condition). Data are means ± s.e.m. (ns, not significant, unpaired two-tailed t-test). Scale bars, 10 μm (**A**).

Lysosomal TRPML1 specifically modulates mitochondrial calcium and mitochondria-lysosome contact dynamics

To further demonstrate that lysosomal TRPML1 activity modulates mitochondrial calcium, we expressed either wild-type TRPML1 (TRPML1 WT-Halo) or the dominant-negative, non-conducting TRPML1 pore mutant (TRPML1 D471K-Halo) in HeLa cells and examined mitochondrial calcium dynamics (Mito-R-GECO1) upon ML-SA1 treatment. We first confirmed that both wild-type TRPML1 and dominant-negative TRPML1 were localized to the lysosomal/late endosomal compartment as evidenced by colocalization with the lysosomal membrane marker, BFP-lysosomes (**Fig. 14A-B**) and that both wild-type and dominant-negative TRPML1 were expressed at similar levels (**Fig. 14C**). Upon ML-SA1 treatment, cells expressing dominant-negative TRPML1 showed a significant reduction in mitochondrial calcium influx compared to wild-type TRPML1-expressing cells (**Fig. 15A-B**). In addition, expression of the dominant-negative TRPML1 mutant significantly reduced the maximum mitochondrial calcium, mean mitochondrial calcium and mitochondrial calcium at multiple time points (**Fig. 15C-E**). These results thus suggest that TRPML1 activity is important for modulating mitochondrial calcium dynamics.

In order to investigate the role of TRPML1 at contact sites, we analyzed whether TRPML1 specifically modulated mitochondrial calcium at mitochondria-lysosome contact sites. HeLa cells expressing wild-type TRPML1 displayed a significantly higher increase in mitochondrial calcium after TRPML1 activation for mitochondria that were in contact with lysosomes, compared to mitochondria not in contact with lysosomes (**Fig. 15F**). In contrast, this difference in contact-dependent calcium transfer was entirely abolished in cells expressing the dominant-negative TRPML1 mutant (**Fig. 15F**). To probe downstream effects of calcium transfer at mitochondria-

lysosome contacts, we investigated whether TRPML1-mediated mitochondrial calcium influx promoted mitochondrial permeability transition pore (mPTP) opening, which can be assessed by the quenching of mitochondrial-localized calcein in the presence of $CoCl_2$ (**Fig. 16A**). In contrast to ionomycin treatment which induced mPTP opening and rapid quenching of calcein, neither the TRPML1 agonist ML-SA1 or vehicle control reduced mitochondrial calcein fluorescence (**Fig. 16B-C**), suggesting that TRPML1-mediated mitochondrial calcium influx does not induce sustained mPTP opening. We also investigated whether TRPML1-mediated mitochondrial calcium influx activated apoptotic pathways via endogenous cytochrome C staining (**Fig. 16D**). Relative to staurosporine which induced release of cytochrome C from the mitochondria into the cytosol, we did not observe significant changes in mitochondrial distribution of cytochrome C in cells treated with TRPML1 agonist ML-SA1 or vehicle control at multiple points (**Fig. 16E-G**).

In addition to modulating contact-dependent calcium transfer, we found that TRPML1 modulated mitochondria-lysosome contact-site dynamics. In cells expressing the dominant-negative TRPML1 mutant, there was both a higher percentage of lysosomes in stable contact with mitochondria (**Fig. 15G**) and a significant increase in minimum duration of mitochondria-lysosome contacts (**Fig. 15H-I**). We further verified whether TRPML1 localized preferentially to mitochondria-lysosome contacts in cells expressing HA-tagged TRPML1 and an HA-mCherry nanobody. TRPML1-HA puncta marked a subset of contact sites (**Fig. 17A**) and TRPML1-HA localization at the contact sites was significantly greater than expected by random chance (**Fig. 17B**). These findings highlight a role for TRPML1 in regulating mitochondria-lysosome contact site dynamics and contact-dependent calcium transfer into mitochondria.

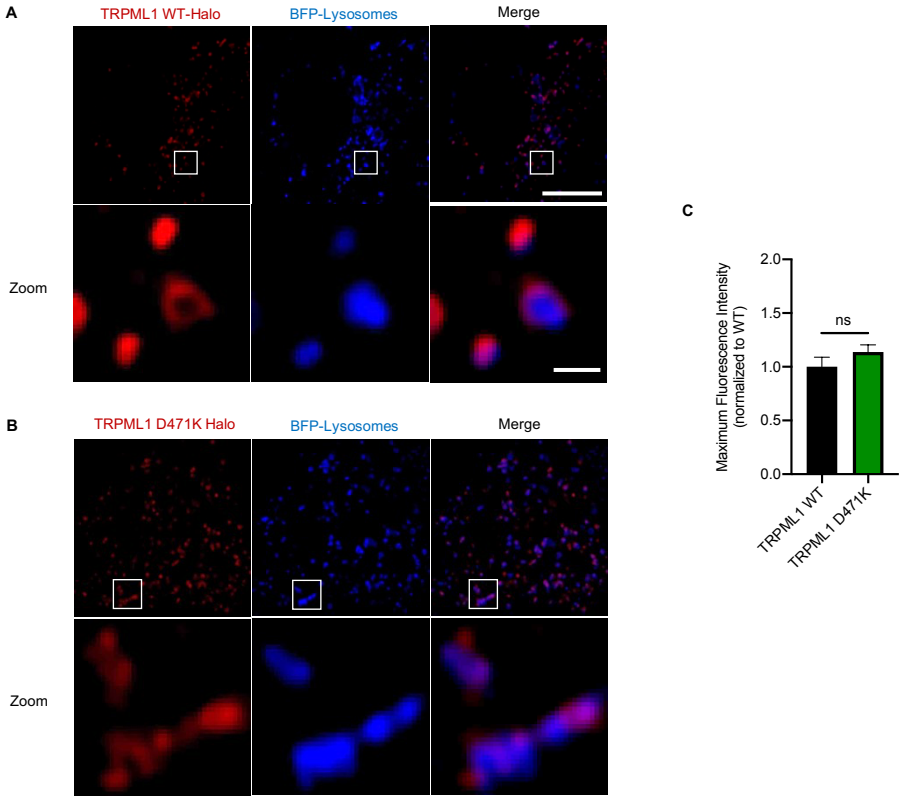

Figure 14: Wild-type and dominant-negative (D471K) TRPML1 preferentially localize to lysosomes/late endosomes. A, Colocalization of TRPML1 WT-Halo (incubated with PA Janelia Fluor 646, red) with lysosomal marker, BFP-lysosomes in live HeLa cells. **B**, Colocalization of TRPML1 D471K-Halo (incubated with PA Janelia Fluor 646, red) with lysosomal marker, BFP-lysosome in live HeLa cells. **C**, Expression level measured by mean fluorescence intensity of Halo-tagged wild-type or mutant (D471K) TRPML1 in live HeLa cells labeled with PA Janelia Fluor 646 ligand (n = 20 cells for each condition). Data are means ± s.e.m. (ns, not significant, unpaired two-tailed t-test). Scale bar, 1 μm (**A-B**).

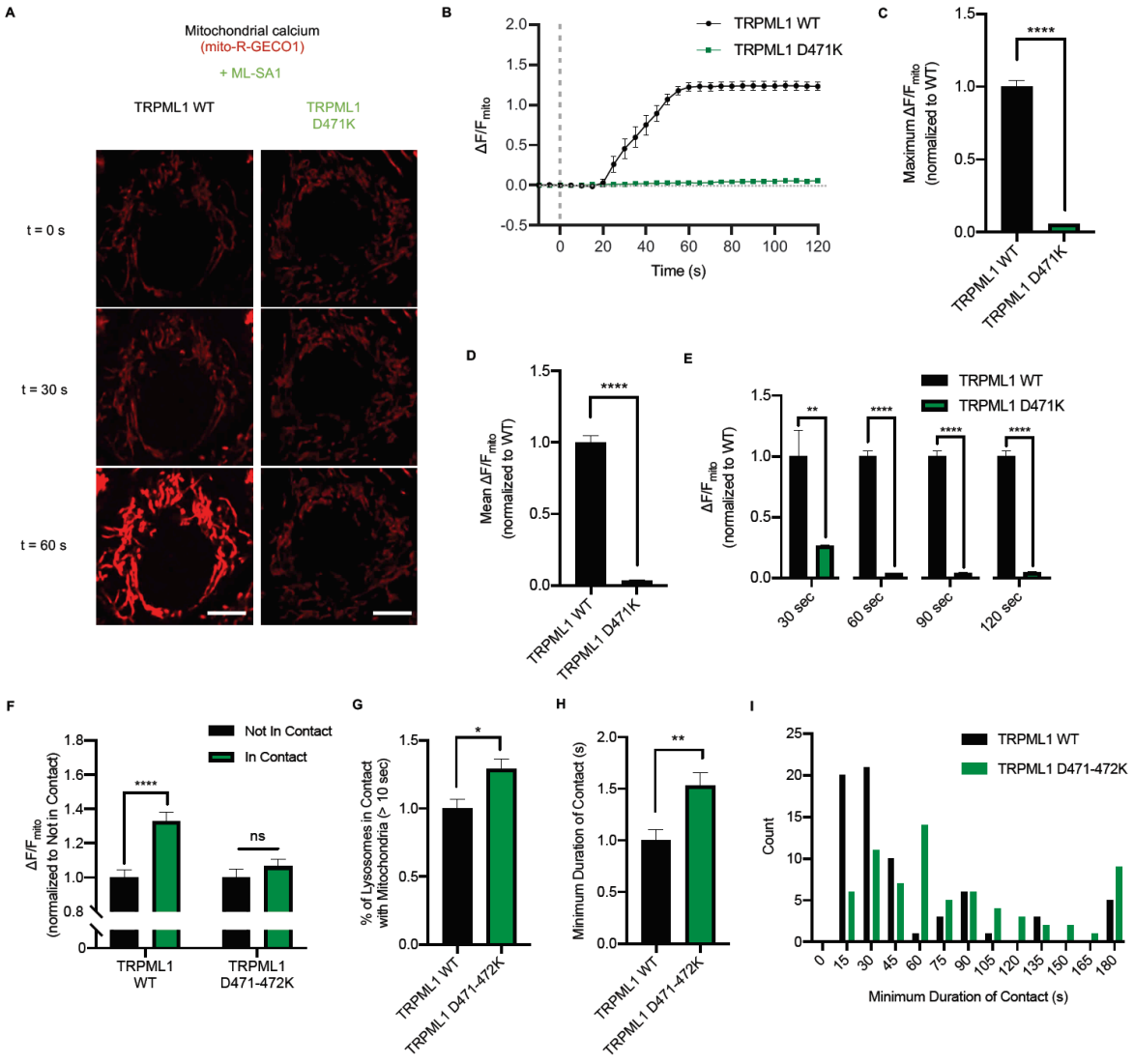
A
Mitochondrial calcium
(mito-R-GECO1)
+ ML-SA1
TRPML1 WT
TRPML1 D471K
t = 0 s
t = 30 s
t = 60 s
B
TRPML1 WT
TRPML1 D471K
ΔF/F mito
Time (s)
C
Maximum ΔF/F mito (normalized to WT)
****
TRPML1 WT
TRPML1 D471K
D
Mean ΔF/F mito (normalized to WT)
****
TRPML1 WT
TRPML1 D471K
E
TRPML1 WT
TRPML1 D471K
ΔF/F mito (normalized to WT)
**
****
****
****
30 sec
60 sec
90 sec
120 sec
F
Not In Contact
In Contact
ΔF/F mito (normalized to Not in Contact)
****
ns
TRPML1 WT
TRPML1 D471-472K
G
% of Lysosomes in Contact with Mitochondria (> 10 sec)
*
TRPML1 WT
TRPML1 D471-472K
H
Minimum Duration of Contact (s)
**
TRPML1 WT
TRPML1 D471-472K
I
TRPML1 WT
TRPML1 D471-472K
Count
Minimum Duration of Contact (s)

Figure 15: TRPML1 specifically modulates mitochondrial calcium and mitochondria-lysosome contact dynamics. **A**, **B**, Mitochondrial calcium response in live HeLa cells expressing Mito-R-GECO1 and either wild-type (WT) or dominant-negative (D471K) TRPML1 mutant, in response to TRPML1 activation with ML-SA1 (31.25 μM) at $t = 0$ s with representative time-lapse confocal images (**A**, n = 20 cells for each condition) and mitochondrial calcium traces (ΔF/F) (**B**, $n = 20$ cells for each condition). **C-E**, Quantification of maximum mitochondrial calcium response (**C**), mean mitochondrial calcium response (**D**) and mitochondrial calcium response at 30, 60, 90 and 120 seconds (**E**) after TRPML1 activation with ML-SA1 (31.25 μM) in live HeLa cells expressing TRPML1 WT or TRPML1 D471K mutant from **A** (n = 20 cells for each condition). **F**, Quantification of mitochondrial calcium responses of mitochondria in contact and not in contact with lysosomes following TRPML1 activation with ML-SA1 (31.25 μM) in live HeLa cells expressing Mito-R-GECO1, lamp1-mGFP, and either TRPML1 WT-pHcRed or dominant-negative TRPML1 D471-472K-pHcRed (n = 100 events from 20 cells foreach condition). **G-I**, Quantification of percentage of mitochondria-lysosome contacts (> 10 s; **G**, n = 10 cells for each condition) and duration of contacts (**H, I**, n = 70 events from 10 cells for each condition) in live HeLa cells expressing Tom20-mEmerald, BFP-lysosomes and either TRPML1 WT-pHcRed or TRPML1 D471-472K-pHcRed**.** Data are means ± s.e.m. (*P<0.05, **P<0.01, ****P<0.0001, ns, not significant, unpaired two-tailed t-test). Scale bars, 10 μm (**A**).

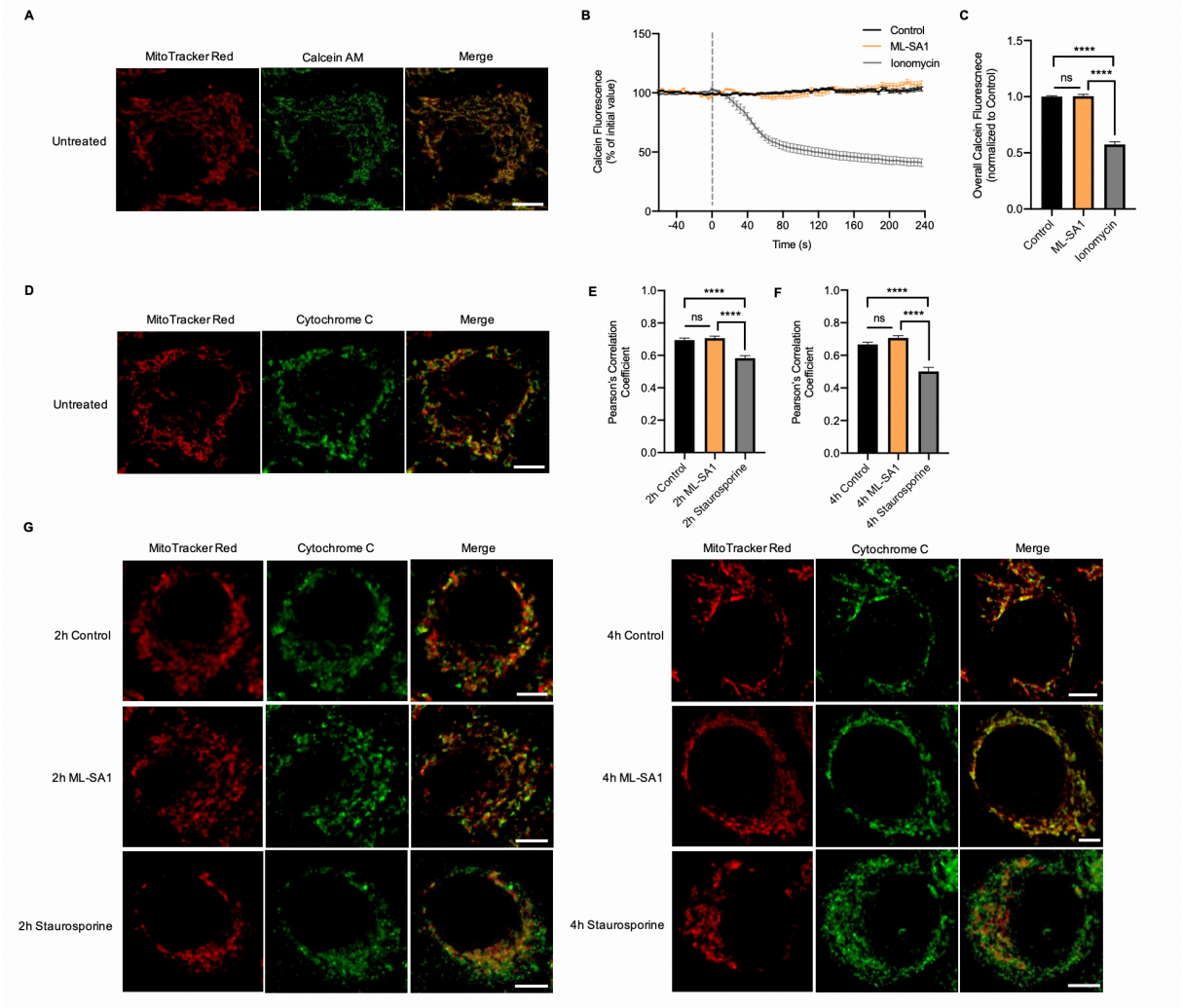
A
MitoTracker Red
Calcein AM
Merge
Untreated
B
Control
ML-SA1
Ionomycin
Calcein Fluorescence (% of initial value)
Time (s)
C
Overall Calcein Fluorescnece (normalized to Control)
ns
****
Control
ML-SA1
Ionomycin
D
MitoTracker Red
Cytochrome C
Merge
Untreated
E
Pearson's Correlation Coefficient
2h Control
2h ML-SA1
2h Staurosporine
F
4h Control
4h ML-SA1
4h Staurosporine
G
2h Control
2h ML-SA1
2h Staurosporine
4h Control
4h ML-SA1
4h Staurosporine

Figure 16: TRPML1-mediated mitochondrial calcium influx does not trigger sustained mPTP opening or cytochrome C release. **A**, Colocalization of calcein-AM with MitoTracker Red in live HeLa cells in the presence of $CoCl_2$. **B**, Calcein fluorescence response as % of initial fluorescence in live HeLa cells pre-incubated for 15 minutes with calcein-AM (1 μM), $CoCl_2$ (8 mM) and MitoTracker Red (200 nM) then treated with vehicle control, ML-SA1 (31.25 μM) or ionomycin (2 μM) (n = 20 cells for each condition). **C**, Quantification of overall calcein fluorescence in live HeLa treated with vehicle control, ML-SA1 (31.25 μM) or ionomycin (2 μM, positive control) (from **B**) (n = 20 cells for each condition). **D**, Colocalization of endogenous cytochrome C with MitoTracker in fixed, untreated HeLa cells (Pearson's correlation coefficient = 0.70 ± 0.01) (n = 25 cells). **E, F**, Quantification of Pearson's correlation coefficients between endogenous cytochrome C and MitoTracker Red in fixed HeLa cells treated for 2 h (**E**) or 4 h (**F**) with vehicle control, ML-SA1 (31.25 μM) or staurosporine (1 μM, positive control) (n = 30 cells for each condition). **G**, Representative confocal images of fixed HeLa cells labeled with MitoTracker Red treated for 2 h or 4 h with vehicle control, ML-SA1 (31.25 μM) or staurosporine (1 μM, positive control) and stained for endogenous cytochrome C (from **E**, **F**) (from n = 30 cells for each condition). Data are means ± s.e.m. (****P<0.0001, ns, not significant, one-way ANOVA with Tukey's post-hoc test). Scale bar, 5 μm (**A, D, G**).

VDAC1 and MCU mediate mitochondrial uptake of lysosomal calcium at mitochondria-lysosome contact sites

Having shown that TRPML1-mediated lysosomal calcium release increased mitochondrial calcium at mitochondria-lysosome contacts, we next sought to identify the mitochondrial components promoting uptake of lysosomal calcium. Voltage-dependent anion channels (VDACs) on the outer mitochondrial membrane have been implicated in mitochondrial calcium uptake (Bathori, Csordas, Garcia-Perez, Davies, & Hajnoczky, 2006; Gincel, Zaid, & Shoshan-Barmatz, 2001; Min et al., 2012; Naghdi & Hajnóczky, 2016; Rapizzi et al., 2002; Subedi et al., 2011) and specifically, VDAC1 was previously identified as a potential interactor of lysosomal TRPML1 (Spooner et al., 2013). To first confirm the interaction of TRPML1 with VDAC1, we conducted co-immunoprecipitation experiments in cells expressing TRPML1-GFP and found that TRPML1 interacted with endogenous VDAC1 (**Fig. 17C**), but not endogenous VDAC2 or VDAC3 (**Fig. 17C**). We next investigated whether VDAC1 is important for the mitochondrial uptake of lysosomal calcium by assessing mitochondrial calcium dynamics upon TRPML1 activation in cells expressing either wild-type human VDAC1 or a VDAC1 mutant (E73Q) with a single amino acid substitution in a putative calcium-binding site (Israelson, Abu-Hamad, Zaid, Nahon, & Shoshan-Barmatz, 2007; Israelson, Zaid, Abu-Hamad, Nahon, & Shoshan-Barmatz, 2008). In response to TRPML1 activation with ML-SA1, cells expressing the VDAC1 mutant showed significantly lower increase in mitochondrial calcium (Mito-R-GECO1) (**Fig. 18A; Fig. 17D**) as well as significantly decreased maximum mitochondrial calcium, mean mitochondrial calcium and mitochondrial calcium at multiple time points compared to wild-type cells following activation of TRPML1 (**Fig. 18B-D**). After verifying that wild-type and mutant VDAC1 were expressed at similar levels (**Fig. 17F**), we next assessed whether VDAC1 regulated calcium transfer

preferentially at mitochondria-lysosome contact sites. While mitochondria in contact with lysosomes had significantly elevated calcium influx after TRPML1 activation compared to mitochondria not in contact with lysosomes in cells expressing wild-type VDAC1, there was no difference in mitochondrial calcium response between mitochondria in and not in contact with lysosomes in VDAC1 mutant-expressing cells (**Fig. 18E**). These findings thus suggest that VDAC1 on the outer mitochondrial membrane serves as a mediator of mitochondrial uptake of lysosomal calcium at mitochondria-lysosome contacts.

The mitochondrial calcium uniporter (MCU) is the major transporter of calcium across the inner mitochondrial membrane into the mitochondrial matrix (Baughman et al., 2011; De Stefani, Raffaello, Teardo, Szabo, & Rizzuto, 2011). To evaluate the role of the MCU in uptake of lysosomal calcium across the inner mitochondrial membrane, we expressed either wild-type MCU or MCU mutant (E264A) which disrupts calcium uptake (De Stefani et al., 2011; C. B. Phillips, Tsai, & Tsai, 2019). As the expression of MCU mutant was not significantly different from that of wild-type MCU (**Fig. 17G**), we then examined mitochondrial calcium dynamics (Mito-R-GECO1) in these cells in response to TRPML1 activation. Compared to cells expressing wild-type MCU, cells expressing mutant MCU had reduced total mitochondrial calcium increase upon TPRML1 activation (**Fig. 18F; Fig. 17E**), as well as significantly lower maximum mitochondrial calcium, mean mitochondrial calcium and mitochondrial calcium at multiple time points after ML-SA1 treatment (**Fig. 18G-I**). Importantly, the MCU was also important for mitochondria-lysosome contact-dependent calcium transfer. Wild-type MCU-expressing cells showed significant differences in calcium influx for mitochondria in contact with lysosomes compared to mitochondria not in contact, while expression of the MCU mutant (E264A) completely abolished

this difference (**Fig. 18J**). These results indicate that MCU on the inner mitochondrial membrane modulates mitochondrial calcium dynamics at mitochondria-lysosome contact sites.

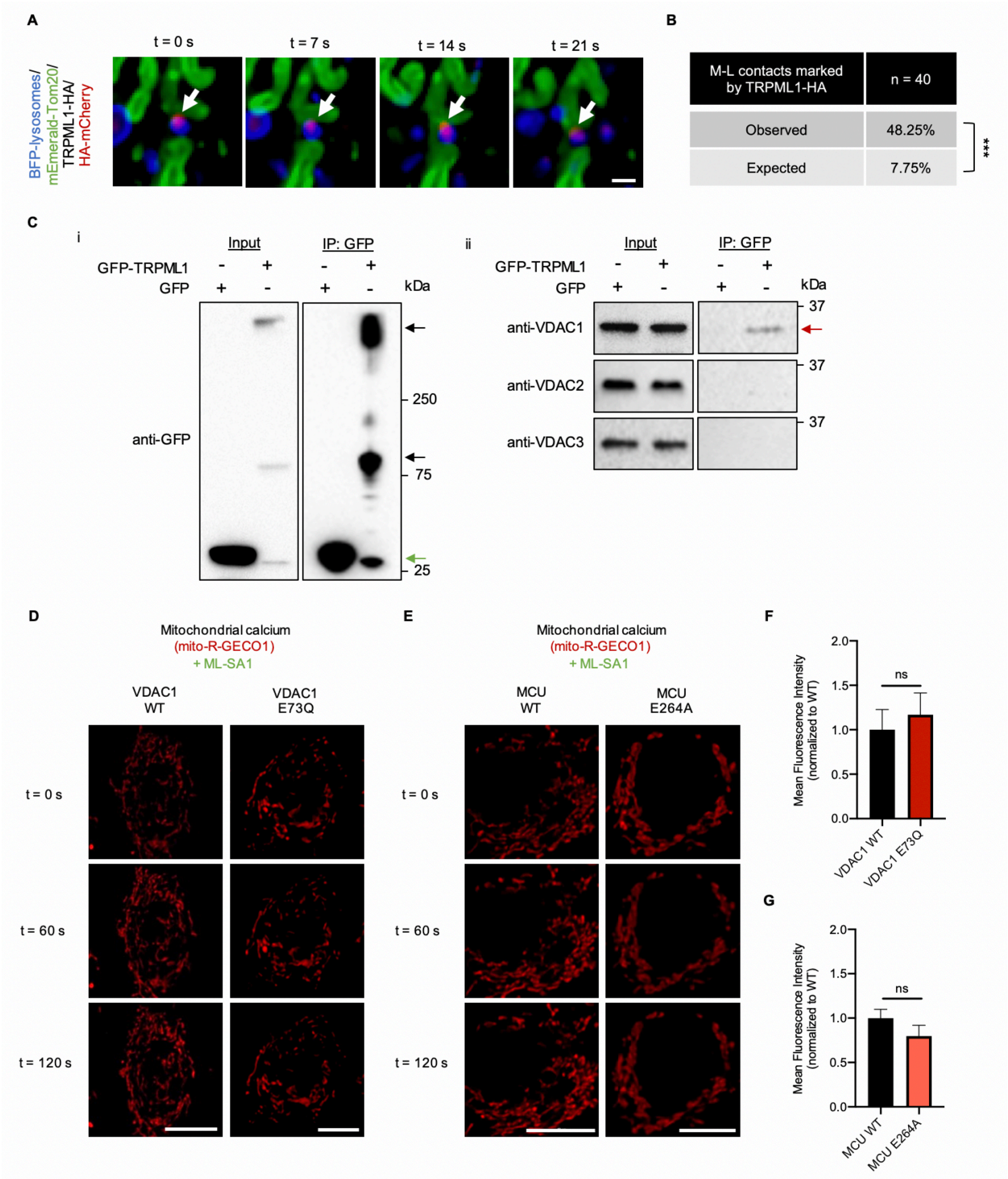

Figure 17: TRPML1, VDAC1 and MCU modulate mitochondrial calcium influx at mitochondria-lysosome contact sites. **A**, Representative time-lapse confocal images showing TRPML1 marking mitochondria-lysosome contact sites (white arrow) in live HeLa cells expressing lysosomal marker, BFP-lysosomes and mitochondrial outer membrane marker, mEmerald-Tom20 along with HA-tagged TRPML1 and HA-tag nanobody, HA-mCherry. **B**, Observed localization of TRPML1-HA marking mitochondria-lysosome contacts compared to TRPML1-HA localization by random chance (expected) in live HeLa cells expressing lysosomal marker, BFP-lysosomes and mitochondrial outer membrane marker, mEmerald-Tom20 along with HA-tagged TRPML1 and HA-tag nanobody, HA-mCherry (n = 40 cells). **C**, Immunoprecipitation of TRPML1-GFP or GFP (control) with anti-GFP beads (i) with indicated bands for TRPML1 monomer and oligomers (black arrows) or GFP (green arrow), and co-immunoprecipitation of TRPML1-GFP with endogenous VDAC1 (red arrow) but not VDAC2 or VDAC3 (ii) (n = 3 biological replicates). **D**, Mitochondrial calcium response in live HeLa cells expressing mitochondrial-matrix targeted calcium sensor, Mito-R-GECO1, and either wild-type (WT) or mutant (E73Q) VDAC1, in response to TRPML1 activation with ML-SA1 (31.25 μM) at t = 0 s with representative time-lapse confocal images (n = 22 cells for each condition). **E**, Mitochondrial calcium response in live HeLa cells expressing mitochondrial-matrix targeted calcium sensor, Mito-R-GECO1, and either wild-type (WT) or mutant (E264A) MCU, in response to TRPML1 activation with ML-SA1 (31.25 μM) at t = 0 s with representative time-lapse confocal images (n = 20 cells for each condition). **F**, Expression level measured by mean fluorescence intensity of SNAP-tagged wild-type or mutant (E73Q) VDAC1 in live HeLa cells labeled with SNAP-Cell 647 ligand (n = 22 cells for each condition). **G**, Expression level measured by mean fluorescence intensity of SNAP-tagged wild-type or mutant (E264A) MCU in live HeLa cells labeled with SNAP-Cell 647 ligand (n = 20 cells for each condition). Data are means ± s.e.m. (****P<0.0001, ns, not significant, Fisher's exact test (**B**) unpaired two-tailed t-test (**F-G**)). Scale bar, 1 μm (**A);** 10 μm (**D-E**).

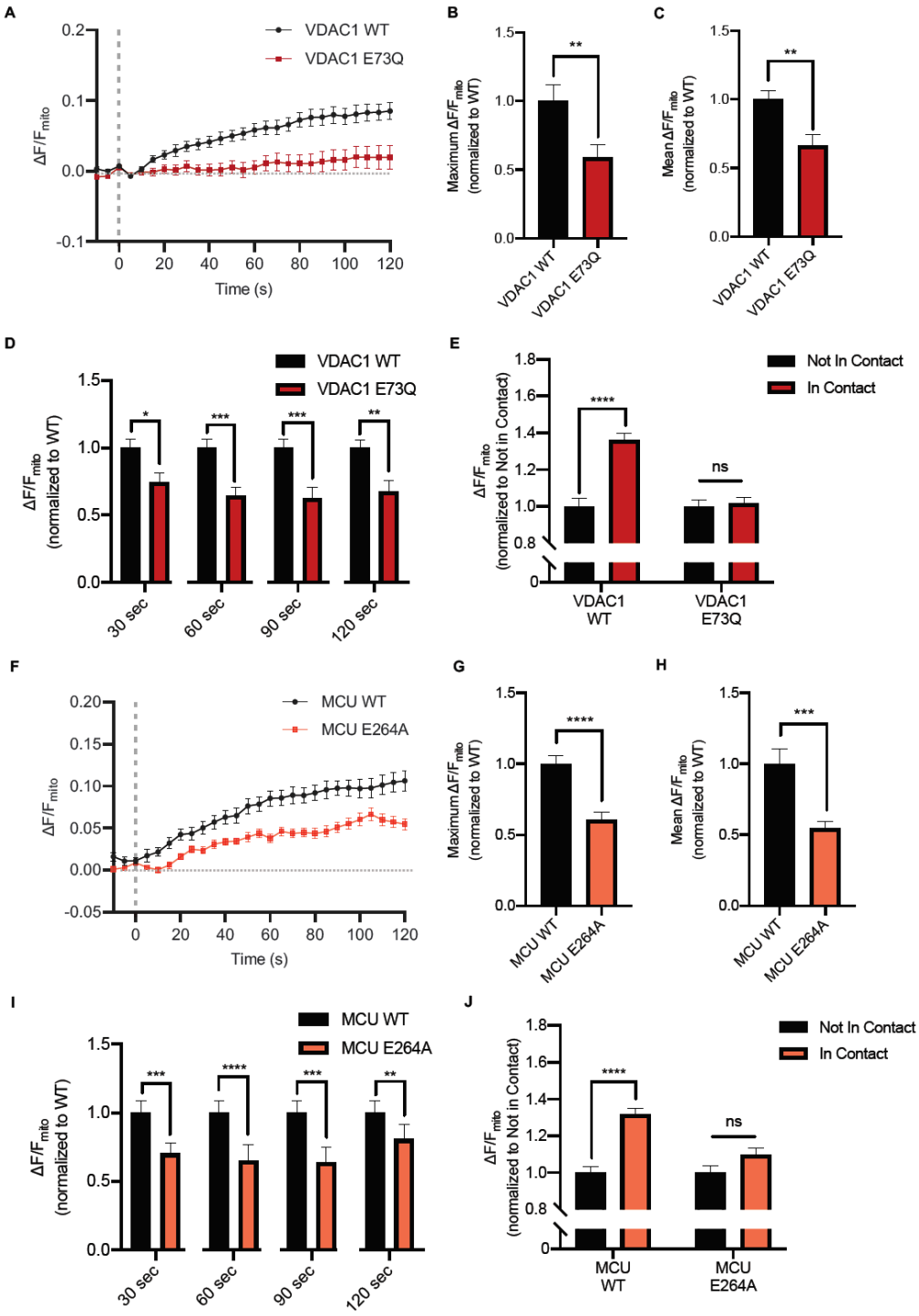
A
VDAC1 WT
VDAC1 E73Q
ΔF/F mito
Time (s)
B
Maximum ΔF/F mito (normalized to WT)
VDAC1 WT
VDAC1 E73Q
C
Mean ΔF/F mito (normalized to WT)
VDAC1 WT
VDAC1 E73Q
D
VDAC1 WT
VDAC1 E73Q
ΔF/F mito (normalized to WT)
30 sec
60 sec
90 sec
120 sec
E
Not In Contact
In Contact
ΔF/F mito (normalized to Not in Contact)
ns
VDAC1 WT
VDAC1 E73Q
F
MCU WT
MCU E264A
ΔF/F mito
Time (s)
G
Maximum ΔF/F mito (normalized to WT)
MCU WT
MCU E264A
H
Mean ΔF/F mito (normalized to WT)
MCU WT
MCU E264A
I
MCU WT
MCU E264A
ΔF/F mito (normalized to WT)
30 sec
60 sec
90 sec
120 sec
J
Not In Contact
In Contact
ΔF/F mito (normalized to Not in Contact)
ns
MCU WT
MCU E264A

Figure 18: VDAC1 and the MCU modulate mitochondrial uptake of lysosomal calcium at mitochondria-lysosome contact sites. **A**, Mitochondrial calcium response (ΔF/F) in live HeLa cells expressing mitochondrial-matrix targeted calcium sensor, Mito-R-GECO1, and either wild-type (WT) or mutant (E73Q) VDAC1 in response to TRPML1 activation with ML-SA1 (31.25 μM) at t = 0 s (n = 22 cells for each condition). **B-D**, Quantification of maximum mitochondrial calcium response (**B**), mean mitochondrial calcium response (**C**) and mitochondrial calcium response at 30, 60, 90 and 120 seconds (**D**) after TRPML1 activation with ML-SA1 (31.25 μM) in live HeLa cells expressing VDAC1 WT or VDAC1 E73Q mutant from confocal time-lapse images (from **A**) (n = 22 cells for each condition). **E**, Quantification of mitochondrial calcium responses of mitochondria in contact and not in contact with lysosomes following TRPML1 activation with ML-SA1 (31.25 μM) in live HeLa cells expressing mitochondrial matrix calcium sensor, Mito-R-GECO1, lysosomal marker, lamp1-mGFP, and either wild-type (WT) or mutant (E73Q) VDAC1 (n = 100 events from 20 cells for each condition). **F**, Mitochondrial calcium response (ΔF/F) in live HeLa cells expressing mitochondrial-matrix targeted calcium sensor, Mito-R-GECO1, and either wild-type (WT) or mutant (E264A) MCU in response to TRPML1 activation with ML-SA1 (31.25 μM) at t = 0 s (n = 20 cells for each condition). **G-I**, Quantification of maximum mitochondrial calcium response (**G**), mean mitochondrial calcium response (**H**) and mitochondrial calcium response at 30, 60, 90 and 120 seconds (**I**) after TRPML1 activation with ML-SA1 (31.25 μM) in live HeLa cells expressing MCU WT or MCU E264A mutant from confocal time-lapse images (from **F**) (n = 20 cells for each condition). **E**, Quantification of mitochondrial calcium responses of mitochondria in contact and not in contact with lysosomes following TRPML1 activation with ML-SA1 (31.25 μM) in live HeLa cells expressing mitochondrial matrix calcium sensor, Mito-R-GECO1, lysosomal marker, lamp1-mGFP, and either wild-type (WT) or mutant (E264A) MCU (n = 100 events from 20 cells for each condition). Data are means ± s.e.m. (*P<0.05, **P<0.01, ***P<0.001, ****P<0.0001, ns, not significant, unpaired two-tailed t-test).

Loss of TRPML1 function in MLIV patient fibroblasts disrupts mitochondria-lysosome contact and calcium dynamics

Loss of function mutations in TRPML1 cause the autosomal recessive lysosomal storage disorder, MLIV (Bassi et al., 2000; M. Sun et al., 2000), which has been associated with both lysosomal (LaPlante et al., 2006; S. Park et al., 2016; Shen et al., 2012; Soyombo et al., 2006; Vergarajauregui et al., 2008) and mitochondrial aberrations (Eichelsdoerfer et al., 2010; Jennings et al., 2006). Given that we found TRPML1 to be important for the regulation of mitochondrial calcium dynamics via direct transfer of calcium at mitochondria-lysosome contact sites, we evaluated whether MLIV patient fibroblasts had defective mitochondrial calcium dynamics as a result of loss of TRPML1 function. We treated fibroblasts from MLIV patients and age-matched healthy controls with ML-SA1 to activate TRPML1 and examined mitochondrial calcium dynamics (Mito-R-GECO1). While control fibroblasts showed a significant increase in total mitochondrial calcium upon TRPML1 activation, this was reduced in MLIV patient fibroblasts (**Fig. 19A**). Consistent with these findings, maximum mitochondrial calcium, mean mitochondrial calcium and mitochondrial calcium at 30 seconds was also significantly decreased in MLIV patient lines (**Fig. 19B-D**). Moreover, MLIV patient fibroblasts showed defects in contact-dependent calcium transfer. In control fibroblasts, mitochondria in contact with lysosomes showed a significantly higher increase in calcium influx following TRPML1 activation compared to those not in contact with lysosomes. In contrast, there was no difference in calcium influx between mitochondria in and not in contact with lysosomes in MLIV fibroblasts (**Fig. 19E**).

In addition to changes in contact-dependent mitochondrial calcium responses, MLIV fibroblasts also displayed abnormal mitochondria-lysosome contact dynamics. Interestingly, MLIV fibroblasts had a significantly increased percentage of lysosomes in stable contact (> 10

seconds) with mitochondria compared to control fibroblasts (**Fig. 19F**) and the duration of mitochondria-lysosome contact tethering was also significantly prolonged (**Fig. 19G**). Together, these data suggest that loss of TRPML1 function in MLIV may contribute to disease pathogenesis by dysregulating mitochondrial calcium dynamics at contact sites and additionally disrupt mitochondria-lysosome contact tethering dynamics. We thus propose a model in which TRPML1-mediated lysosomal calcium efflux results in mitochondrial calcium influx preferentially at mitochondria-lysosome contacts through the mitochondrial channels VDAC1 and the MCU, and that calcium transfer at mitochondria-lysosome contact sites is consequently disrupted in the lysosomal storage disorder MLIV due to loss of function TRPML1 mutations.

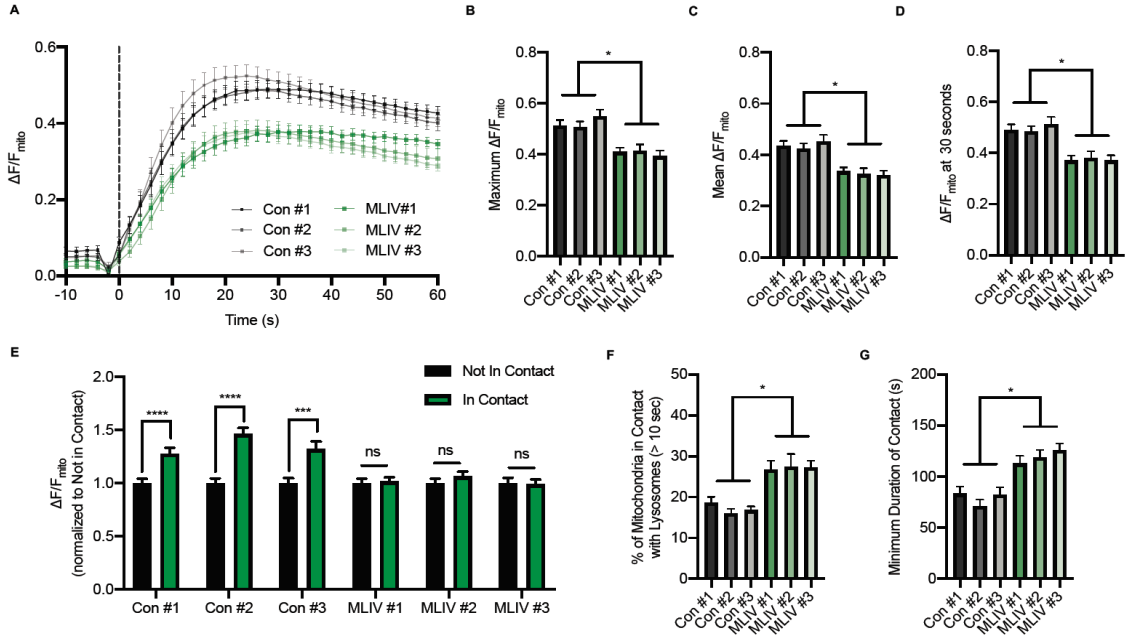

Figure 19: Loss of TRPML1 function in MLIV patient fibroblasts disrupts mitochondria-lysosome contact and calcium dynamics. A, Mitochondrial calcium response (ΔF/F) in fibroblasts from MLIV patients (MLIV #1, MLIV #2, MLIV #3) or age-matched controls (Con #1, Con #2, Con #3) expressing Mito-R-GECO1 in response to TRPML1 activation with ML-SA1 (31.25 μM) at $t = 0$ s ($n = 20$ cells for each condition). **B-D**, Quantification of maximum mitochondrial calcium response (**B**), mean mitochondrial calcium response (**C**) and mitochondrial calcium response at 30 seconds (**D**) after TRPML1 activation with ML-SA1 (31.25 μM) from fibroblasts from **A** ($n = 20$ cells for each condition). **E**, Quantification of mitochondrial calcium responses of mitochondria in contact and not in contact with lysosomes following TRPML1 activation with ML-SA1 (31.25 μM) in MLIV and control fibroblasts expressing Mito-R-GECO1 and lamp1-mGFP ($n = 100$ events from 20 cells for each condition). **F**, **G**, Quantification of percentage of mitochondria-lysosome contacts (> 10 s; **F**, $n = 10$ cells for each condition) and duration of contacts (**G**, $n = 70$ events from 10 cells for each condition) in MLIV and control fibroblasts expressing Tom20-mApple, and lamp1-mGFP. Data are means ± s.e.m. (*P<0.05, ***P<0.001, ****P<0.0001, ns, not significant, one-way ANOVA with Tukey's post-hoc test (**B-E**, **G**), unpaired two-tailed t-test (**F**)).

Conclusions

In summary, we identified a role of mitochondria-lysosome contact sites in modulating intracellular calcium dynamics, whereby TRPML1-mediated lysosomal calcium efflux leads to mitochondrial calcium influx preferentially at mitochondria-lysosome contact sites. TRPML1-mediated increase in mitochondrial calcium is further modulated by VDAC1 and the MCU on the outer and inner mitochondrial membranes, respectively. Importantly, we show that mitochondrial calcium dynamics are disrupted in the lysosomal storage disorder MLIV which results from loss of TRPML1 function and that altered mitochondrial calcium dynamics in MLIV are dependent on mitochondria-lysosome contacts, providing further evidence for the convergence of lysosomal and mitochondrial dysfunction in disease.

CHAPTER 4.

DISCUSSION

Mitochondria-lysosome contacts as regulators of mitochondrial dynamics

Mitochondria-lysosome contacts were previously reported to functionally mark sites of mitochondrial fission (Wong et al., 2018) but whether mitochondria-lysosome contact sites could modulate other forms of mitochondrial dynamics was unknown. Our findings indicate that mitochondria-lysosome contacts also promote inter-mitochondrial contact untethering, which in itself is an important regulator of mitochondrial motility (Wong, Peng, et al., 2019) (**Fig. 20**).

Interestingly, we observed that inter-mitochondrial contact dynamics were further coupled to other inter-organelle contact sites. ER tubules marked inter-mitochondrial contact untethering events, in addition to their previously reported localization at both mitochondrial fission and fusion events (Friedman et al., 2011; Guo et al., 2018) suggesting their ubiquitous localization at multiple mitochondrial events. In addition, while studies labeling mitochondria with matrix markers previously described mitochondrial constriction events prior to fission as marked by both ER tubules and Drp1 oligomers (Chakrabarti et al., 2018; Cho et al., 2017; Friedman et al., 2011), some of these events may have been two distinct mitochondria tethered at inter-mitochondrial contact sites prior to an untethering event which appear similar when visualized with mitochondrial matrix markers, and are also marked by ER tubules and Drp1 oligomers. In contrast, lysosomes preferentially marked inter-mitochondrial untethering events over mitochondrial fusion events, and were also reported to actively promote inter-mitochondrial contact untethering via lysosomal RAB7 GTP hydrolysis at mitochondria-lysosome contact sites (Wong, Peng, et al., 2019; Wong et al., 2018) mediated by the mitochondrial Rab7-GAP (TBC1D15) recruited to mitochondria by

Fis1 (Onoue et al., 2013; Peralta et al., 2010; Wong, Peng, et al., 2019; Yamano et al., 2014; X. M. Zhang et al., 2005). Inter-mitochondrial contact formation and subsequent untethering were further regulated by Mfn1/2 and Drp1 GTP hydrolysis, consistent with early studies showing their effects on mitochondrial clustering and aggregation (Santel & Fuller, 2001; Smirnova et al., 2001; Smirnova, Shurland, Ryazantsev, & Van Der Bliek, 1998). Thus, multiple lysosomal and mitochondrial GTPases together converge to regulate inter-mitochondrial contact dynamics.

Importantly, as multiple human diseases are linked to defective mitochondrial dynamics (Alexander et al., 2000; Burte et al., 2015; Delettre et al., 2000; Zuchner et al., 2004), further elucidating the dynamic inter-organelle interactions shaping mitochondrial networks is critical for understanding disease pathogenesis. Surprisingly, we found that multiple forms of disease-linked Charcot-Marie-Tooth Type 2 including Mfn2 (CMT2A), RAB7 (CMT2B) and TRPV4 (CMT2C) converged on inefficient inter-mitochondrial contact untethering dynamics and defective mitochondrial motility. Of note, mitochondrial motility was also previously shown to be impaired by CMT2-disease linked mutations in Mfn2 (Baloh, Pestronk, & Milbrandt, 2007; A. Misko et al., 2010; A. L. Misko, Sasaki, Tuck, Milbrandt, & Baloh, 2012; Rocha et al., 2018) and recently by mutant Rab7 (Cioni et al., 2019). Our study thus points to a potentially important role for this pathway in CMT Type 2, consistent with a growing list of CMT genes implicated in regulating mitochondrial dynamics (Korobova et al., 2013; J. E. Lee et al., 2016; Wong et al., 2018; Zuchner et al., 2004) Ultimately, understanding the pathways involved in regulating mitochondrial networks will provide insight into both cellular metabolism and pathogenic mitochondrial dysfunction in disease.

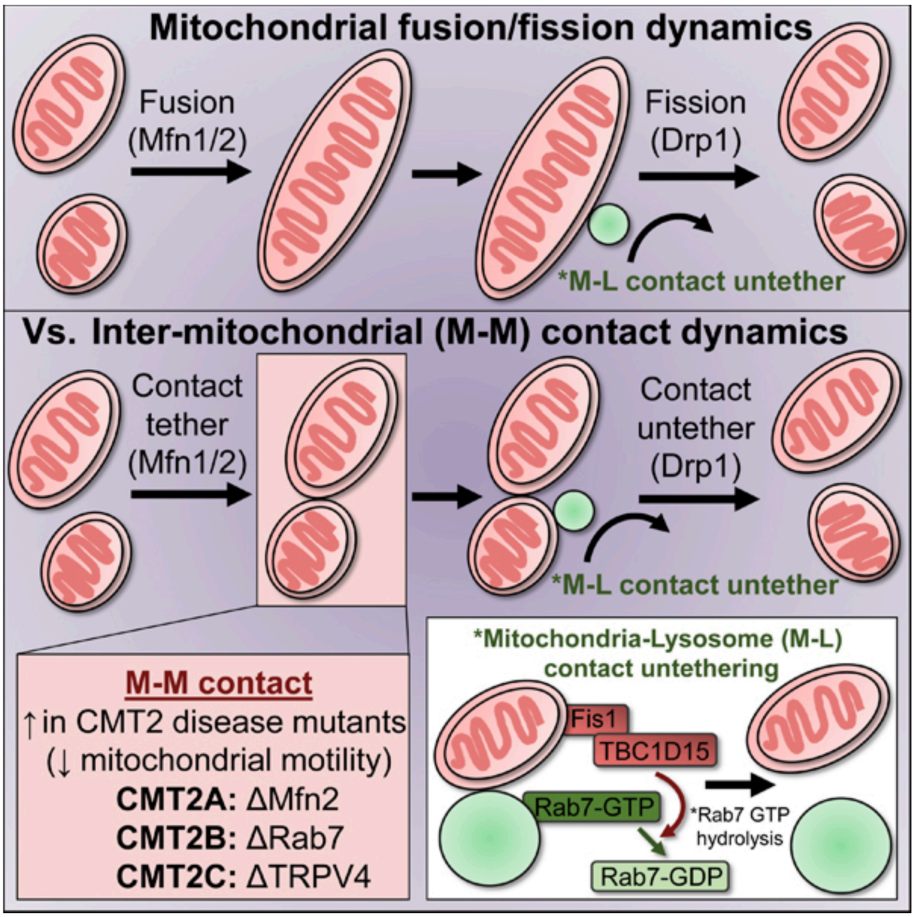

Figure 20: Mitochondria-lysosome contact sites as regulators of mitochondrial dynamics. Model depicting the contribution of inter-mitochondrial contacts to mitochondrial dynamics alongside mitochondrial fusion and fission. Inter-mitochondrial contact tethering is regulated by the GTPases Mfn1/2, whereas inter-mitochondrial contact untethering is mediated by the GTPase Drp1. Inter-mitochondrial contact untethering is further regulated by mitochondria-lysosome contacts wherein lysosomal Rab7 GTP hydrolysis mediated by TBC1D15 recruitment onto mitochondria via Fis1 promotes lysosomal untethering from mitochondria and subsequent untethering of inter-mitochondrial contact sites. Importantly, inter-mitochondrial contacts are perturbed in various forms of Charcot-Marie-Tooth type 2 disease resulting in decreased mitochondrial motility.

Mitochondria-lysosome contacts as regulators of mitochondrial calcium dynamics

Previously, inter-organelle contact sites were shown to be able to act as platforms for metabolite and ion transfer (Bartok et al., 2019; Hayashi & Su, 2007; Hirabayashi et al., 2017; Lim et al., 2019; Rizzuto et al., 1998; Szabadkai et al., 2006). However, whether recently identified mitochondria-lysosome contact sites could similarly serve to promote direct inter-organelle transfer of metabolites and ions, such as calcium, remained unelucidated. Our results indicate that mitochondria-lysosome contacts are able to facilitate the direct transfer of calcium from lysosomes to mitochondria, a process which is mediated by the lysosomal calcium efflux channel TRPML1 and the mitochondrial outer and inner membrane proteins VDAC1 and MCU, respectively (Peng, Wong, & Krainc, 2020) (**Fig. 21**).

Our work further establishes the growing importance of inter-organelle contact sites in the regulation of cellular homeostasis. Defects in inter-organelle contact sites have been implicated in multiple human diseases including lysosomal storage disorders (Lim et al., 2019), peroxisomal diseases (Chu et al., 2015) and neurodegenerative disorders (Allison et al., 2017; K. S. Lee et al., 2018; Liao et al., 2019; Valadas et al., 2018). Recently, mitochondria-lysosome contact sites have been shown to be an important regulator of mitochondrial and lysosomal crosstalk independent of lysosomal degradation of mitochondria (Wong, Kim, et al., 2019; Wong et al., 2018), and to be involved in regulating mitochondrial fission and inter-mitochondrial contact untethering (Wong, Peng, et al., 2019; Wong et al., 2018), as well as the transfer of metabolites such as cholesterol (Hoglinger et al., 2019). Here, we find that mitochondria-lysosome contact sites further play a key role in regulating calcium transfer between these two organelles which is disrupted in a lysosomal storage disorder. Uncovering the diverse functions of mitochondria-lysosome contact sites shall

inform our understanding of how contact sites contribute to both physiological and pathophysiological states.

Our findings also expand upon the previously described physiological roles of TRPML1. TRPML1 is a non-selective cation channel that mediates lysosomal calcium efflux (Q. Chen et al., 2017; Dong et al., 2008; Fine et al., 2018; Hirschi et al., 2017; M. Li et al., 2017; Schmiege et al., 2017) and regulates various lysosomal functions including lysosomal exocytosis, membrane trafficking and lysosomal biogenesis (C. C. Chen et al., 2014; Di Paola, Scotto-Rosato, & Medina, 2018; Medina et al., 2015; Samie et al., 2013; Scotto Rosato et al., 2019; W. Wang et al., 2015; X. Zhang et al., 2016). Our data suggest that in addition to regulating lysosomal dynamics and function, TRPML1 directly impacts mitochondrial homeostasis by modulating mitochondrial calcium dynamics via mitochondria-lysosome contact sites. Mitochondria-lysosome contacts may act as platforms to provide localized pockets of high calcium concentration required for influx into mitochondria and moreover, contact-dependent transfer of calcium from lysosomes to mitochondria may serve as a mechanism to spatially regulate calcium transfer to a subset of mitochondria to facilitate downstream, calcium-dependent mitochondrial functions including oxidative phosphorylation, motility and ROS signaling (Bertero & Maack, 2018; Chang, Niescier, & Min, 2011; Giorgi, Marchi, & Pinton, 2018; Tarasov, Griffiths, & Rutter, 2012; Yi, Weaver, & Hajnóczky, 2004). Indeed, mitochondrial function has also been shown to reciprocally regulate TRPML1 as increased mitochondrial ROS potentiates TRPML1 activity (X. Zhang et al., 2016). Further studies investigating how TRPML1-mediated mitochondrial calcium influx modulates mitochondrial structure, dynamics and function will provide additional insights into the direct communication between lysosomes and mitochondria.

In our study, we also identified VDAC1 on the outer mitochondrial membrane and the MCU on the inner mitochondrial membrane as mediators of mitochondrial calcium influx at mitochondria-lysosome contact sites. Although our finding of TRPML1 interactions with VDAC1 and not other VDAC isoforms is consistent with previous studies (Spooner et al., 2013), it is possible that the other VDAC isoforms, which have also been implicated in mitochondrial calcium uptake (Min et al., 2012; Naghdi & Hajnóczky, 2016; Subedi et al., 2011), may play a role in contact-dependent calcium transfer in other cell types. In addition, while we observed that mutant MCU impaired mitochondrial calcium uptake following TRPML1-mediated lysosomal calcium release, it did not completely abolish mitochondrial uptake at contact sites. Thus, our findings suggest there may be alternative, MCU-independent mechanisms of calcium influx into the mitochondrial matrix at mitochondria-lysosome contacts (Giorgi et al., 2018). Indeed, prior studies have proposed additional transporters mediating mitochondrial matrix calcium influx (Feng et al., 2013; Jiang, Zhao, & Clapham, 2009; Ryu, Beutner, Dirksen, Kinnally, & Sheu, 2010; Trenker, Malli, Fertschai, Levak-Frank, & Graier, 2007), which may also play a role in the uptake of lysosomal calcium.

Of clinical relevance, loss-of-function mutations in TRPML1 cause the autosomal recessive lysosomal storage disorder MLIV, which is characterized by psychomotor retardation, retinal degeneration and neurodevelopmental delay (Bassi et al., 2000; Dong et al., 2008; Marques & Saftig, 2019; M. Sun et al., 2000). Although the pathophysiology of MLIV remains unclear, various cellular phenotypes including defective lysosomal biogenesis, altered lysosomal pH, impaired autophagy and mitochondrial fragmentation have been described (Eichelsdoerfer et al., 2010; Jennings et al., 2006; Medina et al., 2015; Raychowdhury et al., 2004; Scotto Rosato et al., 2019; Soyombo et al., 2006; Venugopal et al., 2009; X. Zhang et al., 2016). Notably, our results

demonstrate that MLIV is also associated with defective mitochondria-lysosome contact dynamics and contact-dependent calcium transfer. It would be important in future studies to elucidate whether these altered organelle contacts in MLIV contribute to previously observed mitochondrial phenotypes and whether MLIV mutations in TRPML1 alter additional mitochondrial functions such as ATP production and mitochondrial fission/fusion dynamics in a contact-dependent manner. Given that many critical mitochondrial functions are regulated by calcium (Giorgi et al., 2018), it is possible that dysregulation of mitochondrial calcium, in conjunction with decreased lysosomal function, potentiates defects in mitochondrial metabolism and dynamics which may consequently contribute to downstream phenotypes such as mitochondrial fragmentation in MLIV disease pathogenesis.

In addition to its role in MLIV, TRPML1 has also been implicated in various neurological and lysosomal storage diseases (Bae et al., 2014; Cheng et al., 2014; J. H. Lee et al., 2015; Santoni et al., 2020; Tsunemi et al., 2019). Several disease models have shown downregulation of TRPML1 which impairs lysosomal function and promotes accumulation of toxic proteins (Tedeschi et al., 2019; L. Zhang et al., 2017). Other studies have reported misregulation of TRPML1 activity due to alterations in lipids or lysosomal pH (Giorgi et al., 2018; Raychowdhury et al., 2004). TRPML1 activity is highly regulated by specific lipids including its endogenous activator $PI(3,5)P_2$ (Dong et al., 2010) which has been suggested to be misregulated in Charcot-Marie Tooth disease and ALS (Chow et al., 2009; Nicholson et al., 2011; X. Zhang et al., 2008), and sphingomyelins and cholesterol which when accumulated in Niemann-Pick Type C, impair TRPML1-mediated lysosomal calcium release (Shen et al., 2012). Moreover, TRPML1 activity is likely regulated upstream by lysosomal pH as it has been shown that TRPML1-mediated calcium dyshomeostasis and autophagic defects are rescued by restoration of lysosomal pH but not calcium

in an Alzheimer's model (J. H. Lee et al., 2015). While these previous studies predominantly describe the role of TRPML1 in regulating lysosomal function in disease (Medina et al., 2015; Scotto Rosato et al., 2019; Shen et al., 2012; Tsunemi et al., 2019), our findings suggest that TRPML1 may also contribute to disease pathogenesis by modulating mitochondrial calcium dynamics. Altered TRPML1-mediated calcium transfer at mitochondria-lysosome contact sites and subsequent dysregulation of mitochondrial calcium dynamics may be an additional contributory mechanism to pathophysiology. Indeed, many of these diseases share cellular hallmarks including mitochondrial and lysosomal dysfunction and calcium dyshomeostasis (15-18). Importantly, TRPML1 has recently emerged as a potential therapeutic target for the treatment of neurodegenerative and lysosomal storage disorders. Studies suggest that TRPML1 agonists may act multimodally by activating various lysosomal pathways including autophagy and lysosomal exocytosis (Scotto Rosato et al., 2019; Shen et al., 2012; Tsunemi et al., 2019). Our results further highlight a potential role for therapeutically targeting TRPML1 in modulating mitochondrial calcium dynamics in disease.

In summary, this work demonstrates that lysosomes can directly transfer calcium to mitochondria at mitochondria-lysosome contacts, thereby further supporting the emerging role for both organelles as critical players in modulating calcium dynamics (Lawrence & Zoncu, 2019; Lie & Nixon, 2019; Misgeld & Schwarz, 2017) and elucidating a novel pathway by which intracellular calcium can be regulated. A broader understanding of the mechanisms underlying intracellular calcium regulation will ultimately inform our understanding of the role of mitochondria and lysosome crosstalk in both cellular homeostasis and disease.

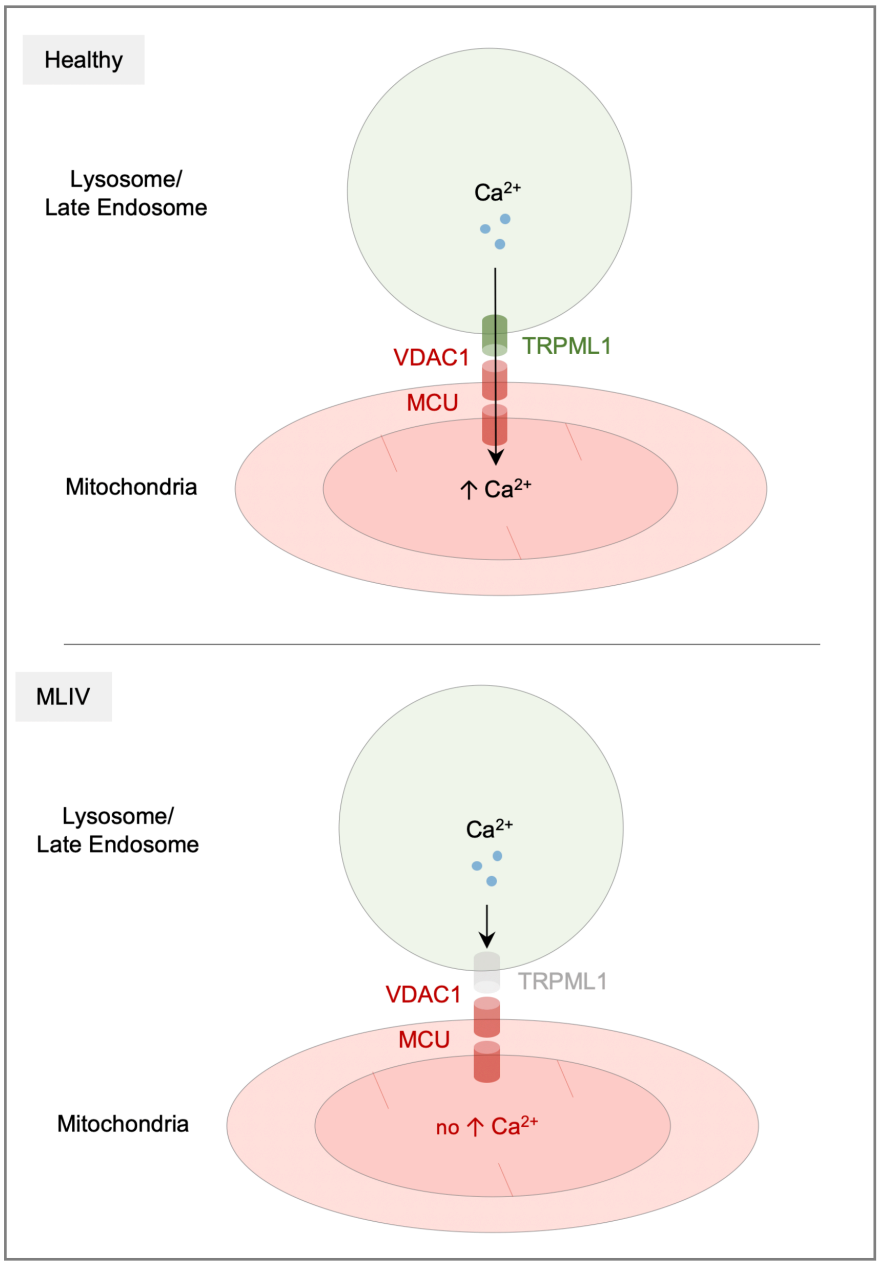

Figure 21: Mitochondria-lysosome contact sites as regulators of mitochondrial calcium dynamics. Model depicting the transfer of calcium from lysosomes to mitochondria at mitochondria-lysosome contacts. Calcium transfer is mediated by the lysosomal calcium efflux channel TRPML1 and the outer and inner mitochondrial membrane proteins VDAC1 and the MCU, respectively. Loss-of-function mutations in TRPML1, which lead to the lysosomal storage disorder Mucolipidosis type IV (MLIV), result in decreased calcium transfer from lysosomes to mitochondria at mitochondria-lysosome contacts.

Additional possible functions of mitochondria-lysosome contact sites

As other inter-organelle contact sites have been shown to be key platforms for regulating metabolite flux between organelles (Gatta & Levine, 2017), mitochondria–lysosome contact sites may similarly mediate additional functions such as transfer of lipids or iron between mitochondria and lysosomes. In addition, mitochondria–lysosome contacts also form under hypoxic conditions, which have been proposed to mediate voltage-dependent anion channel 1 (VDAC1) cleavage by endolysosomal enzymes through mitochondrial–endolysosomal microfusion (Brahimi-Horn et al., 2015).

In yeast, contact sites between mitochondria and the vacuole known as the vacuole and mitochondria patch (vCLAMP) (Elbaz-Alon et al., 2014; Honscher et al., 2014) can regulate phospholipid transport between mitochondria and vacuoles as deletions of both ER-mitochondria encounter structure (ERMES) and vCLAMP, but not ERMES alone, result in severe alterations in phospholipid composition, including accumulation of phosphatidylserine and decreased phosphatidylcholine (Honscher et al., 2014). Interestingly, yeast vCLAMP can be tethered by either: (i) mitochondrial Tom40 binding to VPS39, a protein involved in vacuolar sorting and fusion which interacts with the vacuole membrane via the vacuolar Rab GTPase Ypt7 (Elbaz-Alon et al., 2014; González Montoro et al., 2018); or (ii) mitochondrial MCP1 binding to Vps13, which is localized to the vacuole membrane via its Vps13 adaptor binding (VAB) domain binding a PxP motif on vacuolar Ypt35 (Bean et al., 2018; John Peter et al., 2017). Thus, at mitochondria–lysosome contact sites, there may be different protein complexes mediating distinct tethers or different functions, as has been suggested for VPS39 (physical tether) and VPS13/MCP1 (effectors of lipid transport) in vCLAMP. Of note, in addition to its localization at vCLAMP, yeast Vps13 has also been localized to vacuole–nucleus contact sites in yeast (Lang, John Peter, Walter, &

Kornmann, 2015), and its four human homologs (Vps13A–D) have all been linked to different human diseases. Vps13A, whose mutations are linked to Chorea-acanthocytosis (Rampoldi et al., 2001; Ueno et al., 2001), has been proposed to tether ER to mitochondria and lipid droplets (Kumar et al., 2018) and also localize to and regulate contacts between mitochondria and endolysosomes (Muñoz-Braceras, Tornero-Écija, Vincent, & Escalante, 2019). Vps13B mutations lead to Cohen syndrome (Kolehmainen et al., 2003) but has not been associated with inter-organelle contact sites, while Vps13C, whose mutations are linked to Parkinson's disease (PD) (Lesage et al., 2016), has been proposed to tether ER to late endosome/lysosomes and lipid droplets (Kumar et al., 2018). Recently, Vps13D was linked to childhood onset movement disorder and ataxia (Gauthier et al., 2018; Seong et al., 2018) and found to regulate mitochondrial dynamics (Anding et al., 2018), but its role in inter-organelle contact sites has not been directly studied. Cholesterol has also previously been shown to transport from endolysosomes to mitochondria via the steroidogenic acute regulatory protein-related lipid transfer (START) domain-containing protein, MLN64 (Charman, Kennedy, Osborne, & Karten, 2010; M. Zhang et al., 2002). More recently, it was shown that the lysosomal cholesterol transporter NPC1 was a regulator of ER-endolysosomal and mitochondria-lysosome contacts. Because the absence of NPC1 resulted in decreased ER-endolysosomal contacts with a concurrent increase in mitochondria-lysosome contacts, it was suggested that mitochondria-lysosome contacts may also serve as platforms for lysosomal cholesterol transfer (Hoglinger et al., 2019).

Iron is another metabolite which can be stored by both mitochondrial and endolysosomal compartments. Entry of iron into mitochondria occurs via mitoferrin-1 and -2 solute carriers on the inner mitochondrial membrane (Richardson et al., 2010), where it is subsequently incorporated into iron–sulfur clusters in the matrix, which act as cofactors for various enzymes in the citric acid

cycle and electron transport chain (Rouault, 2012). While delivery of iron to mitochondria remains poorly understood, one proposed mechanism involves direct endosomal delivery through a 'kiss and run' interaction (Das, Nag, Mason, & Barroso, 2016; Sheftel, Zhang, Brown, Shirihai, & Ponka, 2007). In this model, iron bound to Tf (transferrin) is internalized by the cell and is subsequently released within the endosome upon acidification. Docking of Tf-endosomes onto mitochondria, either through VDAC1 or the divalent metal transporter-1 (DMT1) on the outer mitochondrial membrane (Wolff et al., 2018; Wolff et al., 2014), provides the physical tether to allow for iron transfer. As lysosomes also serve as iron storage compartments, mitochondria–lysosome contact sites may also regulate the labile iron pool, similar to mitochondria–endosome contact sites. Interestingly, transferrin receptor-2 (TfR2) mediates lysosomal transferrin delivery, and deficiency in TfR2 results in reduced mitochondrial size and heme content in erythroid progenitors (Khalil et al., 2017). Furthermore, iron overload in fibroblasts from patients with neurodegeneration with brain iron accumulation (NBIA) results in mitochondrial depolarization, reduced ATP production, and decreased lysosomal proteolytic activity (Seibler et al., 2018), suggesting that mitochondria–lysosome contact site dysfunction and iron flux may be intricately connected.

Additionally, mitochondria–lysosome contact sites may also dynamically interact with other organelles, such as the ER. Indeed, mitochondria and lysosomes in contact with one another can also simultaneously contact the ER (Wong et al., 2018), and mitochondrial fission sites marked by lysosomes are also positive for ER tubules (Wong et al., 2018), which were previously found to mark sites of mitochondrial division (Friedman et al., 2011). Moreover, as ER–mitochondria and ER–late endosome/lysosomal contacts form frequently (Valm et al., 2017) and further regulate both mitochondrial and lysosomal homeostasis (H. Wu et al., 2018), modulation of proteins at ER

contacts such as those involved in regulating late endosomal dynamics (Hoyer et al., 2018; Rowland et al., 2014) may further modulate mitochondria–lysosome contact function and tethering. Conversely, as ER–endosome contacts can be modulated via the Rab7 effector protrudin (Elbaz-Alon et al., 2020; Raiborg et al., 2015), mitochondria–lysosome contacts may also modulate ER function via regulation of Rab7 GTP hydrolysis and the ability of Rab7 to recruit its effector proteins. Finally, as multiple other organelles also form contacts with both mitochondria and lysosome/late endosomes (Gatta & Levine, 2017), it is likely that similar to the regulation of lipid transport in yeast, the maintenance of organelle homeostasis involves multiple different types of inter-organelle contact sites that may regulate and compensate for one another.

Contributions of mitochondria-lysosome contacts to neurological disease

In addition to our data showing dysregulation of mitochondria-lysosome contact sites in Charcot-Marie-Tooth type 2 and mucolipidosis type IV, the role of mitochondrial and lysosomal dysfunction in a broad range of neurological disorders suggests that mitochondria-lysosome contact dyshomeostasis may also be a contributory pathophysiological mechanism.

Parkinson's disease (PD) is the second most common neurodegenerative disorder, with motor symptoms caused by dopaminergic neurodegeneration in the substantia nigra (Kalia & Lang, 2015; Wong & Krainc, 2017). Like CMT2, PD has been both genetically and functionally linked to mitochondrial and lysosomal dysfunction, with the identification of familial mutations in mitochondrial-associated genes (Parkin, PINK1, and DJ-1) and endolysosomal-associated genes (VPS35, PARK9, and GBA1) (Plotegher & Duchen, 2017a). Moreover, both mitochondrial and lysosomal dysfunction have been observed in human dopaminergic neurons from idiopathic PD patients (Burbulla et al., 2017), suggesting that these two organelles play a critical role in disease

progression. As mentioned above, mutations in VPS13C, a human homologue of the yeast Vps13 that mediates vCLAMP tethering (John Peter et al., 2017; Lang et al., 2015; J. S. Park et al., 2016), also lead to autosomal recessive PD (Lesage et al., 2016). Several familial PD mutations, such as in VPS35 and Parkin, also decrease Rab7 GTP-binding (Jia et al., 2016; Song, Trajkovic, Tsunemi, & Krainc, 2016), further highlighting a potential role for defective mitochondria–lysosome contact regulation in PD pathogenesis.

Lysosomal storage disorders (LSDs) encompass a group of more than 70 diseases involving lysosomal dysfunction (Mc Donald & Krainc, 2017; Platt, d'Azzo, Davidson, Neufeld, & Tifft, 2018). The most common LSD is caused by autosomal recessive mutations in glucocerebrosidase 1 (GBA1), which leads to Gaucher's disease and is also a risk factor for PD. Interestingly, mitochondrial dysfunction, such as decreased mitochondrial membrane potential, increased ROS and impaired respiration, and morphological abnormalities have been observed in multiple Gaucher's models, including patient fibroblasts, flies, and mouse primary neurons (Cleeter et al., 2013; de la Mata et al., 2015; H. Li et al., 2019; Osellame et al., 2013; Schöndorf et al., 2018; Xu et al., 2014). Additionally, mitochondrial dysfunction and increased oxidative stress have been found in multiple other LSDs, including Niemann-Pick disease type C and neuronal ceroid lipofuscinosis (Plotegher & Duchen, 2017b), suggesting that mitochondrial defects may be a common theme across LSDs and may be partially mediated by defective mitochondria–lysosome contact site function secondary to lysosomal dysfunction. Of note, mitochondrial dysfunction may further exacerbate lysosomal storage defects, as mitochondrial respiration deficiency via TFAM mutation is sufficient to cause lysosomal sphingomyelin accumulation and elicit a proinflammatory response (Baixauli et al., 2015). Likewise, mitochondrial oxidant stress can lead to the oxidation of specific cysteine residues in the catalytic

region of GBA1, further contributing to decreased GBA1 enzymatic activity (Burbulla et al., 2017). Interestingly, it was recently observed that mitochondria-lysosome contact site dynamics were disrupted in a *GBA1* human iPSC-derived dopaminergic neuronal model of Parkinson's disease, further suggesting the contribution of mitochondria-lysosome contact sites to neurological disease phenotypes (Kim, Wong, Gao, & Krainc, 2021).

Future studies on mitochondria-lysosome contact sites

Looking forward, multiple techniques and approaches will be crucial for shedding further light on the organization and function of mitochondria–lysosome contact sites. These include new advanced imaging techniques, such as grazing incidence structured illumination microscopy (GI-SIM) for nanoscale resolution over millisecond timescales (Guo et al., 2018)combined with internal tagging of endogenous proteins (Kumar et al., 2018) and single molecule tracking to visualize protein dynamics at contact sites. In addition, techniques such as the use of protein-fragment complementation libraries, which enable systematic analysis of membrane protein topology (Weill et al., 2018), or proximity biotinylation with APEX2 (Hung et al., 2017) will help to identify new regulators of membrane contact sites. Ultimately, future studies on the function and regulation of these contacts will be critical for advancing our understanding of the roles mitochondria and lysosomes play in health and disease.

REFERENCES

Abeliovich, A., & Gitler, A. D. (2016). Defects in trafficking bridge Parkinson's disease pathology and genetics. *Nature, 539*(7628), 207-216. doi:10.1038/nature20414

Aits, S., & Jaattela, M. (2013). Lysosomal cell death at a glance. *J Cell Sci, 126*(Pt 9), 1905-1912. doi:10.1242/jcs.091181

Alexander, C., Votruba, M., Pesch, U. E., Thiselton, D. L., Mayer, S., Moore, A., . . . Wissinger, B. (2000). OPA1, encoding a dynamin-related GTPase, is mutated in autosomal dominant optic atrophy linked to chromosome 3q28. *Nat Genet, 26*(2), 211-215. doi:10.1038/79944

Allison, R., Edgar, J. R., Pearson, G., Rizo, T., Newton, T., Gunther, S., . . . Reid, E. (2017). Defects in ER-endosome contacts impact lysosome function in hereditary spastic paraplegia. *J Cell Biol, 216*(5), 1337-1355. doi:10.1083/jcb.201609033

Anding, A. L., Wang, C., Chang, T. K., Sliter, D. A., Powers, C. M., Hofmann, K., . . . Baehrecke, E. H. (2018). Vps13D Encodes a Ubiquitin-Binding Protein that Is Required for the Regulation of Mitochondrial Size and Clearance. *Curr Biol, 28*(2), 287-295.e286. doi:10.1016/j.cub.2017.11.064

Aston, D., Capel, R. A., Ford, K. L., Christian, H. C., Mirams, G. R., Rog-Zielinska, E. A., . . . Terrar, D. A. (2017). High resolution structural evidence suggests the Sarcoplasmic Reticulum forms microdomains with Acidic Stores (lysosomes) in the heart. *Sci Rep, 7*, 40620. doi:10.1038/srep40620

Auer-Grumbach, M., Olschewski, A., Papi, L., Kremer, H., McEntagart, M. E., Uhrig, S., . . . Guelly, C. (2010). Alterations in the ankyrin domain of TRPV4 cause congenital distal SMA, scapuloperoneal SMA and HMSN2C. *Nature Genetics, 42*(2), 160-164. doi:10.1038/ng.508

Bae, M., Patel, N., Xu, H., Lee, M., Tominaga-Yamanaka, K., Nath, A., . . . Haughey, N. J. (2014). Activation of TRPML1 clears intraneuronal Abeta in preclinical models of HIV infection. *J Neurosci, 34*(34), 11485-11503. doi:10.1523/jneurosci.0210-14.2014

Baixauli, F., Acín-Pérez, R., Villarroya-Beltrí, C., Mazzeo, C., Nuñez-Andrade, N., Gabandé-Rodriguez, E., . . . Mittelbrunn, M. (2015). Mitochondrial Respiration Controls Lysosomal Function during Inflammatory T Cell Responses. *Cell Metab, 22*(3), 485-498. doi:10.1016/j.cmet.2015.07.020

Balderhaar, H. J., & Ungermann, C. (2013). CORVET and HOPS tethering complexes - coordinators of endosome and lysosome fusion. *J Cell Sci, 126*(Pt 6), 1307-1316. doi:10.1242/jcs.107805

Baloh, R. H., Pestronk, A., & Milbrandt, J. (2007). Altered axonal mitochondrial transport in the pathogenesis of Charcot-Marie-Tooth disease from mitofusin 2 mutations. *Neurology, 68*, A340-A341.

Bannerman, P., Burns, T., Xu, J., Miers, L., & Pleasure, D. (2016). Mice hemizygous for a pathogenic mitofusin- 2 allele exhibit hind limb/foot gait deficits and phenotypic perturbations in nerve and muscle. *PLoS ONE, 11*(12). doi:10.1371/journal.pone.0167573

Bartok, A., Weaver, D., Golenar, T., Nichtova, Z., Katona, M., Bansaghi, S., . . . Hajnoczky, G. (2019). IP3 receptor isoforms differently regulate ER-mitochondrial contacts and local calcium transfer. *Nat Commun, 10*(1), 3726. doi:10.1038/s41467-019-11646-3

Bassi, M. T., Manzoni, M., Monti, E., Pizzo, M. T., Ballabio, A., & Borsani, G. (2000). Cloning of the gene encoding a novel integral membrane protein, mucolipidin-and identification of the two major founder mutations causing mucolipidosis type IV. *Am J Hum Genet, 67*(5), 1110-1120. doi:10.1016/s0002-9297(07)62941-3

Bathori, G., Csordas, G., Garcia-Perez, C., Davies, E., & Hajnoczky, G. (2006). Ca2+-dependent control of the permeability properties of the mitochondrial outer membrane and voltage-dependent anion-selective channel (VDAC). *J Biol Chem, 281*(25), 17347-17358. doi:10.1074/jbc.M600906200

Baughman, J. M., Perocchi, F., Girgis, H. S., Plovanich, M., Belcher-Timme, C. A., Sancak, Y., . . . Mootha, V. K. (2011). Integrative genomics identifies MCU as an essential component of the mitochondrial calcium uniporter. *Nature, 476*(7360), 341-345. doi:10.1038/nature10234

Bean, B. D. M., Dziurdzik, S. K., Kolehmainen, K. L., Fowler, C. M. S., Kwong, W. K., Grad, L. I., . . . Conibear, E. (2018). Competitive organelle-specific adaptors recruit Vps13 to membrane contact sites. *J Cell Biol, 217*(10), 3593-3607. doi:10.1083/jcb.201804111

Bertero, E., & Maack, C. (2018). Calcium Signaling and Reactive Oxygen Species in Mitochondria. *Circ Res, 122*(10), 1460-1478. doi:10.1161/circresaha.118.310082

Bononi, A., Missiroli, S., Poletti, F., Suski, J. M., Agnoletto, C., Bonora, M., . . . Pinton, P. (2012). Mitochondria-associated membranes (MAMs) as hotspot Ca(2+) signaling units. *Adv Exp Med Biol, 740*, 411-437. doi:10.1007/978-94-007-2888-2_17

Bonora, M., Morganti, C., Morciano, G., Giorgi, C., Wieckowski, M. R., & Pinton, P. (2016). Comprehensive analysis of mitochondrial permeability transition pore activity in living cells using fluorescence-imaging-based techniques. *Nat Protoc, 11*(6), 1067-1080. doi:10.1038/nprot.2016.064

Brahimi-Horn, M. C., Lacas-Gervais, S., Adaixo, R., Ilc, K., Rouleau, M., Notte, A., . . . Mazure, N. M. (2015). Local mitochondrial-endolysosomal microfusion cleaves voltage-dependent anion channel 1 to promote survival in hypoxia. *Mol Cell Biol, 35*(9), 1491-1505. doi:10.1128/mcb.01402-14

Britton, S., Dernoncourt, E., Delteil, C., Froment, C., Schiltz, O., Salles, B., . . . Calsou, P. (2014). DNA damage triggers SAF-A and RNA biogenesis factors exclusion from

chromatin coupled to R-loops removal. *Nucleic Acids Res, 42*(14), 9047-9062. doi:10.1093/nar/gku601

Burbulla, L. F., Song, P., Mazzulli, J. R., Zampese, E., Wong, Y. C., Jeon, S., . . . Krainc, D. (2017). Dopamine oxidation mediates mitochondrial and lysosomal dysfunction in Parkinson's disease. *Science, 357*(6357), 1255-1261. doi:10.1126/science.aam9080

Burte, F., Carelli, V., Chinnery, P. F., & Yu-Wai-Man, P. (2015). Disturbed mitochondrial dynamics and neurodegenerative disorders. *Nat Rev Neurol, 11*(1), 11-24. doi:10.1038/nrneurol.2014.228

Chakrabarti, R., Ji, W. K., Stan, R. V., Sanz, J. J., Ryan, T. A., & Higgs, H. N. (2018). INF2-mediated actin polymerization at the ER stimulates mitochondrial calcium uptake, inner membrane constriction, and division. *Journal of Cell Biology, 217*(1), 251-268. doi:10.1083/jcb.201709111

Chang, K. T., Niescier, R. F., & Min, K. T. (2011). Mitochondrial matrix Ca2+ as an intrinsic signal regulating mitochondrial motility in axons. *Proc Natl Acad Sci U S A, 108*(37), 15456-15461. doi:10.1073/pnas.1106862108

Charman, M., Kennedy, B. E., Osborne, N., & Karten, B. (2010). MLN64 mediates egress of cholesterol from endosomes to mitochondria in the absence of functional Niemann-Pick Type C1 protein. *J Lipid Res, 51*(5), 1023-1034. doi:10.1194/jlr.M002345

Chen, C. C., Keller, M., Hess, M., Schiffmann, R., Urban, N., Wolfgardt, A., . . . Grimm, C. (2014). A small molecule restores function to TRPML1 mutant isoforms responsible for mucolipidosis type IV. *Nat Commun, 5*, 4681. doi:10.1038/ncomms5681

Chen, H., Vermulst, M., Wang, Y. E., Chomyn, A., Prolla, T. A., McCaffery, J. M., & Chan, D. C. (2010). Mitochondrial fusion is required for mtdna stability in skeletal muscle and tolerance of mtDNA mutations. *Cell, 141*(2), 280-289. doi:10.1016/j.cell.2010.02.026

Chen, Q., Jin, C., Shao, X., Guan, R., Tian, Z., Wang, C., . . . Diao, J. (2018). Super-Resolution Tracking of Mitochondrial Dynamics with An Iridium(III) Luminophore. *Small, 14*(41), e1802166. doi:10.1002/smll.201802166

Chen, Q., She, J., Zeng, W., Guo, J., Xu, H., Bai, X. C., & Jiang, Y. (2017). Structure of mammalian endolysosomal TRPML1 channel in nanodiscs. *Nature, 550*(7676), 415-418. doi:10.1038/nature24035

Chen, Y., & Dorn Ii, G. W. (2013). PINK1-phosphorylated mitofusin 2 is a parkin receptor for culling damaged mitochondria. *Science, 340*(6131), 471-475. doi:10.1126/science.1231031

Cheng, X., Zhang, X., Gao, Q., Ali Samie, M., Azar, M., Tsang, W. L., . . . Xu, H. (2014). The intracellular Ca(2)(+) channel MCOLN1 is required for sarcolemma repair to prevent muscular dystrophy. *Nat Med, 20*(10), 1187-1192. doi:10.1038/nm.3611

Cho, B., Cho, H. M., Jo, Y., Kim, H. D., Song, M., Moon, C., . . . Sun, W. (2017). Constriction of the mitochondrial inner compartment is a priming event for mitochondrial division. *Nature Communications, 8*(1). doi:10.1038/ncomms15754

Chow, C. Y., Landers, J. E., Bergren, S. K., Sapp, P. C., Grant, A. E., Jones, J. M., . . . Meisler, M. H. (2009). Deleterious variants of FIG4, a phosphoinositide phosphatase, in patients with ALS. *Am J Hum Genet, 84*(1), 85-88. doi:10.1016/j.ajhg.2008.12.010

Chu, B. B., Liao, Y. C., Qi, W., Xie, C., Du, X., Wang, J., . . . Song, B. L. (2015). Cholesterol transport through lysosome-peroxisome membrane contacts. *Cell, 161*(2), 291-306. doi:10.1016/j.cell.2015.02.019

Chung, K. W., Kim, S. B., Park, K. D., Choi, K. G., Lee, J. H., Eun, H. W., . . . Choi, B. O. (2006). Early onset severe and late-onset mild Charcot-Marie-Tooth disease with mitofusin 2 (MFN2) mutations. *Brain, 129*(8), 2103-2118. doi:10.1093/brain/awl174

Cioni, J. M., Lin, J. Q., Holtermann, A. V., Koppers, M., Jakobs, M. A. H., Azizi, A., . . . Holt, C. E. (2019). Late Endosomes Act as mRNA Translation Platforms and Sustain Mitochondria in Axons. *Cell, 176*(1-2), 56-72.e15. doi:10.1016/j.cell.2018.11.030

Cleeter, M. W., Chau, K. Y., Gluck, C., Mehta, A., Hughes, D. A., Duchen, M., . . . Schapira, A. H. (2013). Glucocerebrosidase inhibition causes mitochondrial dysfunction and free radical damage. *Neurochem Int, 62*(1), 1-7. doi:10.1016/j.neuint.2012.10.010

Csordas, G., Renken, C., Varnai, P., Walter, L., Weaver, D., Buttle, K. F., . . . Hajnoczky, G. (2006). Structural and functional features and significance of the physical linkage between ER and mitochondria. *J Cell Biol, 174*(7), 915-921. doi:10.1083/jcb.200604016

Daniele, T., Hurbain, I., Vago, R., Casari, G., Raposo, G., Tacchetti, C., & Schiaffino, M. V. (2014). Mitochondria and melanosomes establish physical contacts modulated by Mfn2 and involved in organelle biogenesis. *Curr Biol, 24*(4), 393-403. doi:10.1016/j.cub.2014.01.007

Das, A., Nag, S., Mason, A. B., & Barroso, M. M. (2016). Endosome-mitochondria interactions are modulated by iron release from transferrin. *J Cell Biol, 214*(7), 831-845. doi:10.1083/jcb.201602069

Dayam, R. M., Saric, A., Shilliday, R. E., & Botelho, R. J. (2015). The Phosphoinositide-Gated Lysosomal Ca(2+) Channel, TRPML1, Is Required for Phagosome Maturation. *Traffic, 16*(9), 1010-1026. doi:10.1111/tra.12303

De Brito, O. M., & Scorrano, L. (2008). Mitofusin 2 tethers endoplasmic reticulum to mitochondria. *Nature, 456*(7222), 605-610. doi:10.1038/nature07534

de la Mata, M., Cotán, D., Oropesa-Ávila, M., Garrido-Maraver, J., Cordero, M. D., Villanueva Paz, M., . . . Sánchez-Alcázar, J. A. (2015). Pharmacological Chaperones and Coenzyme Q10 Treatment Improves Mutant β-Glucocerebrosidase Activity and Mitochondrial

Function in Neuronopathic Forms of Gaucher Disease. *Sci Rep, 5*, 10903. doi:10.1038/srep10903

De Stefani, D., Raffaello, A., Teardo, E., Szabo, I., & Rizzuto, R. (2011). A forty-kilodalton protein of the inner membrane is the mitochondrial calcium uniporter. *Nature, 476*(7360), 336-340. doi:10.1038/nature10230

Delettre, C., Lenaers, G., Griffoin, J. M., Gigarel, N., Lorenzo, C., Belenguer, P., . . . Hamel, C. P. (2000). Nuclear gene OPA1, encoding a mitochondrial dynamin-related protein, is mutated in dominant optic atrophy. *Nat Genet, 26*(2), 207-210. doi:10.1038/79936

Demers-Lamarche, J., Guillebaud, G., Tlili, M., Todkar, K., Bélanger, N., Grondin, M., . . . Germain, M. (2016). Loss of Mitochondrial Function Impairs Lysosomes. *J Biol Chem, 291*(19), 10263-10276. doi:10.1074/jbc.M115.695825

Deng, H. X., Klein, C. J., Yan, J., Shi, Y., Wu, Y., Fecto, F., . . . Siddique, T. (2010). Scapuloperoneal spinal muscular atrophy and CMT2C are allelic disorders caused by alterations in TRPV4. *Nature Genetics, 42*(2), 165-169. doi:10.1038/ng.509

Detmer, S. A., Velde, C. V., Cleveland, D. W., & Chan, D. C. (2008). Hindlimb gait defects due to motor axon loss and reduced distal muscles in a transgenic mouse model of Charcot - Marie - Tooth type 2A. *Human Molecular Genetics, 17*(3), 367-375. doi:10.1093/hmg/ddm314

Di Paola, S., Scotto-Rosato, A., & Medina, D. L. (2018). TRPML1: The Ca((2+))retaker of the lysosome. *Cell Calcium, 69*, 112-121. doi:10.1016/j.ceca.2017.06.006

Dong, X. P., Cheng, X., Mills, E., Delling, M., Wang, F., Kurz, T., & Xu, H. (2008). The type IV mucolipidosis-associated protein TRPML1 is an endolysosomal iron release channel. *Nature, 455*(7215), 992-996. doi:10.1038/nature07311

Dong, X. P., Shen, D., Wang, X., Dawson, T., Li, X., Zhang, Q., . . . Xu, H. (2010). PI(3,5)P(2) controls membrane trafficking by direct activation of mucolipin Ca(2+) release channels in the endolysosome. *Nat Commun, 1*, 38. doi:10.1038/ncomms1037

Eichelsdoerfer, J. L., Evans, J. A., Slaugenhaupt, S. A., & Cuajungco, M. P. (2010). Zinc dyshomeostasis is linked with the loss of mucolipidosis IV-associated TRPML1 ion channel. *J Biol Chem, 285*(45), 34304-34308. doi:10.1074/jbc.C110.165480

Eisenberg-Bord, M., Shai, N., Schuldiner, M., & Bohnert, M. (2016). A Tether Is a Tether Is a Tether: Tethering at Membrane Contact Sites. *Dev Cell, 39*(4), 395-409. doi:10.1016/j.devcel.2016.10.022

El Fissi, N., Rojo, M., Aouane, A., Karatas, E., Poliacikova, G., David, C., . . . Rival, T. (2018). Mitofusin gain and loss of function drive pathogenesis in Drosophila models of CMT2A neuropathy. *EMBO Reports, 19*(8). doi:10.15252/embr.201745241

Elbaz-Alon, Y., Guo, Y., Segev, N., Harel, M., Quinnell, D. E., Geiger, T., . . . Nunnari, J. (2020). PDZD8 interacts with Protrudin and Rab7 at ER-late endosome membrane contact sites associated with mitochondria. *Nat Commun, 11*(1), 3645. doi:10.1038/s41467-020-17451-7

Elbaz-Alon, Y., Rosenfeld-Gur, E., Shinder, V., Futerman, A. H., Geiger, T., & Schuldiner, M. (2014). A dynamic interface between vacuoles and mitochondria in yeast. *Dev Cell, 30*(1), 95-102. doi:10.1016/j.devcel.2014.06.007

Falcon-Perez, J. M., Nazarian, R., Sabatti, C., & Dell'Angelica, E. C. (2005). Distribution and dynamics of Lamp1-containing endocytic organelles in fibroblasts deficient in BLOC-3. *J Cell Sci, 118*(Pt 22), 5243-5255. doi:10.1242/jcs.02633

Feng, S., Li, H., Tai, Y., Huang, J., Su, Y., Abramowitz, J., . . . Wang, Y. (2013). Canonical transient receptor potential 3 channels regulate mitochondrial calcium uptake. *Proc Natl Acad Sci U S A, 110*(27), 11011-11016. doi:10.1073/pnas.1309531110

Fermie, J., Liv, N., Ten Brink, C., van Donselaar, E. G., Muller, W. H., Schieber, N. L., . . . Klumperman, J. (2018). Single organelle dynamics linked to 3D structure by correlative live-cell imaging and 3D electron microscopy. *Traffic, 19*(5), 354-369. doi:10.1111/tra.12557

Fernández-Mosquera, L., Diogo, C. V., Yambire, K. F., Santos, G. L., Luna Sánchez, M., Bénit, P., . . . Raimundo, N. (2017). Acute and chronic mitochondrial respiratory chain deficiency differentially regulate lysosomal biogenesis. *Sci Rep, 7*, 45076. doi:10.1038/srep45076

Fine, M., Schmiege, P., & Li, X. (2018). Structural basis for PtdInsP2-mediated human TRPML1 regulation. *Nat Commun, 9*(1), 4192. doi:10.1038/s41467-018-06493-7

Franco, A., Kitsis, R. N., Fleischer, J. A., Gavathiotis, E., Kornfeld, O. S., Gong, G., . . . Dorn, G. W. (2016). Correcting mitochondrial fusion by manipulating mitofusin conformations. *Nature, 540*(7631), 74-79. doi:10.1038/nature20156

Friedman, J. R., Lackner, L. L., West, M., DiBenedetto, J. R., Nunnari, J., & Voeltz, G. K. (2011). ER tubules mark sites of mitochondrial division. *Science, 334*(6054), 358-362. doi:10.1126/science.1207385

Friedman, J. R., & Nunnari, J. (2014). Mitochondrial form and function. *Nature, 505*(7483), 335-343. doi:10.1038/nature12985

Gafni, J., Munsch, J. A., Lam, T. H., Catlin, M. C., Costa, L. G., Molinski, T. F., & Pessah, I. N. (1997). Xestospongins: potent membrane permeable blockers of the inositol 1,4,5-trisphosphate receptor. *Neuron, 19*(3), 723-733. doi:10.1016/s0896-6273(00)80384-0

Garrity, A. G., Wang, W., Collier, C. M., Levey, S. A., Gao, Q., & Xu, H. (2016). The endoplasmic reticulum, not the pH gradient, drives calcium refilling of lysosomes. *Elife, 5*. doi:10.7554/eLife.15887

Gatta, A. T., & Levine, T. P. (2017). Piecing Together the Patchwork of Contact Sites. *Trends Cell Biol, 27*(3), 214-229. doi:10.1016/j.tcb.2016.08.010

Gauthier, J., Meijer, I. A., Lessel, D., Mencacci, N. E., Krainc, D., Hempel, M., . . . Campeau, P. M. (2018). Recessive mutations in VPS13D cause childhood onset movement disorders. *Ann Neurol, 83*(6), 1089-1095. doi:10.1002/ana.25204

Gincel, D., Zaid, H., & Shoshan-Barmatz, V. (2001). Calcium binding and translocation by the voltage-dependent anion channel: a possible regulatory mechanism in mitochondrial function. *Biochem J, 358*(Pt 1), 147-155. doi:10.1042/0264-6021:3580147

Giorgi, C., Marchi, S., & Pinton, P. (2018). The machineries, regulation and cellular functions of mitochondrial calcium. *Nat Rev Mol Cell Biol, 19*(11), 713-730. doi:10.1038/s41580-018-0052-8

González Montoro, A., Auffarth, K., Hönscher, C., Bohnert, M., Becker, T., Warscheid, B., . . . Ungermann, C. (2018). Vps39 Interacts with Tom40 to Establish One of Two Functionally Distinct Vacuole-Mitochondria Contact Sites. *Dev Cell, 45*(5), 621-636.e627. doi:10.1016/j.devcel.2018.05.011

Gottschling, D. E., & Nyström, T. (2017). The Upsides and Downsides of Organelle Interconnectivity. *Cell, 169*(1), 24-34. doi:10.1016/j.cell.2017.02.030

Guo, Y., Li, D., Zhang, S., Yang, Y., Liu, J. J., Wang, X., . . . Li, D. (2018). Visualizing Intracellular Organelle and Cytoskeletal Interactions at Nanoscale Resolution on Millisecond Timescales. *Cell, 175*(5), 1430-1442.e1417. doi:10.1016/j.cell.2018.09.057

Hamacher-Brady, A., Choe, S. C., Krijnse-Locker, J., & Brady, N. R. (2014). Intramitochondrial recruitment of endolysosomes mediates Smac degradation and constitutes a novel intrinsic apoptosis antagonizing function of XIAP E3 ligase. *Cell Death Differ, 21*(12), 1862-1876. doi:10.1038/cdd.2014.101

Han, Y., Li, M., Qiu, F., Zhang, M., & Zhang, Y. H. (2017). Cell-permeable organic fluorescent probes for live-cell long-term super-resolution imaging reveal lysosome-mitochondrion interactions. *Nat Commun, 8*(1), 1307. doi:10.1038/s41467-017-01503-6

Harel, T., & Lupski, J. R. (2014). Charcot-Marie-Tooth disease and pathways to molecular based therapies. *Clinical Genetics, 86*(5), 422-431. doi:10.1111/cge.12393

Hayashi, T., & Su, T. P. (2007). Sigma-1 receptor chaperones at the ER-mitochondrion interface regulate Ca(2+) signaling and cell survival. *Cell, 131*(3), 596-610. doi:10.1016/j.cell.2007.08.036

Hirabayashi, Y., Kwon, S. K., Paek, H., Pernice, W. M., Paul, M. A., Lee, J., . . . Polleux, F. (2017). ER-mitochondria tethering by PDZD8 regulates Ca(2+) dynamics in mammalian neurons. *Science, 358*(6363), 623-630. doi:10.1126/science.aan6009

Hirschi, M., Herzik, M. A., Jr., Wie, J., Suo, Y., Borschel, W. F., Ren, D., . . . Lee, S. Y. (2017). Cryo-electron microscopy structure of the lysosomal calcium-permeable channel TRPML3. *Nature, 550*(7676), 411-414. doi:10.1038/nature24055

Hoglinger, D., Burgoyne, T., Sanchez-Heras, E., Hartwig, P., Colaco, A., Newton, J., . . . Eden, E. R. (2019). NPC1 regulates ER contacts with endocytic organelles to mediate cholesterol egress. *Nat Commun, 10*(1), 4276. doi:10.1038/s41467-019-12152-2

Honscher, C., Mari, M., Auffarth, K., Bohnert, M., Griffith, J., Geerts, W., . . . Ungermann, C. (2014). Cellular metabolism regulates contact sites between vacuoles and mitochondria. *Dev Cell, 30*(1), 86-94. doi:10.1016/j.devcel.2014.06.006

Houlden, H., King, R. H., Muddle, J. R., Warner, T. T., Reilly, M. M., Orrell, R. W., & Ginsberg, L. (2004). A novel RAB7 mutation associated with ulcero-mutilating neuropathy. *Ann Neurol, 56*(4), 586-590. doi:10.1002/ana.20281

Hoyer, M. J., Chitwood, P. J., Ebmeier, C. C., Striepen, J. F., Qi, R. Z., Old, W. M., & Voeltz, G. K. (2018). A Novel Class of ER Membrane Proteins Regulates ER-Associated Endosome Fission. *Cell, 175*(1), 254-265.e214. doi:10.1016/j.cell.2018.08.030

Hsu, F., Spannl, S., Ferguson, C., Hyman, A. A., Parton, R. G., & Zerial, M. (2018). Rab5 and Alsin regulate stress-activated cytoprotective signaling on mitochondria. *Elife, 7*. doi:10.7554/eLife.32282

Huang, X., Sun, L., Ji, S., Zhao, T., Zhang, W., Xu, J., . . . Cheng, H. (2013). Kissing and nanotunneling mediate intermitochondrial communication in the heart. *Proceedings of the National Academy of Sciences of the United States of America, 110*(8), 2846-2851. doi:10.1073/pnas.1300741110

Hung, V., Lam, S. S., Udeshi, N. D., Svinkina, T., Guzman, G., Mootha, V. K., . . . Ting, A. Y. (2017). Proteomic mapping of cytosol-facing outer mitochondrial and ER membranes in living human cells by proximity biotinylation. *Elife, 6*. doi:10.7554/eLife.24463

Hutagalung, A. H., & Novick, P. J. (2011). Role of Rab GTPases in membrane traffic and cell physiology. *Physiol Rev, 91*(1), 119-149. doi:10.1152/physrev.00059.2009

Ichas, F., Jouaville, L. S., & Mazat, J. P. (1997). Mitochondria are excitable organelles capable of generating and conveying electrical and calcium signals. *Cell, 89*(7), 1145-1153. doi:10.1016/s0092-8674(00)80301-3

Israelson, A., Abu-Hamad, S., Zaid, H., Nahon, E., & Shoshan-Barmatz, V. (2007). Localization of the voltage-dependent anion channel-1 Ca2+-binding sites. *Cell Calcium, 41*(3), 235-244. doi:10.1016/j.ceca.2006.06.005

Israelson, A., Zaid, H., Abu-Hamad, S., Nahon, E., & Shoshan-Barmatz, V. (2008). Mapping the ruthenium red-binding site of the voltage-dependent anion channel-1. *Cell Calcium, 43*(2), 196-204. doi:10.1016/j.ceca.2007.05.006

Itoh, K., Murata, D., Kato, T., Yamada, T., Araki, Y., Saito, A., . . . Sesaki, H. (2019). Brain-specific Drp1 regulates postsynaptic endocytosis and dendrite formation independently of mitochondrial division. *Elife, 8*. doi:10.7554/eLife.44739

Jennings, J. J., Jr., Zhu, J. H., Rbaibi, Y., Luo, X., Chu, C. T., & Kiselyov, K. (2006). Mitochondrial aberrations in mucolipidosis Type IV. *J Biol Chem, 281*(51), 39041-39050. doi:10.1074/jbc.M607982200

Ji, W. K., Hatch, A. L., Merrill, R. A., Strack, S., & Higgs, H. N. (2015). Actin filaments target the oligomeric maturation of the dynamin GTPase Drp1 to mitochondrial fission sites. *Elife, 4*, e11553. doi:10.7554/eLife.11553

Jia, D., Zhang, J. S., Li, F., Wang, J., Deng, Z., White, M. A., . . . Rosen, M. K. (2016). Structural and mechanistic insights into regulation of the retromer coat by TBC1d5. *Nat Commun, 7*, 13305. doi:10.1038/ncomms13305

Jiang, D., Zhao, L., & Clapham, D. E. (2009). Genome-wide RNAi screen identifies Letm1 as a mitochondrial Ca2+/H+ antiporter. *Science, 326*(5949), 144-147. doi:10.1126/science.1175145

Jofuku, A., Ishihara, N., & Mihara, K. (2005). Analysis of functional domains of rat mitochondrial Fis1, the mitochondrial fission-stimulating protein. *Biochem Biophys Res Commun, 333*(2), 650-659. doi:10.1016/j.bbrc.2005.05.154

John Peter, A. T., Herrmann, B., Antunes, D., Rapaport, D., Dimmer, K. S., & Kornmann, B. (2017). Vps13-Mcp1 interact at vacuole-mitochondria interfaces and bypass ER-mitochondria contact sites. *J Cell Biol, 216*(10), 3219-3229. doi:10.1083/jcb.201610055

Jordens, I., Fernandez-Borja, M., Marsman, M., Dusseljee, S., Janssen, L., Calafat, J., . . . Neefjes, J. (2001). The Rab7 effector protein RILP controls lysosomal transport by inducing the recruitment of dynein-dynactin motors. *Curr Biol, 11*(21), 1680-1685. Retrieved from https://www.ncbi.nlm.nih.gov/pubmed/11696325

Kalia, L. V., & Lang, A. E. (2015). Parkinson's disease. *Lancet, 386*(9996), 896-912. doi:10.1016/s0140-6736(14)61393-3

Karbowski, M., Arnoult, D., Chen, H., Chan, D. C., Smith, C. L., & Youle, R. J. (2004). Quantitation of mitochondrial dynamics by photolabeling of individual organelles shows that mitochondrial fusion is blocked during the Bax activation phase of apoptosis. *J Cell Biol, 164*(4), 493-499. doi:10.1083/jcb.200309082

Katajisto, P., Döhla, J., Chaffer, C. L., Pentinmikko, N., Marjanovic, N., Iqbal, S., . . . Sabatini, D. M. (2015). Stem cells. Asymmetric apportioning of aged mitochondria between

daughter cells is required for stemness. *Science, 348*(6232), 340-343. doi:10.1126/science.1260384

Khalil, S., Holy, M., Grado, S., Fleming, R., Kurita, R., Nakamura, Y., & Goldfarb, A. (2017). A specialized pathway for erythroid iron delivery through lysosomal trafficking of transferrin receptor 2. *Blood Adv, 1*(15), 1181-1194. doi:10.1182/bloodadvances.2016003772

Khan, N. A., Nikkanen, J., Yatsuga, S., Jackson, C., Wang, L., Pradhan, S., . . . Suomalainen, A. (2017). mTORC1 Regulates Mitochondrial Integrated Stress Response and Mitochondrial Myopathy Progression. *Cell Metab, 26*(2), 419-428.e415. doi:10.1016/j.cmet.2017.07.007

Kilpatrick, B. S., Yates, E., Grimm, C., Schapira, A. H., & Patel, S. (2016). Endo-lysosomal TRP mucolipin-1 channels trigger global ER Ca2+ release and Ca2+ influx. *J Cell Sci, 129*(20), 3859-3867. doi:10.1242/jcs.190322

Kim, S., Wong, Y. C., Gao, F., & Krainc, D. (2021). Dysregulation of mitochondria-lysosome contacts by GBA1 dysfunction in dopaminergic neuronal models of Parkinson's disease. *Nat Commun, 12*(1), 1807. doi:10.1038/s41467-021-22113-3

Kolehmainen, J., Black, G. C., Saarinen, A., Chandler, K., Clayton-Smith, J., Träskelin, A. L., . . . Lehesjoki, A. E. (2003). Cohen syndrome is caused by mutations in a novel gene, COH1, encoding a transmembrane protein with a presumed role in vesicle-mediated sorting and intracellular protein transport. *Am J Hum Genet, 72*(6), 1359-1369. doi:10.1086/375454

Korobova, F., Ramabhadran, V., & Higgs, H. N. (2013). An actin-dependent step in mitochondrial fission mediated by the ER-associated formin INF2. *Science, 339*(6118), 464-467. doi:10.1126/science.1228360

Kumar, N., Leonzino, M., Hancock-Cerutti, W., Horenkamp, F. A., Li, P., Lees, J. A., . . . De Camilli, P. (2018). VPS13A and VPS13C are lipid transport proteins differentially localized at ER contact sites. *J Cell Biol, 217*(10), 3625-3639. doi:10.1083/jcb.201807019

Landouré, G., Zdebik, A. A., Martinez, T. L., Burnett, B. G., Stanescu, H. C., Inada, H., . . . Sumner, C. J. (2010). Mutations in TRPV4 cause Charcot-Marie-Tooth disease type 2C. *Nat Genet, 42*(2), 170-174. doi:10.1038/ng.512

Lang, A. B., John Peter, A. T., Walter, P., & Kornmann, B. (2015). ER-mitochondrial junctions can be bypassed by dominant mutations in the endosomal protein Vps13. *J Cell Biol, 210*(6), 883-890. doi:10.1083/jcb.201502105

Langemeyer, L., Frohlich, F., & Ungermann, C. (2018). Rab GTPase Function in Endosome and Lysosome Biogenesis. *Trends Cell Biol, 28*(11), 957-970. doi:10.1016/j.tcb.2018.06.007

LaPlante, J. M., Sun, M., Falardeau, J., Dai, D., Brown, E. M., Slaugenhaupt, S. A., & Vassilev, P. M. (2006). Lysosomal exocytosis is impaired in mucolipidosis type IV. *Mol Genet Metab, 89*(4), 339-348. doi:10.1016/j.ymgme.2006.05.016

Lawrence, R. E., & Zoncu, R. (2019). The lysosome as a cellular centre for signalling, metabolism and quality control. *Nat Cell Biol, 21*(2), 133-142. doi:10.1038/s41556-018-0244-7

Lawson, V. H., Graham, B. V., & Flanigan, K. M. (2005). Clinical and electrophysiologic features of CMT2A with mutations in the mitofusin 2 gene. *Neurology, 65*(2), 197-204. doi:10.1212/01.wnl.0000168898.76071.70

Lazarou, M., Sliter, D. A., Kane, L. A., Sarraf, S. A., Wang, C., Burman, J. L., . . . Youle, R. J. (2015). The ubiquitin kinase PINK1 recruits autophagy receptors to induce mitophagy. *Nature, 524*(7565), 309-314. doi:10.1038/nature14893

Lee, J. E., Westrate, L. M., Wu, H., Page, C., & Voeltz, G. K. (2016). Multiple dynamin family members collaborate to drive mitochondrial division. *Nature, 540*(7631), 139-143. doi:10.1038/nature20555

Lee, J. H., McBrayer, M. K., Wolfe, D. M., Haslett, L. J., Kumar, A., Sato, Y., . . . Nixon, R. A. (2015). Presenilin 1 Maintains Lysosomal Ca(2+) Homeostasis via TRPML1 by Regulating vATPase-Mediated Lysosome Acidification. *Cell Rep, 12*(9), 1430-1444. doi:10.1016/j.celrep.2015.07.050

Lee, K. S., Huh, S., Lee, S., Wu, Z., Kim, A. K., Kang, H. Y., & Lu, B. (2018). Altered ER-mitochondria contact impacts mitochondria calcium homeostasis and contributes to neurodegeneration in vivo in disease models. *Proc Natl Acad Sci U S A, 115*(38), E8844-e8853. doi:10.1073/pnas.1721136115

Lesage, S., Drouet, V., Majounie, E., Deramecourt, V., Jacoupy, M., Nicolas, A., . . . Brice, A. (2016). Loss of VPS13C Function in Autosomal-Recessive Parkinsonism Causes Mitochondrial Dysfunction and Increases PINK1/Parkin-Dependent Mitophagy. *Am J Hum Genet, 98*(3), 500-513. doi:10.1016/j.ajhg.2016.01.014

Lewis, S. C., Uchiyama, L. F., & Nunnari, J. (2016). ER-mitochondria contacts couple mtDNA synthesis with mitochondrial division in human cells. *Science, 353*(6296), aaf5549. doi:10.1126/science.aaf5549

Li, H., Ham, A., Ma, T. C., Kuo, S. H., Kanter, E., Kim, D., . . . Tang, G. (2019). Mitochondrial dysfunction and mitophagy defect triggered by heterozygous GBA mutations. *Autophagy, 15*(1), 113-130. doi:10.1080/15548627.2018.1509818

Li, M., Zhang, W. K., Benvin, N. M., Zhou, X., Su, D., Li, H., . . . Yang, J. (2017). Structural basis of dual Ca(2+)/pH regulation of the endolysosomal TRPML1 channel. *Nat Struct Mol Biol, 24*(3), 205-213. doi:10.1038/nsmb.3362

Li, X., Rydzewski, N., Hider, A., Zhang, X., Yang, J., Wang, W., . . . Xu, H. (2016). A molecular mechanism to regulate lysosome motility for lysosome positioning and tubulation. *Nat Cell Biol, 18*(4), 404-417. doi:10.1038/ncb3324

Liao, Y. C., Fernandopulle, M. S., Wang, G., Choi, H., Hao, L., Drerup, C. M., . . . Ward, M. E. (2019). RNA Granules Hitchhike on Lysosomes for Long-Distance Transport, Using Annexin A11 as a Molecular Tether. *Cell, 179*(1), 147-164.e120. doi:10.1016/j.cell.2019.08.050

Lie, P. P. Y., & Nixon, R. A. (2019). Lysosome trafficking and signaling in health and neurodegenerative diseases. *Neurobiol Dis, 122*, 94-105. doi:10.1016/j.nbd.2018.05.015

Lim, C. Y., Davis, O. B., Shin, H. R., Zhang, J., Berdan, C. A., Jiang, X., . . . Zoncu, R. (2019). ER-lysosome contacts enable cholesterol sensing by mTORC1 and drive aberrant growth signalling in Niemann-Pick type C. *Nat Cell Biol, 21*(10), 1206-1218. doi:10.1038/s41556-019-0391-5

Liu, X., Weaver, D., Shirihai, O., & Hajnóczky, G. (2009). Mitochondrial 'kiss-and-run': interplay between mitochondrial motility and fusion-fission dynamics. *Embo j, 28*(20), 3074-3089. doi:10.1038/emboj.2009.255

Manganelli, F., Pisciotta, C., Provitera, V., Taioli, F., Iodice, R., Topa, A., . . . Santoro, L. (2012). Autonomic nervous system involvement in a new CMT2B family. *J Peripher Nerv Syst, 17*(3), 361-364. doi:10.1111/j.1529-8027.2012.00415.x

Manor, U., Bartholomew, S., Golani, G., Christenson, E., Kozlov, M., Higgs, H., . . . Lippincott-Schwartz, J. (2015). A mitochondria-anchored isoform of the actin-nucleating spire protein regulates mitochondrial division. *Elife, 4*. doi:10.7554/eLife.08828

Mansueto, G., Armani, A., Viscomi, C., D'Orsi, L., De Cegli, R., Polishchuk, E. V., . . . Ballabio, A. (2017). Transcription Factor EB Controls Metabolic Flexibility during Exercise. *Cell Metab, 25*(1), 182-196. doi:10.1016/j.cmet.2016.11.003

Marques, A. R. A., & Saftig, P. (2019). Lysosomal storage disorders - challenges, concepts and avenues for therapy: beyond rare diseases. *J Cell Sci, 132*(2). doi:10.1242/jcs.221739

Mason, T. A., Goldenring, J. R., & Kolobova, E. (2014). AKAP350C targets to mitochondria via a novel amphipathic alpha helical domain. *Cell Logist, 4*(3), e943597. doi:10.4161/21592780.2014.943597

Mazzulli, J. R., Xu, Y. H., Sun, Y., Knight, A. L., McLean, P. J., Caldwell, G. A., . . . Krainc, D. (2011). Gaucher disease glucocerebrosidase and α-synuclein form a bidirectional pathogenic loop in synucleinopathies. *Cell, 146*(1), 37-52. doi:10.1016/j.cell.2011.06.001

Mc Donald, J. M., & Krainc, D. (2017). Lysosomal Proteins as a Therapeutic Target in Neurodegeneration. *Annu Rev Med, 68*, 445-458. doi:10.1146/annurev-med-050715-104432

McCray, B. A., Skordalakes, E., & Taylor, J. P. (2010). Disease mutations in Rab7 result in unregulated nucleotide exchange and inappropriate activation. *Hum Mol Genet, 19*(6), 1033-1047. doi:10.1093/hmg/ddp567

McLelland, G. L., Soubannier, V., Chen, C. X., McBride, H. M., & Fon, E. A. (2014). Parkin and PINK1 function in a vesicular trafficking pathway regulating mitochondrial quality control. *Embo j, 33*(4), 282-295. doi:10.1002/embj.201385902

Medina, D. L., Di Paola, S., Peluso, I., Armani, A., De Stefani, D., Venditti, R., . . . Ballabio, A. (2015). Lysosomal calcium signalling regulates autophagy through calcineurin and TFEB. *Nat Cell Biol, 17*(3), 288-299. doi:10.1038/ncb3114

Meggouh, F., Bienfait, H. M., Weterman, M. A., de Visser, M., & Baas, F. (2006). Charcot-Marie-Tooth disease due to a de novo mutation of the RAB7 gene. *Neurology, 67*(8), 1476-1478. doi:10.1212/01.wnl.0000240068.21499.f5

Min, C. K., Yeom, D. R., Lee, K. E., Kwon, H. K., Kang, M., Kim, Y. S., . . . Kim, D. H. (2012). Coupling of ryanodine receptor 2 and voltage-dependent anion channel 2 is essential for Ca^{2+} transfer from the sarcoplasmic reticulum to the mitochondria in the heart. *Biochem J, 447*(3), 371-379. doi:10.1042/bj20120705

Minckley, T. F., Zhang, C., Fudge, D. H., Dischler, A. M., LeJeune, K. D., Xu, H., & Qin, Y. (2019). Sub-nanomolar sensitive GZnP3 reveals TRPML1-mediated neuronal Zn(2+) signals. *Nat Commun, 10*(1), 4806. doi:10.1038/s41467-019-12761-x

Misgeld, T., & Schwarz, T. L. (2017). Mitostasis in Neurons: Maintaining Mitochondria in an Extended Cellular Architecture. *Neuron, 96*(3), 651-666. doi:10.1016/j.neuron.2017.09.055

Mishra, P., & Chan, D. C. (2016). Metabolic regulation of mitochondrial dynamics. *J Cell Biol, 212*(4), 379-387. doi:10.1083/jcb.201511036

Misko, A., Jiang, S., Wegorzewska, I., Milbrandt, J., & Baloh, R. H. (2010). Mitofusin 2 is necessary for transport of axonal mitochondria and interacts with the Miro/Milton complex. *J Neurosci, 30*(12), 4232-4240. doi:10.1523/jneurosci.6248-09.2010

Misko, A. L., Sasaki, Y., Tuck, E., Milbrandt, J., & Baloh, R. H. (2012). Mitofusin2 mutations disrupt axonal mitochondrial positioning and promote axon degeneration. *Journal of Neuroscience, 32*(12), 4145-4155. doi:10.1523/JNEUROSCI.6338-11.2012

Monteleon, C. L., Agnihotri, T., Dahal, A., Liu, M., Rebecca, V. W., Beatty, G. L., . . . Ridky, T. W. (2018). Lysosomes Support the Degradation, Signaling, and Mitochondrial Metabolism Necessary for Human Epidermal Differentiation. *J Invest Dermatol, 138*(9), 1945-1954. doi:10.1016/j.jid.2018.02.035

Moore, A. S., Wong, Y. C., Simpson, C. L., & Holzbaur, E. L. (2016). Dynamic actin cycling through mitochondrial subpopulations locally regulates the fission-fusion balance within mitochondrial networks. *Nat Commun, 7*, 12886. doi:10.1038/ncomms12886

Muñoz-Braceras, S., Tornero-Écija, A. R., Vincent, O., & Escalante, R. (2019). VPS13A is closely associated with mitochondria and is required for efficient lysosomal degradation. *Dis Model Mech, 12*(2). doi:10.1242/dmm.036681

Naghdi, S., & Hajnóczky, G. (2016). VDAC2-specific cellular functions and the underlying structure. *Biochim Biophys Acta, 1863*(10), 2503-2514. doi:10.1016/j.bbamcr.2016.04.020

Nicholson, G., Lenk, G. M., Reddel, S. W., Grant, A. E., Towne, C. F., Ferguson, C. J., . . . Meisler, M. H. (2011). Distinctive genetic and clinical features of CMT4J: a severe neuropathy caused by mutations in the PI(3,5)P_2 phosphatase FIG4. *Brain, 134*(Pt 7), 1959-1971. doi:10.1093/brain/awr148

Norambuena, A., Wallrabe, H., Cao, R., Wang, D. B., Silva, A., Svindrych, Z., . . . Bloom, G. S. (2018). A novel lysosome-to-mitochondria signaling pathway disrupted by amyloid-β oligomers. *Embo j, 37*(22). doi:10.15252/embj.2018100241

Onoue, K., Jofuku, A., Ban-Ishihara, R., Ishihara, T., Maeda, M., Koshiba, T., . . . Ishihara, N. (2013). Fis1 acts as a mitochondrial recruitment factor for TBC1D15 that is involved in regulation of mitochondrial morphology. *J Cell Sci, 126*(Pt 1), 176-185. doi:10.1242/jcs.111211

Osellame, L. D., Rahim, A. A., Hargreaves, I. P., Gegg, M. E., Richard-Londt, A., Brandner, S., . . . Duchen, M. R. (2013). Mitochondria and quality control defects in a mouse model of Gaucher disease--links to Parkinson's disease. *Cell Metab, 17*(6), 941-953. doi:10.1016/j.cmet.2013.04.014

Ozaki, S., DeWald, D. B., Shope, J. C., Chen, J., & Prestwich, G. D. (2000). Intracellular delivery of phosphoinositides and inositol phosphates using polyamine carriers. *Proc Natl Acad Sci U S A, 97*(21), 11286-11291. doi:10.1073/pnas.210197897

Pankiv, S., Alemu, E. A., Brech, A., Bruun, J. A., Lamark, T., Overvatn, A., . . . Johansen, T. (2010). FYCO1 is a Rab7 effector that binds to LC3 and PI3P to mediate microtubule plus end-directed vesicle transport. *J Cell Biol, 188*(2), 253-269. doi:10.1083/jcb.200907015

Park, J. S., Thorsness, M. K., Policastro, R., McGoldrick, L. L., Hollingsworth, N. M., Thorsness, P. E., & Neiman, A. M. (2016). Yeast Vps13 promotes mitochondrial function and is localized at membrane contact sites. *Mol Biol Cell, 27*(15), 2435-2449. doi:10.1091/mbc.E16-02-0112

Park, S., Ahuja, M., Kim, M. S., Brailoiu, G. C., Jha, A., Zeng, M., . . . Muallem, S. (2016). Fusion of lysosomes with secretory organelles leads to uncontrolled exocytosis in the

lysosomal storage disease mucolipidosis type IV. *EMBO Rep, 17*(2), 266-278. doi:10.15252/embr.201541542

Pchitskaya, E., Popugaeva, E., & Bezprozvanny, I. (2018). Calcium signaling and molecular mechanisms underlying neurodegenerative diseases. *Cell Calcium, 70*, 87-94. doi:10.1016/j.ceca.2017.06.008

Pease, D. C. (1962). Demonstration of a highly ordered pattern upon a mitochondrial surface. *The Journal of cell biology, 15*, 385-389. doi:10.1083/jcb.15.2.385

Peng, W., Minakaki, G., Nguyen, M., & Krainc, D. (2019). Preserving Lysosomal Function in the Aging Brain: Insights from Neurodegeneration. *Neurotherapeutics, 16*(3), 611-634. doi:10.1007/s13311-019-00742-3

Peng, W., Wong, Y. C., & Krainc, D. (2020). Mitochondria-lysosome contacts regulate mitochondrial Ca(2+) dynamics via lysosomal TRPML1. *Proc Natl Acad Sci U S A, 117*(32), 19266-19275. doi:10.1073/pnas.2003236117

Peralta, E. R., Martin, B. C., & Edinger, A. L. (2010). Differential effects of TBC1D15 and mammalian Vps39 on Rab7 activation state, lysosomal morphology, and growth factor dependence. *J Biol Chem, 285*(22), 16814-16821. doi:10.1074/jbc.M110.111633

Phillips, C. B., Tsai, C. W., & Tsai, M. F. (2019). The conserved aspartate ring of MCU mediates MICU1 binding and regulation in the mitochondrial calcium uniporter complex. *Elife, 8*. doi:10.7554/eLife.41112

Phillips, M. J., & Voeltz, G. K. (2016). Structure and function of ER membrane contact sites with other organelles. *Nat Rev Mol Cell Biol, 17*(2), 69-82. doi:10.1038/nrm.2015.8

Picard, M., McManus, M. J., Csordás, G., Várnai, P., Dorn, G. W., Williams, D., . . . Wallace, D. C. (2015). Trans-mitochondrial coordination of cristae at regulated membrane junctions. *Nature Communications, 6*. doi:10.1038/ncomms7259

Pickrell, A. M., & Youle, R. J. (2015). The roles of PINK1, parkin, and mitochondrial fidelity in Parkinson's disease. *Neuron, 85*(2), 257-273. doi:10.1016/j.neuron.2014.12.007

Platt, F. M., d'Azzo, A., Davidson, B. L., Neufeld, E. F., & Tifft, C. J. (2018). Lysosomal storage diseases. *Nat Rev Dis Primers, 4*(1), 27. doi:10.1038/s41572-018-0025-4

Plotegher, N., & Duchen, M. R. (2017a). Crosstalk between Lysosomes and Mitochondria in Parkinson's Disease. *Front Cell Dev Biol, 5*, 110. doi:10.3389/fcell.2017.00110

Plotegher, N., & Duchen, M. R. (2017b). Mitochondrial Dysfunction and Neurodegeneration in Lysosomal Storage Disorders. *Trends Mol Med, 23*(2), 116-134. doi:10.1016/j.molmed.2016.12.003

Pryor, P. R., Reimann, F., Gribble, F. M., & Luzio, J. P. (2006). Mucolipin-1 is a lysosomal membrane protein required for intracellular lactosylceramide traffic. *Traffic, 7*(10), 1388-1398. doi:10.1111/j.1600-0854.2006.00475.x

Raffaello, A., Mammucari, C., Gherardi, G., & Rizzuto, R. (2016). Calcium at the Center of Cell Signaling: Interplay between Endoplasmic Reticulum, Mitochondria, and Lysosomes. *Trends Biochem Sci, 41*(12), 1035-1049. doi:10.1016/j.tibs.2016.09.001

Raiborg, C., Wenzel, E. M., Pedersen, N. M., Olsvik, H., Schink, K. O., Schultz, S. W., . . . Stenmark, H. (2015). Repeated ER-endosome contacts promote endosome translocation and neurite outgrowth. *Nature, 520*(7546), 234-238. doi:10.1038/nature14359

Rambold, A. S., Kostelecky, B., Elia, N., & Lippincott-Schwartz, J. (2011). Tubular network formation protects mitochondria from autophagosomal degradation during nutrient starvation. *Proceedings of the National Academy of Sciences of the United States of America, 108*(25), 10190-10195. doi:10.1073/pnas.1107402108

Rampoldi, L., Dobson-Stone, C., Rubio, J. P., Danek, A., Chalmers, R. M., Wood, N. W., . . . Monaco, A. P. (2001). A conserved sorting-associated protein is mutant in chorea-acanthocytosis. *Nat Genet, 28*(2), 119-120. doi:10.1038/88821

Rapizzi, E., Pinton, P., Szabadkai, G., Wieckowski, M. R., Vandecasteele, G., Baird, G., . . . Rizzuto, R. (2002). Recombinant expression of the voltage-dependent anion channel enhances the transfer of Ca2+ microdomains to mitochondria. *J Cell Biol, 159*(4), 613-624. doi:10.1083/jcb.200205091

Raychowdhury, M. K., Gonzalez-Perrett, S., Montalbetti, N., Timpanaro, G. A., Chasan, B., Goldmann, W. H., . . . Cantiello, H. F. (2004). Molecular pathophysiology of mucolipidosis type IV: pH dysregulation of the mucolipin-1 cation channel. *Hum Mol Genet, 13*(6), 617-627. doi:10.1093/hmg/ddh067

Richardson, D. R., Lane, D. J., Becker, E. M., Huang, M. L., Whitnall, M., Suryo Rahmanto, Y., . . . Ponka, P. (2010). Mitochondrial iron trafficking and the integration of iron metabolism between the mitochondrion and cytosol. *Proc Natl Acad Sci U S A, 107*(24), 10775-10782. doi:10.1073/pnas.0912925107

Rizzo, M. A., Davidson, M. W., & Piston, D. W. (2009). Fluorescent protein tracking and detection: fluorescent protein structure and color variants. *Cold Spring Harb Protoc, 2009*(12), pdb.top63. doi:10.1101/pdb.top63

Rizzuto, R., Pinton, P., Carrington, W., Fay, F. S., Fogarty, K. E., Lifshitz, L. M., . . . Pozzan, T. (1998). Close contacts with the endoplasmic reticulum as determinants of mitochondrial Ca2+ responses. *Science, 280*(5370), 1763-1766. doi:10.1126/science.280.5370.1763

Rocha, A. G., Franco, A., Krezel, A. M., Rumsey, J. M., Alberti, J. M., Knight, W. C., . . . Dorn, G. W. (2018). MFN2 agonists reverse mitochondrial defects in preclinical models of

Charcot-Marie-Tooth disease type 2A. *Science, 360*(6386), 336-341. doi:10.1126/science.aao1785

Rosales, K. R., Peralta, E. R., Guenther, G. G., Wong, S. Y., & Edinger, A. L. (2009). Rab7 activation by growth factor withdrawal contributes to the induction of apoptosis. *Molecular Biology of the Cell, 20*(12), 2831-2840. doi:10.1091/mbc.E08-09-0911

Rouault, T. A. (2012). Biogenesis of iron-sulfur clusters in mammalian cells: new insights and relevance to human disease. *Dis Model Mech, 5*(2), 155-164. doi:10.1242/dmm.009019

Rowland, A. A., Chitwood, P. J., Phillips, M. J., & Voeltz, G. K. (2014). ER contact sites define the position and timing of endosome fission. *Cell, 159*(5), 1027-1041. doi:10.1016/j.cell.2014.10.023

Ryu, S. Y., Beutner, G., Dirksen, R. T., Kinnally, K. W., & Sheu, S. S. (2010). Mitochondrial ryanodine receptors and other mitochondrial Ca2+ permeable channels. *FEBS Lett, 584*(10), 1948-1955. doi:10.1016/j.febslet.2010.01.032

Samie, M., Wang, X., Zhang, X., Goschka, A., Li, X., Cheng, X., . . . Xu, H. (2013). A TRP channel in the lysosome regulates large particle phagocytosis via focal exocytosis. *Dev Cell, 26*(5), 511-524. doi:10.1016/j.devcel.2013.08.003

Santel, A., & Fuller, M. T. (2001). Control of mitochondrial morphology by a human mitofusin. *Journal of Cell Science, 114*(5), 867-874.

Santo-Domingo, J., Giacomello, M., Poburko, D., Scorrano, L., & Demaurex, N. (2013). OPA1 promotes pH flashes that spread between contiguous mitochondria without matrix protein exchange. *EMBO Journal, 32*(13), 1927-1940. doi:10.1038/emboj.2013.124

Santoni, G., Maggi, F., Amantini, C., Marinelli, O., Nabissi, M., & Morelli, M. B. (2020). Pathophysiological Role of Transient Receptor Potential Mucolipin Channel 1 in Calcium-Mediated Stress-Induced Neurodegenerative Diseases. *Front Physiol, 11*, 251. doi:10.3389/fphys.2020.00251

Schmiege, P., Fine, M., Blobel, G., & Li, X. (2017). Human TRPML1 channel structures in open and closed conformations. *Nature, 550*(7676), 366-370. doi:10.1038/nature24036

Schöndorf, D. C., Ivanyuk, D., Baden, P., Sanchez-Martinez, A., De Cicco, S., Yu, C., . . . Deleidi, M. (2018). The NAD+ Precursor Nicotinamide Riboside Rescues Mitochondrial Defects and Neuronal Loss in iPSC and Fly Models of Parkinson's Disease. *Cell Rep, 23*(10), 2976-2988. doi:10.1016/j.celrep.2018.05.009

Schrepfer, E., & Scorrano, L. (2016). Mitofusins, from Mitochondria to Metabolism. *Molecular Cell, 61*(5), 683-694. doi:10.1016/j.molcel.2016.02.022

Scotto Rosato, A., Montefusco, S., Soldati, C., Di Paola, S., Capuozzo, A., Monfregola, J., . . . Medina, D. L. (2019). TRPML1 links lysosomal calcium to autophagosome biogenesis

through the activation of the CaMKKbeta/VPS34 pathway. *Nat Commun, 10*(1), 5630. doi:10.1038/s41467-019-13572-w

Seibler, P., Burbulla, L. F., Dulovic, M., Zittel, S., Heine, J., Schmidt, T., . . . Klein, C. (2018). Iron overload is accompanied by mitochondrial and lysosomal dysfunction in WDR45 mutant cells. *Brain, 141*(10), 3052-3064. doi:10.1093/brain/awy230

Sena, L. A., & Chandel, N. S. (2012). Physiological roles of mitochondrial reactive oxygen species. *Mol Cell, 48*(2), 158-167. doi:10.1016/j.molcel.2012.09.025

Seong, E., Insolera, R., Dulovic, M., Kamsteeg, E. J., Trinh, J., Brüggemann, N., . . . Burmeister, M. (2018). Mutations in VPS13D lead to a new recessive ataxia with spasticity and mitochondrial defects. *Ann Neurol, 83*(6), 1075-1088. doi:10.1002/ana.25220

Sheftel, A. D., Zhang, A. S., Brown, C., Shirihai, O. S., & Ponka, P. (2007). Direct interorganellar transfer of iron from endosome to mitochondrion. *Blood, 110*(1), 125-132. doi:10.1182/blood-2007-01-068148

Shen, D., Wang, X., Li, X., Zhang, X., Yao, Z., Dibble, S., . . . Xu, H. (2012). Lipid storage disorders block lysosomal trafficking by inhibiting a TRP channel and lysosomal calcium release. *Nat Commun, 3*, 731. doi:10.1038/ncomms1735

Simmen, T., & Herrera-Cruz, M. S. (2018). Plastic mitochondria-endoplasmic reticulum (ER) contacts use chaperones and tethers to mould their structure and signaling. *Curr Opin Cell Biol, 53*, 61-69. doi:10.1016/j.ceb.2018.04.014

Smirnova, E., Griparic, L., Shurland, D. L., & van der Bliek, A. M. (2001). Dynamin-related protein Drp1 is required for mitochondrial division in mammalian cells. *Mol Biol Cell, 12*(8), 2245-2256. doi:10.1091/mbc.12.8.2245

Smirnova, E., Shurland, D. L., Ryazantsev, S. N., & Van Der Bliek, A. M. (1998). A human dynamin-related protein controls the distribution of mitochondria. *Journal of Cell Biology, 143*(2), 351-358. doi:10.1083/jcb.143.2.351

Song, P., Trajkovic, K., Tsunemi, T., & Krainc, D. (2016). Parkin Modulates Endosomal Organization and Function of the Endo-Lysosomal Pathway. *J Neurosci, 36*(8), 2425-2437. doi:10.1523/jneurosci.2569-15.2016

Soyombo, A. A., Tjon-Kon-Sang, S., Rbaibi, Y., Bashllari, E., Bisceglia, J., Muallem, S., & Kiselyov, K. (2006). TRP-ML1 regulates lysosomal pH and acidic lysosomal lipid hydrolytic activity. *J Biol Chem, 281*(11), 7294-7301. doi:10.1074/jbc.M508211200

Spinosa, M. R., Progida, C., De Luca, A., Colucci, A. M. R., Alifano, P., & Bucci, C. (2008). Functional characterization of Rab7 mutant proteins associated with Charcot-Marie-Tooth type 2B disease. *Journal of Neuroscience, 28*(7), 1640-1648. doi:10.1523/JNEUROSCI.3677-07.2008

Spooner, E., McLaughlin, B. M., Lepow, T., Durns, T. A., Randall, J., Upchurch, C., . . . Fares, H. (2013). Systematic screens for proteins that interact with the mucolipidosis type IV protein TRPML1. *PLoS One, 8*(2), e56780. doi:10.1371/journal.pone.0056780

Subedi, K. P., Kim, J. C., Kang, M., Son, M. J., Kim, Y. S., & Woo, S. H. (2011). Voltage-dependent anion channel 2 modulates resting Ca^{2+} sparks, but not action potential-induced Ca^{2+} signaling in cardiac myocytes. *Cell Calcium, 49*(2), 136-143. doi:10.1016/j.ceca.2010.12.004

Sugiura, A., McLelland, G. L., Fon, E. A., & McBride, H. M. (2014). A new pathway for mitochondrial quality control: mitochondrial-derived vesicles. *Embo j, 33*(19), 2142-2156. doi:10.15252/embj.201488104

Sun, M., Goldin, E., Stahl, S., Falardeau, J. L., Kennedy, J. C., Acierno, J. S., Jr., . . . Slaugenhaupt, S. A. (2000). Mucolipidosis type IV is caused by mutations in a gene encoding a novel transient receptor potential channel. *Hum Mol Genet, 9*(17), 2471-2478. doi:10.1093/hmg/9.17.2471

Sun, N., Youle, R. J., & Finkel, T. (2016). The Mitochondrial Basis of Aging. *Mol Cell, 61*(5), 654-666. doi:10.1016/j.molcel.2016.01.028

Sun, Q., Westphal, W., Wong, K. N., Tan, I., & Zhong, Q. (2010). Rubicon controls endosome maturation as a Rab7 effector. *Proceedings of the National Academy of Sciences of the United States of America, 107*(45), 19338-19343. doi:10.1073/pnas.1010554107

Szabadkai, G., Bianchi, K., Varnai, P., De Stefani, D., Wieckowski, M. R., Cavagna, D., . . . Rizzuto, R. (2006). Chaperone-mediated coupling of endoplasmic reticulum and mitochondrial Ca2+ channels. *J Cell Biol, 175*(6), 901-911. doi:10.1083/jcb.200608073

Tarasov, A. I., Griffiths, E. J., & Rutter, G. A. (2012). Regulation of ATP production by mitochondrial Ca(2+). *Cell Calcium, 52*(1), 28-35. doi:10.1016/j.ceca.2012.03.003

Tedeschi, V., Petrozziello, T., Sisalli, M. J., Boscia, F., Canzoniero, L. M. T., & Secondo, A. (2019). The activation of Mucolipin TRP channel 1 (TRPML1) protects motor neurons from L-BMAA neurotoxicity by promoting autophagic clearance. *Sci Rep, 9*(1), 10743. doi:10.1038/s41598-019-46708-5

Todkar, K., Ilamathi, H. S., & Germain, M. (2017). Mitochondria and Lysosomes: Discovering Bonds. *Front Cell Dev Biol, 5*, 106. doi:10.3389/fcell.2017.00106

Trenker, M., Malli, R., Fertschai, I., Levak-Frank, S., & Graier, W. F. (2007). Uncoupling proteins 2 and 3 are fundamental for mitochondrial Ca2+ uniport. *Nat Cell Biol, 9*(4), 445-452. doi:10.1038/ncb1556

Tsunemi, T., Perez-Rosello, T., Ishiguro, Y., Yoroisaka, A., Jeon, S., Hamada, K., . . . Krainc, D. (2019). Increased Lysosomal Exocytosis Induced by Lysosomal Ca(2+) Channel

Agonists Protects Human Dopaminergic Neurons from alpha-Synuclein Toxicity. *J Neurosci, 39*(29), 5760-5772. doi:10.1523/jneurosci.3085-18.2019

Ueno, S., Maruki, Y., Nakamura, M., Tomemori, Y., Kamae, K., Tanabe, H., . . . Sano, A. (2001). The gene encoding a newly discovered protein, chorein, is mutated in chorea-acanthocytosis. *Nat Genet, 28*(2), 121-122. doi:10.1038/88825

Valadas, J. S., Esposito, G., Vandekerkhove, D., Miskiewicz, K., Deaulmerie, L., Raitano, S., . . . Verstreken, P. (2018). ER Lipid Defects in Neuropeptidergic Neurons Impair Sleep Patterns in Parkinson's Disease. *Neuron, 98*(6), 1155-1169.e1156. doi:10.1016/j.neuron.2018.05.022

Valm, A. M., Cohen, S., Legant, W. R., Melunis, J., Hershberg, U., Wait, E., . . . Lippincott-Schwartz, J. (2017). Applying systems-level spectral imaging and analysis to reveal the organelle interactome. *Nature, 546*(7656), 162-167. doi:10.1038/nature22369

Venkatachalam, K., Hofmann, T., & Montell, C. (2006). Lysosomal localization of TRPML3 depends on TRPML2 and the mucolipidosis-associated protein TRPML1. *J Biol Chem, 281*(25), 17517-17527. doi:10.1074/jbc.M600807200

Venugopal, B., Mesires, N. T., Kennedy, J. C., Curcio-Morelli, C., Laplante, J. M., Dice, J. F., & Slaugenhaupt, S. A. (2009). Chaperone-mediated autophagy is defective in mucolipidosis type IV. *J Cell Physiol, 219*(2), 344-353. doi:10.1002/jcp.21676

Vergarajauregui, S., Connelly, P. S., Daniels, M. P., & Puertollano, R. (2008). Autophagic dysfunction in mucolipidosis type IV patients. *Hum Mol Genet, 17*(17), 2723-2737. doi:10.1093/hmg/ddn174

Verhoeven, K., De Jonghe, P., Coen, K., Verpoorten, N., Auer-Grumbach, M., Kwon, J. M., . . . Timmerman, V. (2003). Mutations in the small GTP-ase late endosomal protein RAB7 cause Charcot-Marie-Tooth type 2B neuropathy. *Am J Hum Genet, 72*(3), 722-727. doi:10.1086/367847

Vernay, A., Marchetti, A., Sabra, A., Jauslin, T. N., Rosselin, M., Scherer, P. E., . . . Cosson, P. (2017). MitoNEET-dependent formation of intermitochondrial junctions. *Proceedings of the National Academy of Sciences of the United States of America, 114*(31), 8277-8282. doi:10.1073/pnas.1706643114

Wai, T., & Langer, T. (2016). Mitochondrial Dynamics and Metabolic Regulation. *Trends in Endocrinology and Metabolism, 27*(2), 105-117. doi:10.1016/j.tem.2015.12.001

Wang, W., Gao, Q., Yang, M., Zhang, X., Yu, L., Lawas, M., . . . Xu, H. (2015). Up-regulation of lysosomal TRPML1 channels is essential for lysosomal adaptation to nutrient starvation. *Proc Natl Acad Sci U S A, 112*(11), E1373-1381. doi:10.1073/pnas.1419669112

Wang, X., Han, C., Liu, W., Wang, P., & Zhang, X. (2014). A novel RAB7 mutation in a Chinese family with Charcot-Marie-Tooth type 2B disease. *Gene, 534*(2), 431-434.

Weill, U., Yofe, I., Sass, E., Stynen, B., Davidi, D., Natarajan, J., . . . Schuldiner, M. (2018). Genome-wide SWAp-Tag yeast libraries for proteome exploration. *Nat Methods, 15*(8), 617-622. doi:10.1038/s41592-018-0044-9

Wolff, N. A., Garrick, M. D., Zhao, L., Garrick, L. M., Ghio, A. J., & Thévenod, F. (2018). A role for divalent metal transporter (DMT1) in mitochondrial uptake of iron and manganese. *Sci Rep, 8*(1), 211. doi:10.1038/s41598-017-18584-4

Wolff, N. A., Ghio, A. J., Garrick, L. M., Garrick, M. D., Zhao, L., Fenton, R. A., & Thévenod, F. (2014). Evidence for mitochondrial localization of divalent metal transporter 1 (DMT1). *Faseb j, 28*(5), 2134-2145. doi:10.1096/fj.13-240564

Wong, Y. C., & Holzbaur, E. L. (2014). Optineurin is an autophagy receptor for damaged mitochondria in parkin-mediated mitophagy that is disrupted by an ALS-linked mutation. *Proc Natl Acad Sci U S A, 111*(42), E4439-4448. doi:10.1073/pnas.1405752111

Wong, Y. C., Kim, S., Peng, W., & Krainc, D. (2019). Regulation and Function of Mitochondria-Lysosome Membrane Contact Sites in Cellular Homeostasis. *Trends Cell Biol, 29*(6), 500-513. doi:10.1016/j.tcb.2019.02.004

Wong, Y. C., & Krainc, D. (2017). α-synuclein toxicity in neurodegeneration: mechanism and therapeutic strategies. *Nat Med, 23*(2), 1-13. doi:10.1038/nm.4269

Wong, Y. C., Peng, W., & Krainc, D. (2019). Lysosomal Regulation of Inter-mitochondrial Contact Fate and Motility in Charcot-Marie-Tooth Type 2. *Dev Cell, 50*(3), 339-354.e334. doi:10.1016/j.devcel.2019.05.033

Wong, Y. C., Ysselstein, D., & Krainc, D. (2018). Mitochondria-lysosome contacts regulate mitochondrial fission via RAB7 GTP hydrolysis. *Nature, 554*(7692), 382-386. doi:10.1038/nature25486

Wu, H., Carvalho, P., & Voeltz, G. K. (2018). Here, there, and everywhere: The importance of ER membrane contact sites. *Science, 361*(6401). doi:10.1126/science.aan5835

Wu, J., Liu, L., Matsuda, T., Zhao, Y., Rebane, A., Drobizhev, M., . . . Campbell, R. E. (2013). Improved orange and red Ca(2)+/- indicators and photophysical considerations for optogenetic applications. *ACS Chem Neurosci, 4*(6), 963-972. doi:10.1021/cn400012b

Wu, Y., Whiteus, C., Xu, C. S., Hayworth, K. J., Weinberg, R. J., Hess, H. F., & De Camilli, P. (2017). Contacts between the endoplasmic reticulum and other membranes in neurons. *Proceedings of the National Academy of Sciences of the United States of America, 114*(24), E4859-E4867. doi:10.1073/pnas.1701078114

Xu, Y. H., Xu, K., Sun, Y., Liou, B., Quinn, B., Li, R. H., . . . Grabowski, G. A. (2014). Multiple pathogenic proteins implicated in neuronopathic Gaucher disease mice. *Hum Mol Genet, 23*(15), 3943-3957. doi:10.1093/hmg/ddu105

Yamano, K., Fogel, A. I., Wang, C., van der Bliek, A. M., & Youle, R. J. (2014). Mitochondrial Rab GAPs govern autophagosome biogenesis during mitophagy. *Elife, 3*, e01612. doi:10.7554/eLife.01612

Yamano, K., Wang, C., Sarraf, S. A., Münch, C., Kikuchi, R., Noda, N. N., . . . Youle, R. J. (2018). Endosomal Rab cycles regulate Parkin-mediated mitophagy. *Elife, 7*. doi:10.7554/eLife.31326

Yi, M., Weaver, D., & Hajnóczky, G. (2004). Control of mitochondrial motility and distribution by the calcium signal: a homeostatic circuit. *J Cell Biol, 167*(4), 661-672. doi:10.1083/jcb.200406038

Zhang, K., Ben Kenan, R. F., Osakada, Y., Xu, W., Sinit, R. S., Chen, L., . . . Wu, C. (2013). Defective axonal transport of Rab7 GTPase results in dysregulated trophic signaling. *Journal of Neuroscience, 33*(17), 7451-7462. doi:10.1523/JNEUROSCI.4322-12.2013

Zhang, L., Fang, Y., Cheng, X., Lian, Y., Xu, H., Zeng, Z., & Zhu, H. (2017). TRPML1 Participates in the Progression of Alzheimer's Disease by Regulating the PPARγ/AMPK/Mtor Signalling Pathway. *Cell Physiol Biochem, 43*(6), 2446-2456. doi:10.1159/000484449

Zhang, M., Liu, P., Dwyer, N. K., Christenson, L. K., Fujimoto, T., Martinez, F., . . . Strauss, J. F., 3rd. (2002). MLN64 mediates mobilization of lysosomal cholesterol to steroidogenic mitochondria. *J Biol Chem, 277*(36), 33300-33310. doi:10.1074/jbc.M200003200

Zhang, X., Cheng, X., Yu, L., Yang, J., Calvo, R., Patnaik, S., . . . Xu, H. (2016). MCOLN1 is a ROS sensor in lysosomes that regulates autophagy. *Nat Commun, 7*, 12109. doi:10.1038/ncomms12109

Zhang, X., Chow, C. Y., Sahenk, Z., Shy, M. E., Meisler, M. H., & Li, J. (2008). Mutation of FIG4 causes a rapidly progressive, asymmetric neuronal degeneration. *Brain, 131*(Pt 8), 1990-2001. doi:10.1093/brain/awn114

Zhang, X. M., Walsh, B., Mitchell, C. A., & Rowe, T. (2005). TBC domain family, member 15 is a novel mammalian Rab GTPase-activating protein with substrate preference for Rab7. *Biochem Biophys Res Commun, 335*(1), 154-161. doi:10.1016/j.bbrc.2005.07.070

Zhao, N., Kamijo, K., Fox, P. D., Oda, H., Morisaki, T., Sato, Y., . . . Stasevich, T. J. (2019). A genetically encoded probe for imaging nascent and mature HA-tagged proteins in vivo. *Nat Commun, 10*(1), 2947. doi:10.1038/s41467-019-10846-1

Zhen, Y., & Stenmark, H. (2015). Cellular functions of Rab GTPases at a glance. *J Cell Sci, 128*(17), 3171-3176. doi:10.1242/jcs.166074

Zuchner, S., Mersiyanova, I. V., Muglia, M., Bissar-Tadmouri, N., Rochelle, J., Dadali, E. L., . . . Vance, J. M. (2004). Mutations in the mitochondrial GTPase mitofusin 2 cause Charcot-Marie-Tooth neuropathy type 2A. *Nat Genet, 36*(5), 449-451. doi:10.1038/ng1341